IMPACT OF LIGAND SHELL ARCHITECTURE ON STRUCTURE AND REACTIVITY OF DNA APTAMER-LINKED GOLD NANOPARTICLE ASSEMBLIES

by

BRANDI LEE BALDOCK

A DISSERTATION

Presented to the Department of Chemistry and Biochemistry
and the Graduate School of the University of Oregon
in partial fulfillment of the requirements
for the degree of
Doctor of Philosophy

March 2016

DISSERTATION APPROVAL PAGE

Student: Brandi Lee Baldock

Title: Impact of Ligand Shell Architecture on Structure and Reactivity of DNA Aptamer-Linked Gold Nanoparticle Assemblies

This dissertation has been accepted and approved in partial fulfillment of the requirements for the Doctor of Philosophy degree in the Department of Chemistry and Biochemistry by:

Dr. Mark C. Lonergan	Chairperson
Dr. James E. Hutchison	Advisor
Dr. J. Andrew Berglund	Core Member
Dr. Karen Guillemin	Institutional Representative

and

Dr. Scott L. Pratt	Dean of the Graduate School

Original approval signatures are on file with the University of Oregon Graduate School.

Degree awarded: March 2016

DISSERTATION ABSTRACT

Brandi Lee Baldock

Doctor of Philosophy

Department of Chemistry and Biochemistry

March 2016

Title: Impact of Ligand Shell Architecture on Structure and Reactivity of DNA Aptamer-Linked Gold Nanoparticle Assemblies

DNA-functionalized gold nanoparticles (DNA-NPs) have enormous potential as building blocks for materials due to their ability to specifically recognize and respond to target molecules and surfaces. The ability of DNA aptamers to adopt different conformations and bind either complementary DNA sequences or analyte molecules allows them to mediate nanoparticle assembly or disassembly, generating selective colorimetric responses.

Aptamer-mediated nanoparticle assembly and disassembly is sensitive to the nanoparticle ligand shell composition and structure, yet these topics have not been extensively explored. In this dissertation, a method for determining the ligand shell composition of DNA-NPs is described and a framework for understanding the impact of the DNA assembly arrangement and recognition strand density upon aptamer-mediated nanoparticle assembly and disassembly is developed. Design rules for creating sensors with desired properties are elucidated, leading to creation of sensors with improved detection limits and quantification ranges.

A technique was needed to determine the number of DNA strands of any base composition attached to gold nanoparticles (AuNPs) of any core size. A rapid, convenient and inexpensive method to quantify the number of label-free DNA strands attached to

AuNPs was therefore developed. This technique was extended to determine two different DNA sequences bound to AuNPs using UV-visible and fluorescence spectroscopy. Based on the results of quantifying the ligand shells of DNA-NPs functionalized with two sequences, disulfide-terminated DNA non-specifically adsorbs and then rearranges to specifically bind the gold surface.

The position of the AuNPs and DNA strands within DNA-NP assemblies had a profound influence on their ability to assemble and sense adenosine. Assemblies designed for large inter-AuNP spacing were stable but unable to sense adenosine. Assemblies designed for short inter-AuNP spacing were unstable until the DNA ligand shell was diluted.

AuNPs functionalized with the fewest number of aptamers produced assemblies with the lowest detection limit and apparent disassociation constant and the largest analyte quantification range. Increasing the number of aptamer strands per AuNP increased the cooperativity of the AuNP disassembly response to adenosine.

This dissertation includes previously unpublished co-authored material.

CURRICULUM VITAE

NAME OF AUTHOR: Brandi Lee Baldock

GRADUATE AND UNDERGRADUATE SCHOOLS ATTENDED:

University of Oregon, Eugene, Oregon, USA
Trent University, Peterborough, Ontario, Canada

DEGREES AWARDED:

Doctor of Philosophy in Chemistry, 2016, University of Oregon
Master of Science in Chemistry, 2009, University of Oregon
Bachelor of Science with Honours in Chemistry, 2008, Trent University

AREAS OF SPECIAL INTEREST:

Nanomaterials Chemistry
Chemical Education
Biochemistry
Green Chemistry
Analytical Chemistry

PROFESSIONAL EXPERIENCE:

General Chemistry Faculty and Curriculum Coordinator, Department of Chemistry and Biochemistry, University of Oregon, Eugene, OR, 2015

Graduate Student Chemistry Consultant, University of Oregon CH 114: Green Product Design, 2015

Graduate Research Assistant, Department of Chemistry and Biochemistry, University of Oregon, Eugene, OR, 2008-2015

Graduate Teaching Assistant, Department of Chemistry and Biochemistry, University of Oregon, Eugene, OR, 2008-2009; 2013-2015

Webmaster for University of Oregon Women in Graduate Sciences, 2013-2014

Graduate Student Organizer of UO Materials Science Institute and Oregon Centre for Optics Symposium, 2012 and 2013

Undergraduate Teaching Assistant, Department of Chemistry, University of Oregon, Eugene, OR, 2007-2008

Undergraduate Research Assistant, Department of Chemistry, Trent University, Peterborough, Ontario, Canada, 2007

Undergraduate Teaching Assistant, Department of Chemistry, Trent University, Peterborough, Ontario, Canada, 2006

GRANTS, AWARDS, AND HONORS:

Post-doctoral fellowship, "Learning Chemistry", Tom and Carol Williams Foundation for Undergraduate Education, 2015-2016

National Academies Education Fellow, Summer Institute on Undergraduate Education, National Academies and Howard Hughes Medical Institution, 2015-2016

Graduate Teaching Initiative-Advanced Certificate of Completion, University of Oregon Teaching Effectiveness Program, 2015. In preparation.

Science Literacy Program Fellow, Howard Hughes Medical Institute, University of Oregon, 2015

Graduate Student Award for Excellence in the Teaching of Chemistry Department of Chemistry and Biochemistry, University of Oregon, 2014

Graduate Student Travel Award, Department of Chemistry and Biochemistry, 2014

Dean's Honour Roll, President's Honour Roll and Cranston Scholarship, Trent University, Peterborough, Ontario, Canada

PUBLICATIONS:

Brandi L. Baldock and Deborah Berkshire Exton, 2016. CH 6. "Determination of the Heat Exchanged in Chemical Reactions", Hayden McNeil LLC, University of Oregon Department of Chemistry and Biochemistry "Experiments in General Chemistry" p. 39-46

Brandi L. Baldock and Deborah Berkshire Exton, 2014, CH 6. "Determination of the Heat Exchanged in Chemical Reactions", McGraw-Hill Education LLC, University of Oregon CH 227 General Chemistry Laboratory Manual p. 65-69

ACKNOWLEDGMENTS

Grad school was a long and complicated journey, during which I underwent a lot of personal and professional growth. I thank my advisor Jim Hutchison, who invited me on this journey. I would not have attended graduate school without his encouragement. Jim is a patient man who always saw my potential, even when I could not. His persistent optimism and interest in science and my development as a researcher saw me through several challenging time periods. I would never have completed my dissertation without his willingness to "dig in" and his insistence that I do the same.

Thank you to my dissertation committee members Andy Berglund, Mark Lonergan and Karen Guillemin, who provided great advice and encouraged me to challenge myself and strive for my personal best. I especially thank Andy, who generously shared experimental and editorial guidance, lab space, and research materials with me.

I acknowledge the Air Force Research Laboratory (USAF Nano #23570), the W. M. Keck Foundation, Howard Hughes Medical Institute, University of Oregon's Science Literacy Program, University of Oregon's Materials Science Institute and Department of Chemistry and Biochemistry for financial support. I thank CAMCOR and the Institute of Molecular Biology for use of their facilities and technical support.

Thank you to the lab mates who supported me over the years. I was grateful for thoughtful advice and emotional support provided by Tatiana Zaikova and Ruth Siboni. Sam Lohse, Rick Glover, Erik Richman, Zack Kennedy, Adam Jansons, Samantha Young and Kenyon Plummer were considerate, supportive and helpful colleagues.

I thank my teaching mentors, Deborah Exton and Tom Greenbowe, who provided endless encouragement and advice. Giving a talk about our education work at the Biennial Conference on Chemical Education was an amazing experience, and helped me set my goals for my next step. Thank you to the Department of Chemistry and Biochemistry for funding the trip. I look forward to performing more curriculum development and education research with Deb and Tom next year, as we revise the "Learning Chemistry" program we designed and implemented in Fall 2015. Thank you to members of the Science Literacy Program; spending time talking to other enthusiastic educators at our Teaching Journal Club was a highlight of each week.

I thank my family and friends for their endless love and support, particularly Mom, Dad, Kensi and Kelsi Dickinson. I always looked forward to the next board game, RPG night and camping trip with Ethan Walker, Brandon Schabes, Erin Moody, Zac Sandine, Dan Gerold, Lysse Stokes and Clay Stephens. Dawn Potter, Lena Trotochaud and Rachel Ulrich provided much needed support and comic relief in the form of wisecracks. Marco Esters, Lisa Enman and Hillary Henthorn were also great friends.

Most importantly, I thank my husband and greatest cheerleader, James Baldock. I would never have completed my dissertation without his love and his relentless optimism and encouragement. He provided the jokes I needed when times were rough, led the celebration when times were good, and constantly reminded me to eat, to sleep and to take breaks to socialize. I look forward to many more years exploring the outdoors, and playing hockey and board games together.

This dissertation is dedicated to my Mom, who taught me that I can do anything I want

TABLE OF CONTENTS

LIST OF FIGURES

Figure Page

Figure Page

LIST OF TABLES

CHAPTER I

INTRODUCTION

INTRODUCTION

Nanoparticle Applications

Nanoparticles are used in a large and expanding number of exciting applications, including biosensing,[1–3] drug delivery,[4–8] therapeutics,[6,9,10] diagnostics,[11] solar energy conversion,[12] and catalysis.[13,14] Nanoparticles are defined as particles that possess one dimension in the 1-100 nm range and exhibit size-dependent properties that differ from those of the bulk material.[14,15] To design and create functional nanomaterials tailored for specific applications, it is critical to understand and control their properties. The expanding number of nanoparticle applications and their increasing market value makes the study of nanoparticle structure-property relationships a particularly compelling area of research.

Biosensors are a particularly intriguing class of nanomaterials that transduce specific binding recognition events by biomolecules (i.e. antibodies, proteins, peptides, DNA or RNA) into colorimetric, surface enhanced raman spectroscopy (SERS), fluorescence resonance energy transfer (FRET) or electrochemical responses. [3,16–25]

Small nanoparticles are well suited for biosensing applications because they preferentially localize to areas of tumor growth and inflammation,[26] and enter cells more rapidly than small molecules,[6] which is advantageous for therapeutic and cellular imaging applications. They can be functionalized with multiple copies of targeting and/or binding ligands, and thereby interact strongly with biological systems and biomolecules. [6,15]

The widespread implementation of many biosensors is prevented by the technical expertise and specialized equipment required to collect and analyze FRET, SERS or electrochemical responses. Fluorophore labels required for FRET-based sensors are expensive, are susceptible to photobleaching, and can affect interactions between biomolecule and their targets.[27,28] To avoid these drawbacks, biomolecule-functionalized gold nanoparticles have been used to generate colorimetric responses to analytes. Colorimetric sensors are advantageous because their responses can be analyzed by eye or by using a simple hand-held reader or cell phone, without requiring technical expertise or expensive instruments.[29,30] To produce specific user-friendly sensors that respond to analytes over desired concentration ranges, an advance in the fundamental understanding of the structure-property relationships of these materials is required.

Unique Properties of Gold Nanoparticles

Gold nanoparticles (AuNPs) are of particular interest as response elements for biosensing applications due to their unique optical properties,[7,10,15,31] biocompatibility[32] and ability to be modified to display antibodies, nucleic acid or peptide recognition sequences.[33,34] The large extinction coefficients and increased photostability of AuNPs compared to fluorescent dye molecules[10] makes them ideal reporters for biosensors.

AuNPs, like other noble metal nanoparticles, exhibit an intense absorbance band in the UV-visible region of the electromagnetic spectrum. [7,10,15,31] The oscillating electromagnetic field of the light induces collective coherent oscillation of electrons in the conduction band of the AuNPs, a phenomenon known as surface plasmon resonance (SPR).[7,10,15,31] The wavelength of light at which the amplitude of the electrons reaches a maximum corresponds to their UV-visible absorbance peak.[10] The position and shape of

this peak is sensitive to the size and shape of the AuNPs, their local environment (i.e. ligand shell) and the solvent. [7,10,15,31]

The SPR peak of AuNPs is also sensitive to interactions between AuNPs. [7,10,15,31] During light propagation, the instantaneous polarization of the AuNP electron cloud induces repulsive surface charges within each AuNP.[35] The instantaneous dipoles of closely adjacent AuNPs can couple during light propogation, weakening the repulsive surface charges.[35] This causes their SPR peak to shift to longer wavelengths.[36] The position and shape of the SPR band of AuNPs therefore provides information about the interactions between AuNPs in solution. [7,10,15,31]

Because the SPR peak is in the visible region of the electromagnetic spectrum, AuNPs exhibit a colorimetric response when they are assembled or disassembled. This property is extensively exploited by AuNP biosensors, which transduce binding events by biomolecules into assembly or disassembly-based colorimetric responses.

AuNPs can be functionalized with multiple ligands, including DNA or peptide targeting sequences, covalently or non-covalently bound drugs and solubilizing diluent ligands. S-Au interactions are widely used to anchor biomolecules to AuNPs, though DNA base-gold interactions have also been used.[37] The versatile ligands that can be attached means that properties of biomolecule-functionalized AuNPs have the potential to be tuned for specific applications.[33] However, the relationship between moles of each ligand added and bound to AuNPs is complex, and characterization methods are not straightforward. Predicting how the ligand shell composition and structure will affect the sensing properties of new materials is challenging. Elucidating the design rules for

creating biomolecule-functionalized materials with enhanced properties has the potential to significantly advance the field of biosensing. One ligand of particular interest is DNA.

Unique Properties of DNA

Deoxyribonucleic acid (DNA) is a linear polymer composed of nitrogenous bases (adenine (A), thymine (T), guanine (G) or cytosine (C)) covalently linked by a phosphodiester-ribose backbone.[38] Individual DNA molecules are referred to as DNA strands, and the exact order in which bases are arranged in a DNA strand is considered its sequence.[38] Individual DNA strands can form a double-stranded DNA helix by hydrogen bonding, or base pairing, to their complementary sequence (also called hybridization).[38] Typically, adenine base pairs to thymine and guanine base pairs to cytosine.[38] DNA also interacts strongly with planar gold surfaces and AuNPs.

Interactions between DNA Strands and Planar Gold Surfaces

Individual DNA bases and DNA strands interact strongly with planar gold surfaces. It was found that individual DNA bases formed relatively strong bonds with planar gold surfaces, forming the strongest bonds with guanine (127-139 kJ/mol) and adenine (124 kJ/mol), followed by cytosine (122 kJ/mol) and thymine (104 kJ/mol).[39] The DNA base composition of a polynucleotide sequence (i.e. A_{25}, C_{25}, T_{25}) significantly affected its rate of adsorption to planar gold, with polyadenosine adsorbing the most quickly, followed by polycytosine and polythymidine.[40] For polynucleotide sequences terminated in thiol functionalities (i.e. HS-A_{25}, HS-C_{25}, HS-T_{25}), the initial adsorption kinetics were not affected by the sequence's base composition, but the final surface coverage was significantly lower for polyadenosine sequences than for polycytosine or polythymine sequences.[40] This suggests that they initially lie flat on the Au surface, and

do not adopt a fully vertical orientation during adsorption.[40] The thiol anchor on the DNA sequence was found to significantly increased the surface coverage of DNA probes on Au surfaces; this effect was greatest for short oligonucleotide strands, suggesting that DNA bases interact with the gold surface after their additional adsorption and thiol binding to the surface.[41]

These results from the functionalization of gold films have important implications for the attachment of DNA strands to AuNPs, since they highlight the importance of including a sulfur-containing anchoring group and using an excess of DNA to promote adsorption during ligand exchange. They also highlight the importance of carefully choosing the base composition of DNA sequences.

Interactions between DNA Strands and AuNPs

The most commonly used method to functionalize AuNPs with DNA is to perform ligand exchange by mixing thiol-terminated DNA with citrate-stabilized AuNPs and gradually increase the sodium chloride concentration of the solution until a high surface coverage of DNA strands on the AuNPs is attained.[42] A more recently established method promotes DNA adsorption during ligand exchange by decreasing the pH of the solution to 3, thereby protonating adenosine bases and reducing the electrostatic repulsion between strands during functionalization.[43,44] The adsorption of unthiolated DNA can also promoted by increasing the dielectric constant of the solution during functionalization.[45] After ligand exchange, DNA-functionalized nanoparticles (DNA-NPs) are typically purified by centrifugation.

Sandstrom et al.[46] studied the interactions between AuNPs and unthiolated or thiolated DNA strands. Similar to when DNA strands bind planar gold, adding the thiol

anchor group to the DNA sequences significantly increased the surface coverage of DNA on the AuNPs. Functionalizing AuNPs with short (12 base) DNA sequences resulted in higher DNA surface coverages than when long (25 base) DNA sequences were added, suggesting that longer DNA sequences prevented additional DNA binding via enduring base interactions with the AuNP surface.

Hurst et al.[42] found that using a polyethylene glycol spacer near the thiol anchor group significantly increased the final surface coverage of DNA strands on the AuNPs. Sonicating the DNA-NPs after the initial adsorption promoted additional DNA binding to the AuNPs, suggesting that the DNA bases initially laid flat on the surface of AuNPs, then rearranged to permit additional DNA binding.[42] Sonication was much more effective at promoting the adsorption of DNA sequences containing a T_{10} spacer than those containing A_{10} spacers, suggesting that adenosine bases more tightly bind the AuNP surface.

Brown et al.[47] found that sequences designed to contain adenosine or cytidine nucleotides adjacent to the thiol-AuNP bond exhibited significantly lower surface coverages than those with thymidine nucleotides adjacent to the gold suface. These findings were unsurprising given that adenine forms a higher enthalpy bond with gold than cytosine or thymine, and therefore is more likely to interact with the surface.[39] These findings have important implications for the design of sequences to hybridize at the surface of AuNPs.

Hybridization of DNA Strands to DNA-NPs

The hybridization of DNA strands to DNA-functionalized surfaces and AuNPs is integral to most technologies involving DNA-NPs. Peterson et al.[48] found that DNA

hybridization to strands immobilized on thin gold films was highly dependent on the surface density of DNA. At low DNA surface densities, hybridization efficiency was very high, and binding kinetics were fast.[48] Conversely, DNA binding to surfaces covered with a high density of immobilized DNA strands was slow and inefficient.[48] Herne and Tarlov[49] were able to promote DNA hybridization to DNA-functionalized gold films by diluting their DNA monolayer using mercaptohexanol.

Demers et al.[50] studied DNA hybridization to DNA-NPs and found that the hybridization efficiency of their DNA-NPs increased as a function of the surface density of DNA on the AuNPs. However, the surface density of DNA on all their DNA-NPs[50] was similar to the optimum DNA ligand density identified by Herne and Tarlov.[49] Park et al[51]were able to increase hybridization efficiency of their DNA-NPs by diluting their ligand shell using mercaptohexanol. Brown et al. found that sequences containing guanosine or thymidine adjacent to the thiol anchor to the AuNP surface exhibited greater hybridization efficiency than sequences containing adenosine or cytosine adjacent to the thiol anchor, which suggests that their hybridization efficiency decreased as DNA base interactions with the AuNP surface increased.[52]

There are two primary reasons why DNA hybridization to DNA-functionalized surfaces and DNA-NPs is promoted by diluting the ligand shell: (1) Decreasing the density of DNA strands decreases the electrostatic repulsion between immobilized DNA strands and DNA strands in solution[53] and (2) Using a diluent ligand to decrease the density of DNA ligands on the AuNP surface can prevent DNA bases from interacting with the Au surface, promoting the adoption of a vertical position that facilitates hybridization.[54]

Therefore, the density of the DNA ligand shell is an important design criteria when preparing assemblies of DNA-NPs for biosensing applications. This density can be manipulated by selecting DNA strands that interact significantly with the gold surface, by not using ligand exchange conditions in which DNA loading onto AuNPs is maximized or by deliberately diluting the DNA ligand shell using a diluent ligand. Selecting DNA strands that significantly interact with the gold surface could prevent subsequent DNA hybridization. Simply performing ligand exchange under conditions in which DNA loading is not maximized could destabilize the AuNPs. Therefore, it is preferable to use a diluent ligand to decrease the surface density of DNA strands bound to AuNPs.

DNA-Mediated AuNP Assembly

Single-stranded DNA sequences anchored to AuNPs via a thiol-Au linkage have been extensively used to program interactions between AuNPs. Base-pairing between DNA strands on separate AuNPs and linker DNA molecules has been used to guide the formation and structure of large crystalline AuNP assemblies.[21,55–57] These base pairing interactions are sensitive to single-base imperfections, which permits the sensitive and selective detection of DNA.[58] DNA-functionalized AuNPs have also been used to detect cellular mRNA levels[32] and regulate biological events *in vivo*[32,59].

The formation and thermal melting (dehybridization) of DNA-NP assemblies formed by binding DNA-NPs to one another via interactions with linking DNA strands (linker-mediated hybridization) has been studied extensively in the literature.[60,61] Jin et al.[62] studied this behavior and found that the melting temperature was directly proportional to the salt concentration, inter-particle distance and DNA strand density, and inversely proportional to the core size of the AuNPs. A theoretical model was developed

to explain the melting behavior of DNA-NP assemblies, and this model showed that the melting temperature and apparent cooperativity of the dehybridization events were proportional to the number of linkers between DNA-NPs.[62]

Thermodynamic modeling of DNA-NP assembly formation found that the DNA-NP hybridization efficiency significiantly increased when a spacer sequence (A_{10}) was introduced between the AuNP surface and the linking DNA binding site.[63]

Nykypanchuk et al.[64] experimentally determined that DNA-NP assemblies formed from directly binding the DNA-NPs exhibited significantly less order than assemblies formed by linker-mediated hybridization. The ability of the DNA-NPs to form extended crystalline structures was proportional to the length of the DNA between the DNA-NPs, with systems in which AuNPs were positioned 100 bases apart exhibiting the greatest degree of crystallinity, as assessed by small angle x-ray scattering (SAXS).[65] They proposed that DNA-NPs form amorphous assemblies during the initial stages of hybridization, and reorganize into extended crystalline structures when annealed near their melting temperatures, provided the DNA on the surface of the AuNPs is not electrostatically restrained from doing so.

Macfarlene et al.[66] described DNA-NP crystal formation as a 3-step process involving (1) a random binding phase resulting in disordered assemblies (2) local reorganization by slow cooling through the melting temperature and (3) extended crystal growth. The growth of large crystalline DNA-NP assemblies is promoted by using long, flexible inter-particle linking DNA strands, with large distances between the nanoparticles and the inter-particle binding sequence.[66] The crystal lattice structure can be controlled by the choice of 1-component vs. 2-component linking DNA systems and

the annealing temperature.[66] The hydrodynamic radius of the AuNPs, and ratio of the linking DNA sequence to the AuNP core size[67] were also described as key contributing factors to determining the lattice parameters and structure of the resultant DNA-NP crystal.[68]

A theoretical paper[69] demonstrated that limiting the potential number of bonds between DNA-NPs using inert DNA strands could lead to the formation of small disordered DNA-NP assemblies. Similarly, introducing "overhanging" DNA bases to the end of DNA linking strands decreases the melting temperature of DNA-NP assemblies.[70]

While many papers have studied the formation and melting properties of DNA sequence-linked AuNP assemblies, relatively few have explored the assembly and melting properties of DNA aptamer-linked AuNP assemblies. Fewer still have explored the potential for using small disordered AuNP assemblies in sensing applications.

DNA Aptamers as Recognition Elements

The specific and sensitive binding of antibodies to their targets has long been used in enzyme linked immunosorbent assays,[71] lateral flow assays[72] and northern, southern and western blot assays.[73] Unfortunately, antibodies must be produced in vivo, which inherently limits the number of potential analytes.[74] This also makes them relatively expensive to produce.

Aptamers are short (<100 nucleotide) single-stranded DNA or RNA sequences that switch conformation to form structures capable of binding target analytes with a similar sensitivity and selectivity to that of antibodies.[74–76] An increasing number of sensing and therapeutic applications exploit the ability of DNA aptamers to adopt different conformations and bind either complementary DNA sequences or analyte

molecules.[18,21,74,77] Colorimetric sensors can be created by marrying the binding properties of DNA aptamers to the optical properties of AuNPs.

Sensors based on DNA or RNA aptamers have been developed to detect a large number of potential analytes[17,18,21,74,77], which include small molecules[78,79] , metal ions[80], allergens[47,81–84] microbial and viral pathogens[85,86], proteins[23,87–89] and cells[90].

DNA Aptamer-Mediated AuNP Assembly and Disassembly

One particularly intriguing class of AuNP biosensors are those that exploit the unique structure-switching properties of DNA aptamers.[3,16–20] The aptamer-analyte binding event can be designed to trigger AuNP assembly[91–94] or disassembly.[80,95–97] Disassembly-based sensing is preferable over assembly-based sensing because while AuNPs can be destabilized and aggregate due to many environmental factors, few things cause them to disassemble.[98] In disassembly-based sensing, untethered aptamer-containing crosslinking strands initially act as a bridge between DNA strands on neighboring AuNPs.[80,95–97,99] When the aptamer sequence changes conformation to bind its analyte, the AuNPs disassemble, producing a colorimetric response based on plasmon decoupling.[95,99]

Aptamer-AuNP biosensors are ideally suited for personal or commercial analyte detection because observing their colorimetric response requires no specialized equipment or technical expertise,.[95–97,99–101] Their use in dipstick[102] and lateral flow assays[103] has been demonstrated, which are increasingly used in consumer products[72]. Unfortunately, existing colorimetric sensors based on disassembly-based sensing do not respond to biologically relevant analyte concentrations. In this dissertation, several challenges facing these systems are identified and addressed.

Addressing the Challenges Facing Aptamer-Mediated Sensing Based on AuNP Disassembly

Typical aptamer-mediated sensors based on AuNP disassembly are designed to maximize the linkages between AuNPs. These sensors are composed of extended assemblies of DNA-functionalized nanoparticles (DNA-NPs) that span several microns in size.[95] The large size of these assemblies and the vast number of crosslinks between AuNPs significantly decreases the sensitivity and reproducibility of their sensing responses, compared to if smaller assemblies were used. [97]

Improving the properties of aptamer-mediated disassembly-based AuNP sensors requires an advance in our fundamental understanding of the variables that govern interactions between AuNPs, aptamers and their analytes. This dissertation describes the successful implementation of two strategies designed to decrease the size of the DNA-NP assemblies and improve the sensitivity of their response to adenosine.

Directly hybridizing DNA strands on separate AuNPs to one another produces smaller and less crystalline AuNP assemblies than when they are linked by an untethered crosslinking strand.[64] The distance between AuNPs inside assemblies is directly related to their melting temperature[62] and inversely related to their ability to disassemble as a response to the analyte.[96] We predicted that changing the arrangement of AuNPs and DNA strands within the assemblies so that the DNA-NPs are directly hybridized and positioned closer to one another would decrease the concentration of analyte required to separate individual AuNPs from the assemblies.

The melting temperature of DNA-NPs decreases as a function of the number of DNA recognition strands per AuNP.[62] Theoretical calculations indicate that the melting

temperature of DNA-NP assemblies is directly related to the number of linkages between AuNPs.[62] Decreasing the number of DNA recognition ligands attached per AuNP would decrease the number of reactive groups, thereby limiting the number of linkages that could form between AuNPs. Therefore, we predicted that lowering the density of DNA recognition strands on our AuNPs would also decrease the concentration of analyte required to separate individual AuNPs from the assemblies.

Before we could test our hypotheses, we needed to prepare and fully characterize the DNA-NPs and assemblies of interest.

CHARACTERIZATION OF DNA-NPS

The synthesis and characterization of nanomaterials presents several unique challenges to the researcher. Methods used to synthesize intermediate-sized AuNPs (~12 nm) produce citrate-stabilized AuNPs that have a narrow distribution of sizes centered around a mean.[104–106] The width of this size distribution is referred to as the nanoparticle's polydispersity. Large polydispersities in AuNP core size must be avoided, because it negatively affects the performance of the nanomaterials.

Citrate-stabilized AuNPs are readily functionalized by DNA by ligand exchange and purified by centrifugation.[43,44] Prior to ligand exchange, great care must be taken to avoid destabilizing the AuNPs. Drying, freezing or bringing the colloidal solutions to high ionic strength causes irreversible aggregation of the gold cores. Because DNA-NPs are conjugates containing organic and inorganic materials, the AuNP core size and polydispersity and the ligand shell composition must be analyzed using multiple corroborative and complementary characterization techniques.[107]

Characterization of AuNPs

The position of an AuNP's SPR peak and its extinction coefficient varies according to the diameter of the Au core.[108–110] Once the core size of a particular sample has been determined, its absorbance and extinction coefficient can be used to determine the AuNP concentration.[109] Inter-particle interactions produce shifts in the SPR peak of the AuNPs, and formation of large aggregates results in an increase in the baseline of their absorbance spectrum.[31,36,111,112]

Bright field transmission electron microscopy (TEM) is commonly used to determine the size and polydispersity of AuNPs.[107] Samples are prepared for TEM by immobilizing the AuNPs on the surface of an electron-transparent material such as silicon dioxide.[107] During the TEM experiment, high energy electrons (~80-300 keV) bombard the AuNP sample and electrons that are not scattered by the high density AuNP core are transmitted through the material to be collected by a CCD detector.[113] The AuNP size and shape can then be determined from the micrographs using analysis software such as ImageJ.[114] Collecting statistically significant data regarding the mean size and size distribution of AuNPs using TEM requires a lot of time, because many micrographs containing thousands of AuNPs must be imaged and analyzed. Therefore, TEM was primarily used to confirm the shape of our AuNPs prior to determining the size distribution using SAXS.

Small angle x-ray scattering (SAXS) is a powerful tool to determine the size and polydispersity of colloidal materials.[115] In a SAXS experiment, AuNPs are exposed to a monochromated x-ray beam, and the particles elastically scatter the x-rays in a pattern characteristic of their size and polydispersity.[116] After removing the background

scattering and desmearing data collected from the line x-ray source (rather than a point source), the scattering pattern of the sample can be modeled using existing macros in software packages such as IgorPro,[117–120] and used to determine the mean size and size distribution of the AuNPs.[116]

After the determining the size of the AuNPs using SAXS, their SPR extinction coefficient can be calculated from empirical data and Beer's law can be used to determine the AuNP concentration.[109]

Quantification of the DNA Ligand Shell

The two most common methods used to quantify the concentration of DNA in solution are UV-visible spectroscopy and fluorescent dye binding.[121] DNA bases absorb light strongly at 260 nm, with extinction coefficients corresponding to their base composition,[122] so Beer's law is most often used to quantify DNA in pure, concentrated samples.[123] Multiple contaminants commonly found in DNA solutions absorb light in the UV region of the electromagnetic spectrum (incuding proteins, phenolate ion, thiocyanates, and other organic compounds).[123] Care must be taken to account for these other contributing species. Gold salts and AuNPs absorb near 260 nm,[124] but their contributions to the UV-visible spectrum cannot be normalized because citrate-stabilized AuNPs cannot be adequately purified. Therefore, the DNA concentration cannot be determined directly from the UV-visible spectrum of DNA-NPs.

To quantify DNA strands bound to AuNPs, DNA sequences are often labeled using a fluorophore and quantified using fluorescence spectroscopy. Commonly used fluorophores are organic dye molecules whose resonant emissions originate from optical transitions delocalized over the entire chromophore.[125] These emissions are drastically

quenched near the surface of AuNPs,[126] so the total amount of DNA bound to AuNPs can be calculated by the decrease in solution fluorescence during AuNP functionalization.[43,45]

The ligand shell of AuNPs functionalized with fluorophore-labeled DNA strands is most often determined by displacing the DNA strands using small thiol ligands, separating the fluorophores from the AuNPs, then quantifying the DNA based on a calibration curve.[127]

Unfortunately, fluorophores attached to DNA strands can drastically change the number of DNA strands bound to AuNPs[128] and influence the DNA's structure and reactivity.[27,28] DNA ligands attached to AuNPs have been quantified using the Oligreen fluorescence assay[129] and DNA strand displacement assay.[27] These assays readily quantify sequences that are eighteen and six bases long respectively, but require specialized equipment and reagents. Therefore, a label-free method to determine the number of DNA strands bound to AuNPs of any size was required.

DISSERTATION OVERVIEW

The intent of this dissertation is to develop a framework for understanding the impact of the DNA–NP ligand shell architecture on the structure and reactivity of DNA aptamer-linked gold nanoparticle assemblies.

To understand the impact of the ligand shell on the resulting properties of AuNP sensors, a rapid, convenient, label-free method to determine the number of DNA ligands bound to AuNPs was required. Chapter II describes the development of a UV-visible spectroscopy based method to determine the number of DNA strands bound to AuNPs of any size. This method was extended towards quantifying the ligand shell of DNA-NPs with diluted ligand shells, by using UV-visible spectroscopy in tandem with dye-based

fluorescence quantification. Based on the results of this study, a mechanism for the adsorption of disulfide-terminated DNA strands onto AuNPs was proposed. This work was completed with Jim Hutchison, and is intended for future publication. Jim Hutchison provided experimental and editorial guidance.

In Chapter III, the impact of the assembly arrangement and recognition strand density on the structure and reactivity of DNA-NP disassembly-based sensing systems was investigated. Several assembly systems were designed, in which the distance between AuNPs and the ligand shell density were varied. The assembly arrangement and ligand shell density had dramatic effects on the stability of the resulting DNA-NP assemblies. The distance between AuNPs inside the assemblies was directly related to assembly stability, and inversely related to the ability of aptamer strands within the assembly to dehybridize and sense adenosine. Assemblies of DNA-NPs with diluted ligand shells designed to have short inter-particle distances assembled readily and sensed adenosine at lower detection limits and over greater ranges of quantification than existing sensors. This work was completed with Jim Hutchison, and is intended for future publication. Jim Hutchison provided experimental and editorial guidance.

In Chapter IV, the number of DNA aptamer ligands per AuNP was systematically varied, and the impact of diluting the ligand shell on aptamer-mediated disassembly was determined. The number of aptamers per AuNP had a significant impact on the detection limit, quantification range and disassociation constants for the reactions between assemblies and adenosine. AuNPs functionalized with the fewest number of aptamers exhibited the lowest adenosine detection limits and largest adenosine quantification ranges. The cooperativity of the sensing response increased according to the number of

aptamers per AuNP, then appeared to plateau. The apparent kD values for the sensors increased as a function of the number of aptamers per AuNP, then decreased. This work was completed with Jim Hutchison, and is intended for future publication. Jim Hutchison provided experimental and editorial guidance.

In Chapter V, I reflect on the knowledge gained during these studies, the broader impacts of my research project on the field and discuss potential avenues for future research.

BRIDGE

Before we could determine the impact of changing the arrangement of AuNPs and DNA strands inside DNA-NP assemblies and reducing their polyvalency on the sensing properties of DNA-NP assemblies, we needed to develop a method to quantify the number of label-free DNA strands per AuNP. Chapter II describes this method.

CHAPTER II

LABEL-FREE, UV-VISIBLE SPECTROSCOPY-BASED QUANTIFICATION OF DNA BOUND TO GOLD NANOPARTICLES

Note: Portions of Chapter II are expected to appear in an upcoming publication co-authored with James E. Hutchison. I designed and performed the experiments and composed the manuscript corresponding to Chapter II. James E. Hutchison was the principle investigator for this work and provided experimental and editorial guidance.

INTRODUCTION

DNA-functionalized gold nanoparticles have enormous potential as building blocks for materials due to their ability to both recognize and specifically respond to target molecules and surfaces.[1,2] Analyte binding by DNA recognition sequences can be used to direct DNA-NP assembly[2–4] or disassembly[5] in solution, triggering a colorimetric response based on nanoparticle plasmon resonance coupling. The binding specificity of DNA sequences allows DNA-NPs to detect DNA in vitro, differentiating between sequences containing single base imperfections.[6] DNA-NP biocompatibility and colloidal stability[7,8] make them ideally suited for use *in cellulo* sensing. They can detect cellular mRNA levels[9] and regulate biological events *in vivo*.[9,10] The myriad of potential DNA-NP sensing applications means it is critical to understand and control their properties.

The properties of DNA-NPs are dependent on their ligand shell composition, which typically consist of a single recognition sequence,[3,11,12] a mixture of two different recognition strands[9,13,14] or a mixture of recognition strands and diluent polyethylene-glycol,[13,15–17] polyadenosine[18,19]or polythymine[16] ligands. The number of complementary sequences bound by DNA-NPs,[18,20] their cellular uptake mediated by protein binding,[15]

resistance to oxidative decomposition[17] and melting temperature of assembled DNA-NPs[19] are directly proportional to the number of recognition strands bound to the AuNP surface. DNA-NPs functionalized with mixtures of DNA sequences of different base compositions have defined targeting, signaling[13] and regulatory properties.[9] To produce DNA-NPs with desired properties, it is critical to control the DNA-NP ligand shell composition and to determine its impact on nanoparticle reactivity. Therefore, rigorous characterization of the ligand shell composition of DNA-NPs is of the utmost importance.

The number of DNA strands per AuNP is typically determined using the highly sensitive fluorescence 'turn-on'[18] or 'turn-off'[21,22] methods. In the 'turn-on' method, fluorophore-labeled DNA is attached to AuNPs and displaced by small thiol ligands before DNA quantification by fluorescent emission. In the 'turn-off' method, the fluorescent emission of a fluorophore labeled DNA solution is determined before and after incubation with AuNPs, and the DNA concentration is quantified from the decrease in fluorescence due to quenching by the AuNPs. Beer's law is used to determine the concentration of AuNPs from their UV-visible absorbance at 520 nm.

The main drawback of these methods is that each sequence to be quantified must be labeled with a different fluorophore. These labels can affect DNA-NP ligand structure, reactivity and the number of recognition strands bound to each AuNP.[23,24] To determine the DNA concentration using the fluorescent turn-on method, it must be assumed that all ligands are completely displaced from the surface of the DNA-NPs. This can be problematic because the rate and extent of thiol:thiol ligand exchange rates varies dramatically based on ligand identity.[25] To determine the DNA concentration using fluorescent turn-off method, it must be assumed that the fluorophore is completely

quenched upon interacting with the AuNPs, which means only very short sequences can be used as ligands.[26] Fluorophores are also time-consuming to synthesize, expensive to purchase and often bleach under light exposure.[23]

Label-free DNA sequences attached to AuNPs have been quantified using the Oligreen fluorescence assay[15,27] and toehold displacement assay.[23] These assays are suitable for quantifying sequences longer than 6 nucleotides[27] and 18 nucleotides[23] in length, but require specialized equipment and reagents.

A simple alternative approach would be to measure the UV-visible spectrum of the DNA-NPs, and use Beer's law to determine the concentration of both AuNPs and DNA. The concentration of AuNPs is conventionally determined using UV-visible spectroscopy, based on their absorbance at 520 nm (A_{520}) and empirically determined extinction coefficients.[28] AuNP extinction coefficients do not significantly change upon functionalization with DNA.[18] Therefore established extinction coefficient values can also be used to determine the concentration of DNA-NPs. DNA concentrations are conveniently determined from their absorbance at 260 nm (A_{260}) and extinction coefficients calculated using thermodynamic modeling. [29]

One reason UV-visible spectroscopy has not been used to determine the DNA in solutions of AuNPs is because both AuNPs and gold salts also absorb at 260 nm.[30] To use A_{260} to determine the DNA concentration in a mixture, the contributions to the absorbance from all other reaction solution components must be removed or subtracted from the spectrum. To eliminate the strong absorbance from the AuNP core, we thought it would be feasible to decompose the DNA-NPs by treatment with cyanide prior to determining the DNA concentration. Cyanide etching has long been used to extract gold

from ores and has previously been used to oxidatively decompose gold nanoparticles for quantification of DNA ligand shells based on fluorescence[18] and radioactivity.[31]

In this paper, we describe a simple, inexpensive, general method to quantify any label-free DNA sequence bound to AuNPs of any core size. UV-visible absorbance spectroscopy was used to determine the number of DNA strands bound per AuNP.

We extended this method to determine the composition for two different label-free DNA sequences bound to AuNPs using UV-visible spectroscopy in conjunction with a commercially available dye assay. These data allowed us to refine the model for DNA adsorption onto AuNPs.

EXPERIMENTAL

Materials and Reagents

Citrate-stabilized AuNPs (d_{core} = 5 nm) were purchased from Nanocomposix (San Diego, California). All DNA samples were purchased from Integrated DNA Technologies (Coralville, Iowa). DNA sequences were purified by either the standard desalting method or HPLC. A "Quant-It" OliGreen ssDNA Assay kit was purchased from Thermo Fisher Scientific (Grand Island, NY). 50 kDa spin column purification membranes were purchased from Millipore (Darmstadt, Germany). Clear and amber 1.5 mL microcentrifuge tubes and opaque polypropylene black 96 well plates (Costar) were purchased from VWR (Radnor, PA). Sodium citrate dihydrate, hydrogen tetrachloroaurate hydrate and UV-transparent 96 well plates (Corning) were purchased from Sigma Aldrich (St. Louis, Missouri).

Instrumentation

UV-visible absorbance spectra of AuNP and DNA solutions were obtained using either a BioTek Synergy 2 instrument or a Mikropack DH-2000 UV-vis-NIR light source equipped with an Ocean Optics USB2000 spectrophotometer. UV-visible spectra of DNA were obtained using these or a Thermo Scientific Nanodrop 2000 spectrophotometer path length (10mm) and baseline corrected at 340nm.

The endpoint (after 5-15 minutes) fluorescent emission of the solutions were measured in 96-well opaque black well plates (Costar) using a Biotek Synergy 2 instrument equipped with a tungsten lamp and filters (EX 485/20 nm, EM 528/20 nm). The data collection time was autoscaled, so that 80,000 counts were emitted from the well containing the highest concentration of DNA.

Calculation of UV-visible Extinction Coefficients

AuNP extinction coefficients were calculated using their average core diameters (d_{core} = 12.3 nm: $\varepsilon = 1.98 \times 10^8$; d_{core} = 5.0 nm: $\varepsilon = 9.96 \times 10^6$) and previously reported empirical data[28]. The error associated with these extinction coefficient values is 1-3%.[28] DNA sequence extinction coefficients (ε) were calculated using Integrated DNA Technologies' "Oligo Analyzer" tool, which calculates values from thermodynamic modeling according to DNA base composition and nearest neighbors[29](Table 2.1). DNA extinction coefficient values are accurate within 4% error (IDT-DNA). Concentrations of AuNP solutions were determined from A_{520} and DNA concentrations were determined from A_{260}.

Table 2.1: Names, primary sequences and calculated extinction coefficients[29] of DNA sequences used. All sequences are labeled at their 5' end with disulfide ($HO(CH_2)_6S$-S-5'-DNA-3')

Name	DNA Primary Sequence	Extinction Coefficient ($Lmol^{-1}cm^{-1}$)
DNA_1	5'-AGA GAA CCT GGG GGA GTA TTG CGG AGG AAG GT-3'	331 900
DNA_2	5'-A_5-3'	63 400
DNA_3	5'-A_{12}-3'	147 400
DNA_4	5'-T_5-3'	41 100
DNA_5	5'-CCC AGG TTC TCT-3'	102 500

Preparation of 12 nm DNA-NPs

12 nm citrate-stabilized AuNPs were synthesized using a modified literature method.[32,33] Briefly, a 250 mL 3-neck round bottom flask, glass stopper, magnetic stir bar and condenser were cleaned using aqua regia and rinsed copiously with nanopure water. Sodium citrate dihydrate (408 mg, 1.39 mmoles) was dissolved in 200 mL nanopure water and brought to 100°C while stirring. $HAuCl_4$ (1mL of 200 mM solution) was added using a micropipettor. The solution instantly turned dark blue, a color change previously attributed to nucleation.[32] Within one minute, the solution turned a deep red color, indicating AuNPs were formed. AuNPs were stirred at 100°C for 20 minutes, then removed from heat and allowed to stir overnight before being characterized using Small Angle X-Ray Scattering (SAXS) and Transmission Electron Microscopy (TEM).

The AuNP size determined by SAXS analysis was 12.3 ±1.9 nm (Figure A1; See Appendix A for A Figures). TEM analysis confirmed that the AuNPs were spherical (Figure A2). Complete descriptions of SAXS and TEM data acquisition methods are available in the Supporting Information.

AuNPs were functionalized with DNA using a modified literature method.[21,34] DNA and AuNP solutions were mixed together. Typically, AuNPs and DNA were mixed together to prepare reaction solutions containing 16 nM AuNPs and 16 uM DNA. 10x excess DNA was added to maximize DNA loading on the AuNPs, because a small but measurable increase in DNA density during functionalization was reported when excess DNA was used during ligand exchange.[34] After 5 minutes, pH 3 citric acid buffer was added (10 mM). After 10 minutes, NaCl was added (70 mM). DNA and AuNPs were incubated overnight before being purified using four rounds of centrifugation (15 min at 20 000g). DNA-NPs were redispersed in buffer containing 1mM pH 8.2 Tris Acetate and 100 mM NaCl after each centrifugation step, and finally dissolved in 225 uL nanopure water. Fluorescence spectroscopy was used to determine that this method removed all excess DNA (Figure A3a). After each purification, UV-visible spectroscopy was used to confirm that most excess DNA (>>99%) is removed.

Preparation and Analysis of 5 nm DNA-NPs

The same procedures (with modifications) were used to prepare DNA-NPs from purchased 5 nm AuNPs (Nanocomposix, San Diego) and to analyze their ligand shell composition. SAXS analysis confirmed the AuNPs were 5.0 ± 0.5 nm and TEM confirmed they were spherical. DNA and AuNPs were mixed together. Reaction solutions contained 90 nM AuNPs and 13.5 uM DNA. DNA-NPs were purified by centrifuging

five times (9 min at 13 500g) above a spin filter membrane with a 50 kDa molecular weight cutoff, discarding each flow-through. Fluorescence spectroscopy was performed to determine that this method removed all excess DNA (Figure A3b). DNA-NPs were eluted according to the manufacturer's instructions and redispersed using 230 uL nanopure water.

UV-visible Spectroscopy Determination of DNA Strands per Nanoparticle

The number of DNA strands per AuNP was calculated by dividing the DNA concentration by the AuNP concentration. The concentration of DNA-NPs in each sample was determined using the A_{520} and calculated extinction coefficient of AuNPs of the same core size. The concentration of DNA in each sample was determined using the A_{260} and calculated extinction coefficient of the DNA sequence.

KCN solution (100 mM) was prepared in nanopure water adjusted to pH 12 using NaOH. KCN solution was mixed with 12 nm AuNPs or DNA-NPs and allowed to react overnight before measuring the resultant UV-visible absorbance spectrum. At minimum, 8 moles KCN (4 equivalents) were added for every mole of Au atoms (15 mM typically). The DNA A_{260} was determined by subtracting the contribution of decomposed AuNPs from the A_{260} of the DNA-NP decomposition reaction solution. The concentration of DNA in each sample was determined based on its extinction coefficient and DNA A_{260}.

To validate our method, Quant-It's ssDNA Oligreen quantification assay[27] was used to determine the DNA in the decomposed AuNP solutions, using the supplier's instructions. Briefly: a series of standard DNA solutions (80 nM, 40 nM, 20 nM and 8 nM) were prepared. The decomposed DNA-NP A_{260} was used to determine how much to dilute the decomposed DNA-NP samples for the Oligreen assay. Buffer (10 mM pH 7.5

Tris-HCl, EDTA:1 mM) and water were added to each sample, then Oligreen dye. They were incubated 5-10 minutes before measuring the final fluorescent emission of the dye. The decomposed AuNPs did not affect the assay results.

To perform ligand shell analysis on the 5 nm DNA-NPs, the same procedure was followed, except 2.5 moles KCN (1.25 equivalents) were added for every mole of Au atoms (typically 2-3 mM).

UV-visible and Fluorescence Spectroscopy Determination of Two DNA Sequences Co-Conjugated to Gold Nanoparticles

The number of strands of each DNA per AuNP was determined by dividing the concentration of each DNA sequence by the concentration of AuNPs. The concentration of DNA-NPs was determined as described previously. The concentration of the longer DNA strand was determined using the Oligreen dye assay and used to calculate the number of DNA strands per AuNP. The extinction coefficient of the longer DNA strand was then used to determine its contribution to A_{260} decomposed DNA-NPs. The absorbance of the shorter DNA strand was then calculated by subtracting the contributions from the decomposed nanoparticles and the longer DNA strand from A_{260} decomposed DNA-NPs, and using the DNA's extinction coefficient to calculate its concentration. The percentage of each strand in the ligand shell was then calculated.

RESULTS AND DISCUSSION

Our initial strategy to quantify the number of DNA strands per AuNP was to determine the concentration of the DNA-NPs from their A_{520}, decompose the DNA-NPs using KCN (Figure 2.1) and quantify the DNA based on A_{260}. DNA-NPs were prepared

using an established method,[34] and purified by centrifugation (Figure A3) before being characterized using UV-visible spectroscopy.

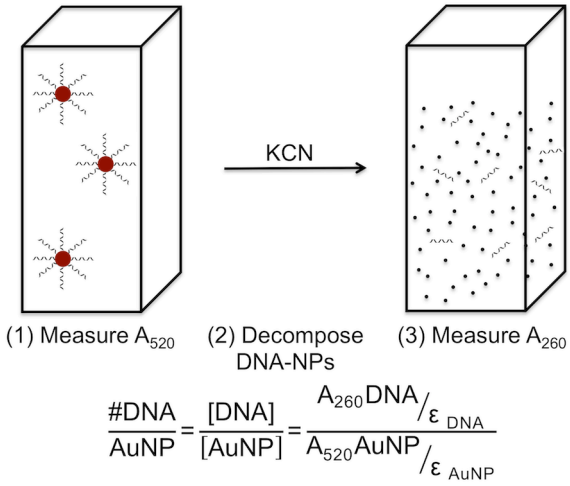

Figure 2.1: Overall strategy for quantifying DNA bound to AuNPs using UV-visible spectroscopy. (1) The concentration of DNA-NPs is determined from their absorbance at 520 nm. (2) DNA-NPs are decomposed using KCN, and (3) the absorbance of the resultant solution is measured at 260 nm. The concentration of DNA is determined from its A_{260}, as shown in the equation.

As expected, the solution of DNA-NPs (Figure 2.2a) exhibited a UV-visible absorbance peak characteristic of AuNPs at 520 nm and an absorbance peak characteristic of DNA at 260 nm. The latter absorbance was absent from the UV-visible spectrum of AuNPs of the same core size (Figure 2.2b), which was normalized to have the same A_{520} as the DNA-NPs. The fact that A_{260} is larger for the citrate-stabilized AuNPs than the DNA-NPs indicates they contain a small but appreciable amount of gold salts or small gold clusters. DNA stabilizes the AuNPs, making it possible to extensively purify the AuNPs, during which unreacted gold salts and clusters are removed. Sodium citrate forms a weakly bound ionic ligand shell on the AuNP surface, so extensive purification of the AuNPs causes irreversible aggregation, which must be avoided. Therefore, DNA A_{260} cannot be directly determined from the DNA-NP absorbance spectrum.

We decomposed DNA-NPs and AuNPs using KCN and then measured the UV-visible spectra of the resultant solutions (Figure 2.2c and 2.2d). The reaction between citrate-stabilized AuNPs and KCN appeared to be complete in 10-15 minutes based on the UV-visible spectrum. DNA-NP decomposition took longer, so all subsequent decomposition reactions were incubated overnight, adding excess KCN to increase the reaction rate.

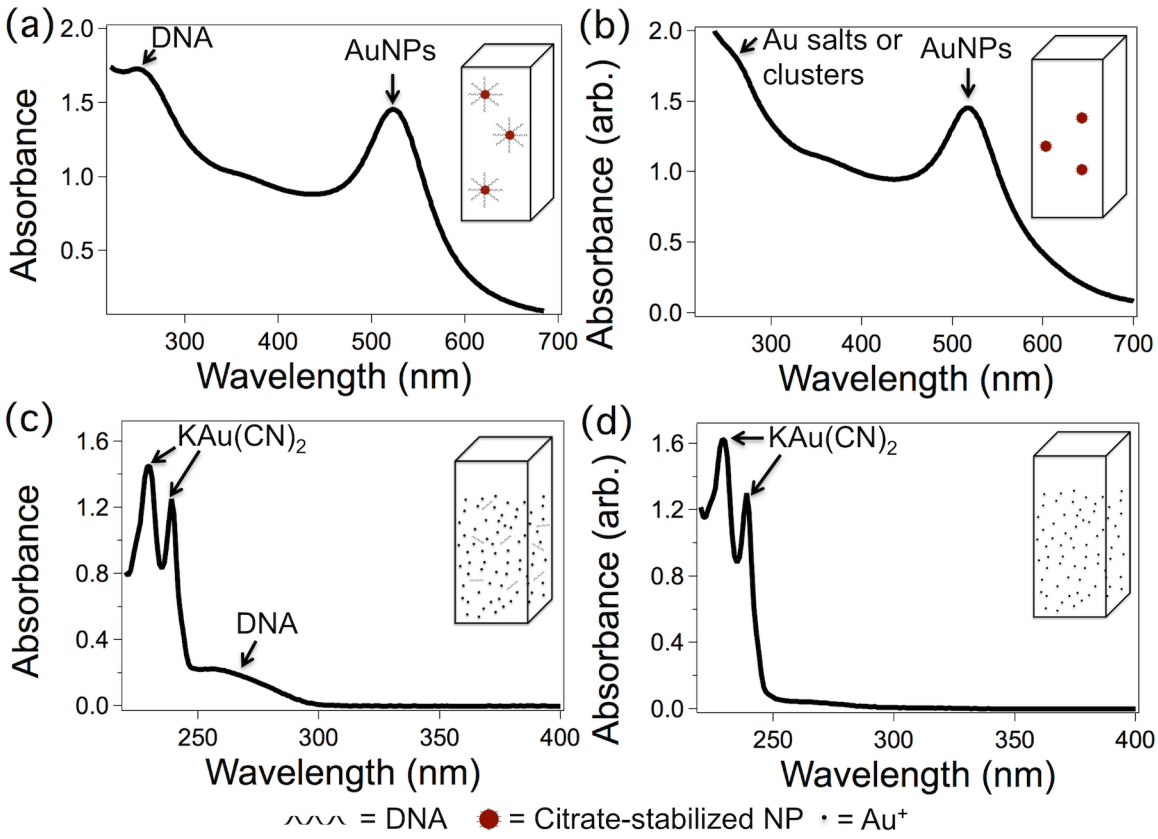

Figure 2.2: UV-visible absorbance spectra of solutions containing AuNPs before and after oxidative KCN decomposition. (a) Intact 12 nm DNA-NPs (b) Intact citrate-stabilized 12 nm AuNPs (c) Products from reaction between 12 nm DNA-NPs and KCN (d) Products from reaction between 12 nm AuNPs and KCN

The decomposed DNA-NPs strongly absorbed light at 230 nm and 240 nm, in addition to the characteristic DNA absorbance at 260 nm (Figure 2.2c). These peaks are characteristic of the $KAu(CN)_2$ salt formed during nanoparticle decomposition,[35] and

solutions resulting from reacting citrate-stabilized NPs (Figure 2.2d) with KCN also absorb at those wavelengths. The baseline absorbance of decomposed AuNPs approached zero near 350 nm at the endpoint of the reaction with KCN, and the spectrum did not change afterwards. The reaction solutions appeared colorless by eye before the AuNPs were fully decomposed. Therefore, A_{350} was used to assess the endpoint of the reaction between KCN and AuNPs prior to quantifying the ligand shell.

To determine the DNA concentration from A_{260}, the overlapping contribution from $KAu(CN)_2$ must be removed. If the $KAu(CN)_2$ A_{260} primarily arises from products of the reaction between KCN and AuNPs, the absorbance should be directly related to the initial AuNP concentration. Solutions containing different concentrations of AuNPs were reacted with KCN and their UV-visible absorbance spectra measured. A_{260} of the resultant solutions directly correlated with the initial AuNP concentration (Figure 2.3a). A plot relating A_{260} of the decomposed AuNPs to the initial AuNP concentration (Figure 2.3b) was prepared. The fact that the plot was linear meant this could be used as a calibration curve to predict A_{260} for unknown solutions of DNA-NPs.

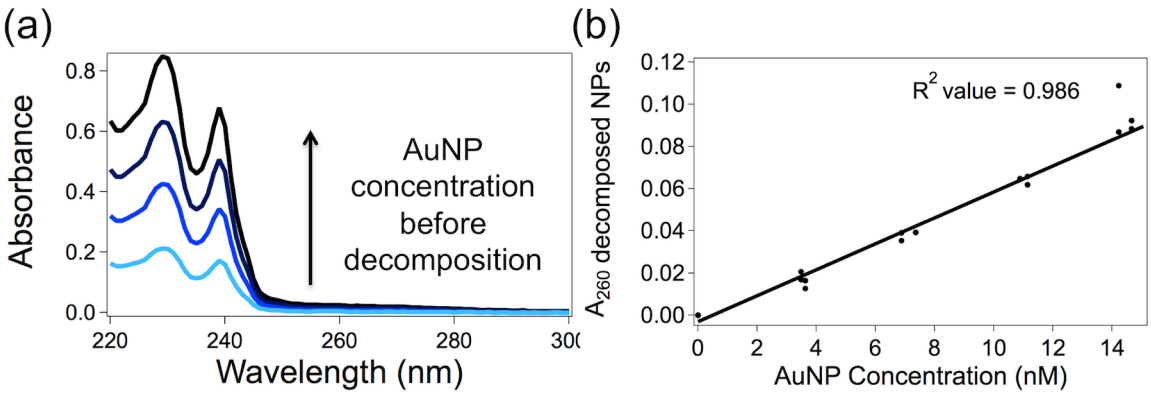

Figure 2.3: (a) Representative UV-visible spectra of solutions prepared by reacting various concentrations (3.5-14.2 nM) of 12 nm AuNPs with KCN (b) Calibration curve used to determine the contribution of decomposed AuNPs to decomposed DNA-NP absorbance spectra (n = 24)

UV-visible Spectroscopy Determination of DNA Bound to AuNPs

We prepared AuNPs functionalized with DNA_1, determined the DNA-NP concentration from A_{520} and used Equation 1 to determine A_{260} of DNA_1. Using DNA_1's extinction coefficient (Table 2.1) and Beer's law, we determined that there were 58±7 DNA strands per 12 nm AuNP (n=9).

$$A_{260}\ DNA_1 = A_{260}\ dDNA\text{-}NPs - A_{260}\ dNPs \qquad \text{(Equation 1)}$$

To validate our method, we also quantified the number of DNA_1 strands per AuNP using an established Oligreen fluorescent dye assay.[15,27] The value calculated using this method (59±4) agreed with that calculated using our method within 1% error, which is within the experimental error introduced by determining the AuNP concentration using UV-visible spectroscopy. This validates our use of UV-visible spectroscopy to determine DNA bound per AuNP.

This value is lower than the number of DNA strands per AuNP previously reported by Zhang and coworkers[34] who found that ~85 DNA strands of a 12 base sequence were attached per 13 nm AuNP. It is therefore likely that part of DNA_1 lies flat on the surface of the AuNPs during functionalization, and electrostatically or sterically hinders the adsorption of additional DNA, leading to the lower number of strands per AuNP, as suggested by others who observed DNA base-dependent surface coverage on planar gold surfaces[36] and AuNPs[37].

UV-visible and Fluorescence Spectroscopy Determination of Two DNA Sequences Co-conjugated to AuNPs

DNA-NPs functionalized with mixed ligand shells and diluted ligand shells are of growing importance due to their defined targeting, signaling[13] and regulatory properties.[9]

DNA-NPs functionalized with limited numbers of recognition strands have been developed as building blocks for programmable materials.[2,38–40] Short DNA sequences have been used to dilute the ligand shell of DNA-NPs to tune the number of DNA recognition sequences displayed on the surface of DNA-NPs.[14,16] Diluting the number of recognition strands is advantageous as it promotes DNA hybridization[18,20,41] while maintaining DNA-NP colloidal stability.

Given the importance of using mixed and diluted DNA ligand shells to control DNA-NP reactivity, we wanted to extend our technique to be able to determine the ligand shell composition of AuNPs functionalized with more than one label-free sequence. We prepared DNA-NPs functionalized with mixtures of two DNA strands by performing ligand exchanges on 12 nm AuNPs using solutions containing various molar ratios of DNA_1:DNA_2. Determining the concentration of each sequence and dividing it by the AuNP concentration (Figure 2.4) allowed the percentage of DNA_1 in the ligand shell to be determined.

The concentration of DNA-NPs was determined using UV-visible spectroscopy and the nanoparticles were decomposed using KCN. The UV-visible spectrum of the resultant solution was measured. The longer sequence, DNA_1, was determined using the Oligreen dye assay. The DNA_1 concentration and its extinction coefficient were used to determine its A_{260}. A_{260} DNA_2 was then calculated from A_{260} decomposed DNA-NP solution by subtracting the contributions from $KAu(CN)_2$ and DNA_1, and then using its extinction coefficient to determine its concentration.

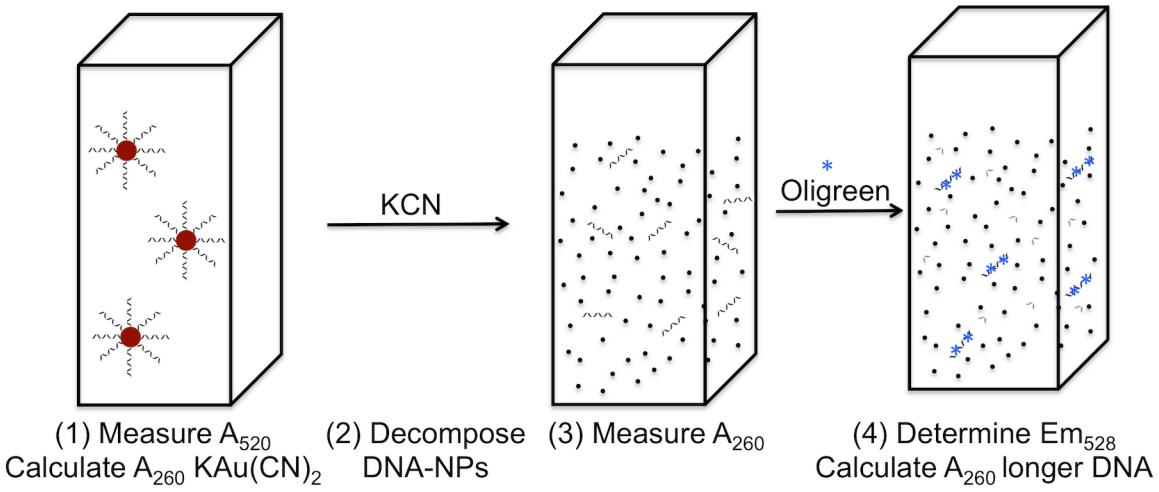

Figure 2.4: UV-visible spectroscopy and fluorescent spectroscopy determination of DNA bound to AuNPs. (1) The concentration of DNA-NPs is determined from A_{520}, and used to determine A_{260} $KAu(CN)_2$. (2) DNA-NPs are decomposed using KCN (3) A_{260} of the resultant solution is measured. (4) The concentration of DNA_1 is determined from a linear (typical R^2= 0.999) calibration curve relating DNA_1 concentration to Em_{528} and used to calculate A_{260} DNA_1. A_{260} DNA_2 is determined by subtracting A_{260} DNA_1 and A_{260} $KAuCN_2$ from A_{260} solution. The DNA_2 concentration is then calculated using its extinction coefficient.

DNA_1 was under-represented in the AuNP ligand shell after functionalization (Figure 2.5), and there was a non-linear relationship between the percentage of DNA_1 during ligand exchange and the percentage of DNA_1 bound to the AuNPs. This was not surprising, because the DNA_1 sequence is longer and less adenosine rich. The adsorption rate of unthiolated[42] and thiolated[43] DNA sequences to AuNPs is inversely related to the chain length of the sequence. The initial rate of DNA adsorption is directly related to the base content of the sequence, with polyadenosine sequences exhibiting the highest adsorption rate.[44]

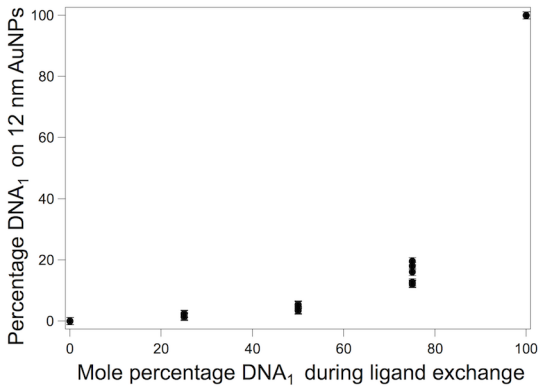

Figure 2.5: Ligand shell composition of DNA-NPs prepared by mixing 12 nm AuNPs with various amounts of DNA_1 and DNA_2 sequences. The percentage of DNA_1 in the ligand shell was determined using UV-visible and fluorescence spectroscopy.

The indeterminate error associated with determining the percentage of DNA_1 in the ligand shell was 2.6%, which reflects the variance between A_{260} DNA_1 determined from UV-visible vs. fluorescence spectroscopy.

Determination of Label-free DNA Sequences Bound to 5 nm AuNPs

5 nm AuNPs functionalized with DNA are of interest for fundamental and applied studies. They are convenient for studying assembly of DNA-NPs in solution, because assembled 5 nm DNA-NPs are less prone to precipitation and therefore produce more uniform SAXS patterns.[45] Small AuNPs are often preferred for *in vivo* bioimaging and drug delivery experiments because of their increased propensity to enter cells.[8,46] Because different sizes of DNA-NPs are desirable for different applications, we wanted to evaluate whether our method could be extended towards determining DNA bound to AuNPs of more than one core size.

Solutions containing different concentrations of 5 nm AuNPs were prepared and decomposed, and their UV-visible spectrum was measured. 5 nm AuNPs contain fewer gold atoms than 12 nm AuNPs, so they exhibited a lower A_{260} when decomposed. A_{260} of the decomposed 5 nm DNA-NP solutions varied linearly with the original NP

concentration (Figure 2.6a). A_{260} of decomposed 12nm and 15 nm AuNPs also varied linearly according to their concentration prior to decomposition (data not shown).

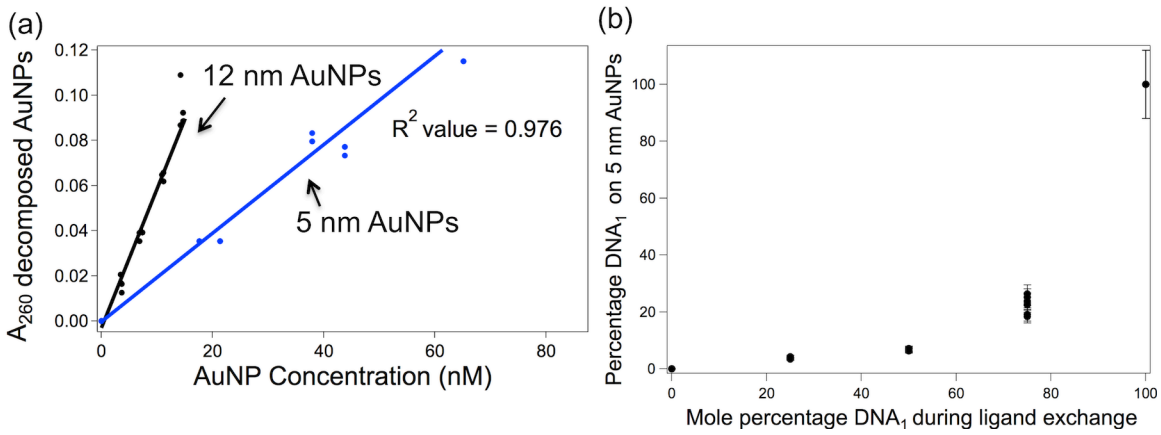

Figure 2.6: (a) Calibration curves for determining A_{260} of decomposed citrate-stabilized AuNPs (b) Percentage DNA_1 in ligand shell of 5nm AuNPs functionalized from different feed ratios of DNA_1:DNA_2 sequences.

5 nm DNA-NPs were prepared by incubating AuNPs with DNA_1. The number of DNA_1 strands per 5 nm AuNP (n = 9) was analyzed using spectrophotometry (18±2) and the fluorescent dye assay (15.1±0.8), which means the calculated ranges of DNA per AuNP agreed reasonably well. Our UV-visible based method is therefore suitable for determining the DNA bound to more than one size of AuNP.

We wanted to further extend our technique towards calculating DNA per AuNP on 5 nm AuNPs, so we performed ligand exchanges on AuNPs in solutions containing various ratios of DNA_1:DNA_2 ligand and analyzed them as done for the 12 nm DNA-NPs. The ligand shell composition of small DNA-NPs exhibited a similar trend to that of the 12 nm DNA-NPs, with DNA_1 being under-represented in DNA-NP ligand shell (Figure 2.6b). Interestingly, the percentage of DNA_1 in the ligand shell of 5 nm DNA-NPs was higher than in the ligand shell of the 12 nm DNA-NPs when the same feed ratio of ligands was used. For example, solutions containing 75% DNA_1 during ligand

exchange produce 12 nm DNA-NPs functionalized with 15 ± 3 % DNA_1 and 5 nm DNA-NPs functionalized with 23 ± 3 % DNA_1. The percentage of DNA_1/DNA_1max (the maximum number of DNA_1 per AuNP) increased from 28% (12 nm DNA-NPs) to 50% (5 nm DNA-NPs).

If chain length and adenosine content were the only factors influencing DNA adsorption, AuNPs of different core sizes functionalized using the same feed ratios of DNA sequences would produce DNA-NPs with the same ligand shell composition. Instead, the adsorption of longer DNA sequences is promoted by increasing the AuNP radius of curvature, which suggests a more complex reaction mechanism.

Based on our observation that the percentage of DNA_1 in the ligand shell is dependent on the AuNP radius of curvature and existing evidence from previous literature, we propose a two-stage model for DNA adsorption under our conditions, in which the disulfide-terminated DNA sequences (i) non-specifically (via DNA bases) adsorb to AuNPs at pH 7 and (ii) re-arrange to form thiol bonds and permit additional DNA binding at pH 3.

Zhang et al.[21] observed that to maintain AuNP stability during DNA-NP preparation, DNA must be incubated with AuNPs for 1 minute prior to adding pH 3 citric acid buffer (30 mM Na^+), suggesting that thiolated DNA strands adsorb quickly onto the AuNPs. DNA adsorption onto AuNPs at pH 7 is dependent upon the sequence chain length[42,43] and base composition.[44] Wang et al.[43] found that thiolated DNA adsorbed quickly and non-specifically to the surface of AuNPs and rearranged to permit additional specific binding between DNA and AuNPs, but that nonthiolated DNA adsorbed non-

specifically in a single fast step. This suggests that the DNA adsorbs quickly and non-specifically during the first stage of our procedure.

Hurst et al.[37]observed that the final surface coverage of DNA on AuNPs is inversely related to the adenosine content of the sequence near the thiol anchoring group, suggesting that bases near the thiol anchoring group continue to lie flat and interact strongly with the gold surface after the AuNPs are saturated with DNA. Additional DNA binding took place when interactions with the surface were disrupted by sonication.[37] Bringing the solution to pH 3 protonates the adenosine residues,[47] thereby reducing their binding affinity for the gold, and adding salt reduces electrostatic repulsion between DNA strands on the AuNPs and DNA in solution. DNA can thus rearrange and additional binding can occur after adding the buffer and salt to our ligand exchange reaction mixtures.

During this rearrangement and additional binding step at pH 3, adsorption of the bulky DNA_1 ligand is hindered, resulting in an increase in the DNA_2 content on the surface of the AuNPs even when it is a minor component of the ligand exchange mixture. This effect is less for AuNPs with a larger radius of curvature, because the gold surface is more accessible for binding. These results therefore support a model for disulfide-terminated DNA adsorption in which there is fast non-specific adsorption of DNA to the gold surface dictated by chain length and base composition, followed by rearrangement and specific binding to the AuNPs.

Strengths and Limitations of Method

UV-visible spectroscopy is sufficiently sensitive to determine the number of DNA strands bound to gold nanoparticles at typical DNA-NP sample concentrations. For

convenience, we used a plate reader to make our UV-visible measurements. Using a small path length spectrometer (i.e. the nanodrop) to perform the same set of measurements would greatly decrease the sample volume required for quantification.

For our method to be accurate, the solution must be free of other species that absorb light at 260 nm. Dilute buffer must be used during nanoparticle purification because commonly used purification buffers exhibit a small but appreciable absorbance at 260 nm (Figure A4).

Any two DNA sequences that exhibit greatly different reactivity towards a commercially available fluorescent dye can be quantified using our method. Oligonucleotide sequences that are short and/or contain few thymine residues do not affect dye assay quantification of other DNA sequences (Figure A5).[27] This method is thereby applicable to any set of label-free sequences that vary significantly in length or thymine composition. For example, the ligand shell composition of NPs concurrently modified using DNA_1 and DNA_3 sequences can be quantified (Figure A5b), as can NPs modified using DNA_1 and DNA_4 ligands (Figure A5c) or DNA_2 and DNA_5 ligands (Figure A5d).

To quantify co-conjugated sequences of similar length, our method can be used concurrently with a different technique. For mixtures of sequences that are longer than 18 nucleotides, one ligand can be quantified using our method, and the other using sequential strand displacement by DNA "toehold sequences".[23]

CONCLUSION

We developed a rapid, convenient and inexpensive method to quantify the number of label-free DNA strands attached to AuNPs. The number of strands per nanoparticle

was easily determined from solutions of DNA-NPs at concentrations typically used in sensing assays. Our technique is broadly applicable, because it can be used to determine the number of DNA strands of any base composition attached to AuNPs of any core size.

UV-visible spectroscopy was used in concert with a conventional Oligreen dye assay to determine two different label-free DNA sequences co-conjugated to AuNPs, without requiring specialized probes. The results of the analysis performed on DNA-NPs with mixed ligand shells support a model for disulfide-terminated DNA adsorption in which there is fast non-specific adsorption of DNA to the gold surface dictated by chain length and base composition, followed by rearrangement and additional binding to the gold surface.

Our method could be further extended to quantify other ligands with visible absorbance signatures that overlap with that of decomposed gold nanoparticles, such as other nucleic acids[48] and synthetic peptides.[49,50] It could also be used to determine DNA bound to silver nanoparticles, which have been assembled in solutions and on surfaces,[51,52] and undergo oxidative decomposition by KCN.[53]

Using this approach, the ligand shell composition of a large of library of nanoparticles functionalized with mixed label-free DNA ligand shells can be precisely determined. It will therefore enable rapid screening of nanomaterial properties as a function of ligand shell composition. This will lead to our enhanced understanding of nanoparticle structure-property relationships, and lead to production of nanoparticles with precisely engineered assembly, sensing and gene regulation properties.

BRIDGE

Having developed a rapid, convenient method to determine the number of active and diluent strands bound to AuNPs, we sought to develop a deeper understanding of the relationship between the AuNP ligand shell composition and reactivity. Chapter 3 explores the effect of changing the arrangement of AuNPs and DNA strands within AuNP assemblies on their disassembly-based sensing properties.

CHAPTER III

EFFECT OF ASSEMBLY ARRANGEMENT ON STRUCTURE AND REACTIVITY OF DNA APTAMER-LINKED GOLD NANOPARTICLE SYSTEMS

Note: Portions of Chapter III are expected to appear in an upcoming publication co-authored with James E. Hutchison I designed and performed the experiments and composed the manuscript corresponding to Chapter III. James E. Hutchison was the principle investigator for this work and provided experimental and editorial guidance.

INTRODUCTION

Twenty years ago, it was demonstrated that DNA strands tethered to gold nanoparticles (AuNPs) can direct their assembly in solution.[1,2] It was subsequently found that the primary sequence of linking DNA strands and the DNA-NP assembly arrangement can control the inter-particle spacing inside large two-dimensional and three-dimensional AuNP arrays.[3–8] More recently, it has been shown that DNA aptamers can control the assembly[9–12] or disassembly[13–18] of AuNPs, creating a new class of highly specific biosensors.

Aptamers are short (<100 nucleotide) single-stranded DNA or RNA sequences that fold into complex 2 or 3-dimensional structures to bind their analyte with high affinity and specificity.[19,20] Many biosensors exploit the ability of DNA aptamers to initially bind a complementary DNA sequence, then switch conformations to bind their target analyte.[20–24] Tethering the aptamer sequence to a response element whose properties change as the aptamer switches conformations is a powerful way to transduce molecular binding events into colorimetric responses.[21,22,24] The optical properties of

AuNPs make them ideal response elements for biosensors, because their surface plasmon resonance (SPR) peak shifts as a result of AuNP assembly or disassembly.[25–28]

In AuNP disassembly-based biosensors, aptamer-containing strands act as a linker between DNA strands on neighboring AuNPs (Figure 3.1a), thereby forming extended AuNP assemblies.[13–17] The plasmons of AuNPs within the assembly are coupled, causing their SPR peak to shift to longer wavelengths and broaden.[29–31] As the aptamers change conformation to bind the analyte, AuNPs separate, causing their SPR peak to return to shorter wavelengths and become narrow.[13,15–17]

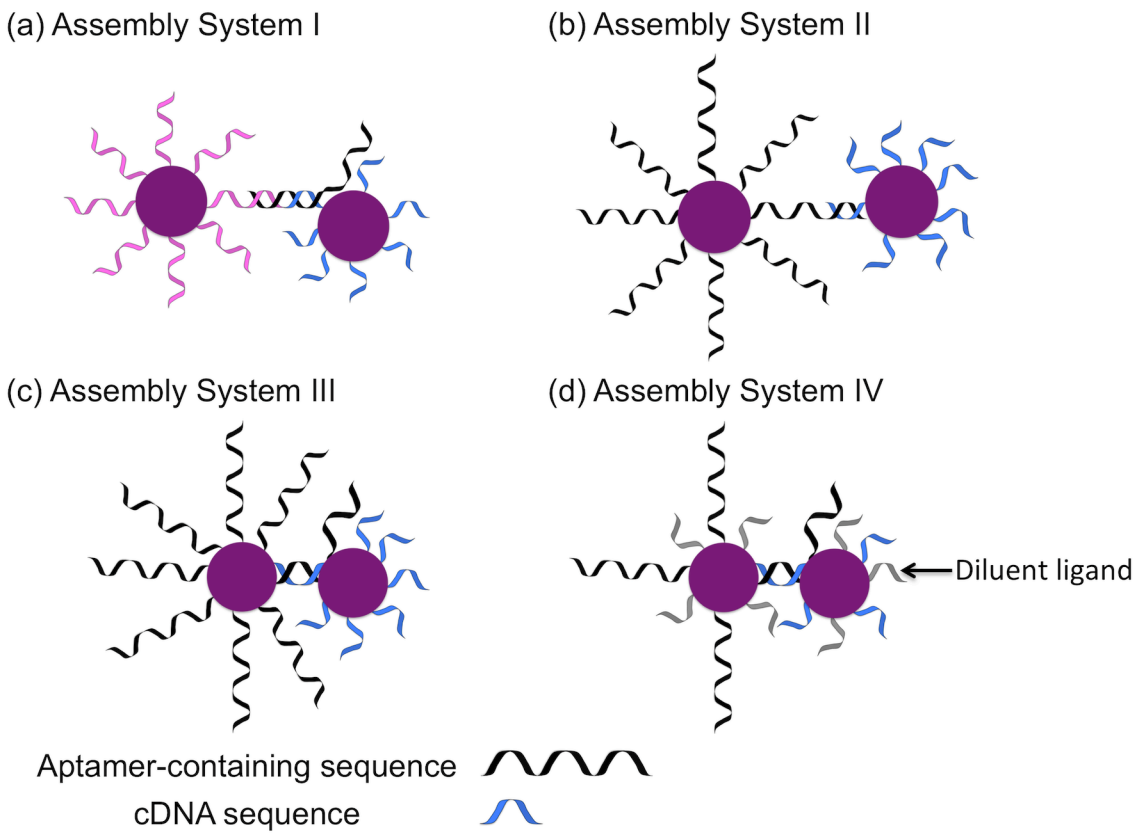

Figure 3.1: Aptamer-mediated assembly systems. (a) System I: DNA-NPs linked together by binding an untethered crosslinking strand (b) System II: DNA-NPs directly hybridized with large (approx. 11 nm) inter-particle distances (c) System III: DNA-NPs directly hybridized at small (approx. 4 nm) inter-particle distances. (d) System IV: DNA-NPs with diluted ligand shells are directly hybridized at small (approx. 4 nm) inter-particle distances.

In most aptamer-mediated disassembly sensors, the AuNPs are designed to maximize the number of linkages between DNA-NPs in the assembly. The DNA-NPs form large insoluble assemblies spanning several microns, which must be agitated just prior to measurement.[15,16] The large size of the assemblies formed using linker-mediated nanoparticle assembly, and the large number of linkages between DNA-NPs, leads to the sensor response being much less sensitive and reproducible than if smaller assemblies were used.[13] In the existing colorimetric aptamer-mediated AuNP disassembly-based sensor, the lowest adenosine concentration that produces a colorimetric response (the sensor's limit of detection, LOD)[15] is higher than biologically relevant adenosine concentrations.[32–34]

Adenosine is a highly important biomarker for hypoxia and ischemia.[32–34]Adenosine plays a critical role in the body's cardiovascular, nervous and immune systems,[35] signal transduction and neuromodulation.[36] It has therefore been the subject of intense research activity, and adenosine sensing has been used as the proof of concept reaction for a number of new biosensors. Adenosine sensors with detection based on luminescence, [37–40] enzymatic assays,[35,41–44] electrochemical reactions,[45–51] surface-enhanced raman spectroscopy,[52,53] fluorescent resonance energy transfer,[38,54–58] aptazyme disassembly,[14] liquid chromatography mass spectrometry,[59]flow cytometry,[60] split aptamer nanoparticle assembly,[61] quartz crystal microbalance,[62] resonance light scattering,[45] and nanoparticle-based lateral flow assays have been produced.[18] Some of these sensors report extremely impressive detection limits, with polymerization-based detection reporting the lowest detection limit at 20 pM. However,

many of these detection methods require significant technical expertise and equipment, and/or would not detect the difference between typical extracellular adenosine concentrations and those during ischemia. The ideal sensing platform would be sufficiently sensitive, respond to adenosine over a reasonable quantification range and be colorimetric in nature so that the approximate adenosine concentration could be determine using a simple handheld device such as a camera or cell phone.

To realize the full potential of aptamer-mediated nanoparticle sensors, their design must be improved so they can respond to biologically relevant analyte concentrations. This requires a systematic understanding of the variables that influence aptamer-mediated assembly and disassembly. The goal of this study was to investigate the impact of the DNA assembly arrangement and the density of the DNA recognition sequences on DNA-NP assembly/disassembly chemistry, thereby elucidating design rules for developing sensitive aptamer-based sensors.

To accomplish this goal, three sets of aptamer-functionalized nanoparticles (aptamer-NPs) and cDNA-functionalized nanoparticles (cDNA-NPs) were designed to form different assembly systems (Figure 3.1b, 3.1c and 3.1d). Each aptamer-containing sequence contained two overlapping regions: the adenosine aptamer sequence[63] and a cDNA-binding sequence. The aptamer-NPs initially directly bind cDNA-NPs, forming AuNP assemblies. Upon adding adenosine, the aptamer strands change conformation to bind adenosine instead, resulting in disassembly.

Our initial prediction was that decreasing the size of the assemblies and the number of linkages between DNA-NPs would increase the sensitivity of these sensors by decreasing the number of bonds between AuNPs required to be broken before a

colorimetric response is generated. Our strategy to reduce the size of the AuNP assemblies was to directly hybridize DNA on neighboring AuNPs to one another (Assembly Systems II, III and IV), which favors formation of smaller, less ordered DNA-NP assembly systems[6].

It has been demonstrated that increasing the distance between individual DNA-NPs inside Assembly System I increases the melting temperature of the assembly and decreases its ability to disassemble via aptamer-analyte interactions.[17] We therefore anticipated that the distance between AuNPs inside Assembly Systems II-IV would be directly related to the extent of AuNP assembly and inversely related to the ability of the assemblies to sense adenosine. Diluting the DNA-NP ligand shell (Assembly IV, Figure 3.1d), thereby reducing the number of reactive groups on the DNA-NPs, was expected to reduce the number of connections formed between DNA-NPs. We hypothesized that this would decrease the limit of detection for our sensing platform by reducing the number of successful aptamer-analyte interactions required to generate a colorimetric response.

The arrangement of AuNPs and DNA within these systems had a dramatic impact on the extent of AuNP assembly and aptamer-mediated disassembly. We demonstrated that diluting the ligand shells of DNA-NPs increases their hybridization efficiency, and that decreasing the inter-particle distance within the assembly system decreased the stability of the assembly, facilitating disassembly-based sensing of adenosine. We develop a sensing platform with a lower detection limit and larger range of quantification than existing sensors. Our results have important implications for the future design of sensors based on aptamer-mediated nanoparticle diassembly, because they identify key criteria for the future design of materials with enhanced properties.

RESULTS AND DISCUSSION

Preparation and Assembly of DNA-NPs and DNA/PEG3-NPs

To test the impact of the inter-particle distance and DNA ligand density on the assembly and reactivity of DNA aptamer-linked gold nanoparticle systems, we prepared a series of DNA-NPs designed to form Asssembly Systems II, III and IV (Figure 3.1).

DNA-NPs needed to form Assembly Systems II and III were prepared by mixing the aptamer or cDNA sequence with 12 nm AuNPs,[64] then adding pH 3 citric acid buffer and NaCl.[65,66] The reaction solution was then incubated overnight.[64] The disulfide at the end of the DNA strand forms a thiolate bond with the surface of the AuNPs without being reduced beforehand.[64,66–68]

DNA/PEG3-NPs designed to assemble into System IV were prepared by introducing a bunte salt-terminated ligand composed of three polyethylene glycol units ($NaSO_3S(CH_2CH_2O)_2CH_2CH_2OH$, PEG3)[69] during ligand exchange. Once bound to the AuNPs, the PEG3 ligand is thought to be neutrally charged.[70] DNA strands bound to AuNPs exert substantial electrostatic repulsive forces towards neighboring DNA strands,[71] so DNA diluent ligands could contribute substantial enthalpy and entropy costs during DNA hybridization.[72] To encourage DNA-NP assembly, we therefore selected a neutral diluent ligand. PEG chain ligands are also biocompatible.[27,73] We selected a bunte salt-terminated ligand instead of a thiol ligand because they form gold-thiolate bonds without requiring reduction by dTT or TCEP.[70] To prepare DNA/PEG3-NPs, disulfide-terminated DNA sequences and PEG3 were mixed and

added to AuNPs, followed by pH 3 citric acid buffer and NaCl. This reaction solution was incubated 18 hours before purification.

DNA-NPs and DNA/PEG3-NPs were purified by four rounds of centrifugation, and stored in water for 2-3 days before assembling. UV-visible spectroscopy and fluorescence spectroscopy were used to quantify their ligand shells (Table 3.1).[64]

Table 3.1: Number of DNA strands attached to DNA-NPs and DNA/PEG3-NPs

Assembly System	Number of aptamer strands per AuNP	Number of cDNA strands per AuNP
II	27±1	124±1
III	59±1	124±4
IV	21±1	55±7

The surface density of cDNA strands attached to DNA-NPs (Systems II and III) was higher than the number of DNA strands per AuNP previously reported by Zhang and coworkers[66] who found that ~85 DNA strands of a 12 base sequence were attached per 13 nm AuNP. This makes sense because we added excess DNA during our ligand exchange, whereas they did not. The assembly system therefore had a minimal impact on the number of cDNA strands bound per AuNP.

Despite the fact that the aptamer-containing strands in Systems II and III were the same length, the position of disulfide group within the aptamer sequence did have a large influence on the number of aptamer strands attached to each AuNP (Table 1). The surface density of aptamer strands attached to DNA-NPs designed to assemble into System III was the same as we previously reported,[64] but the density of aptamer

strands attached DNA-NPs designed to assemble into System II was much lower. The base composition near the DNA anchoring site to the AuNPs therefore had a large effect on the number of DNA strands adsorbed to the AuNP surface during ligand exchange.[64,74] AuNPs co-conjugated with DNA recognition sequences and the PEG3 ligand were functionalized with a lower number of recognition strands than those prepared without PEG3.

Having prepared the DNA-NPs and DNA/PEG3-NPs, we proceeded to assemble them. The concentration of AuNPs in each solution was determined using UV-visible spectroscopy, using the AuNP extinction coefficient and A_{520}.[64] Aptamer-NPs and cDNA-NPs were mixed in a 1:1 ratio in buffered solutions containing 300 mM NaCl and incubated at 4°C. AuNP assemblies were isolated by centrifugation, and redispersed in buffered solutions containing 150 mM NaCl for characterization. We estimated the percentage of AuNPs incorporated into assemblies by dividing the $A_{\lambda max}$ of assembled AuNPs by the $A_{\lambda max}$ of AuNPs.[3]

Characterization of Structure and Reactivity of Assembly System II

DNA-NPs designed to form Assembly System II (Figure 3.2a) began to change color from pink to purple within minutes of mixing them at room temperature. The DNA-NPs were incubated at 4°C for 3 days. 98% of DNA-NPs designed to form System II were incorporated into assemblies.

The UV-visible absorbance spectrum of Assembly System II (Figure 3.2c) changed in several ways compared to that of the individual DNA-NPs. The SPR peak of the AuNPs shifted (11 nm) to longer wavelengths. The maximum absorbance value of the solution decreased and the full width half maximum (FWHM) value of its absorbance

peak increased by 106 nm. These spectral changes are characteristic of AuNP assembly.[29]

In TEM micrographs (Figure 3.2d), we observed a mixture of dimers, trimers and larger groups containing hundreds of DNA-NPs. This corroborated the conclusions drawn from our UV-visible spectroscopy data, and confirmed formation of Assembly System II.

We initially predicted that Assembly System II would produce smaller assemblies than Assembly System I. Previous studies performed on directly hybridized DNA-NPs suggest that the DNA binding rearrangements required for assemblies to equilibrate into a highly ordered structures are inhibited in these systems due to local DNA crowding and hybridization costs.[6]

The UV-visible spectroscopy and TEM data generated from observing Assembly System II support our hypothesis that it forms smaller assemblies than Assembly System I. Assembly System II exhibited a smaller SPR shift and increase in FWHM than Assembly System I.[14,15] The relatively modest shift in the AuNP SPR suggests that fewer AuNPs were incorporated into the resultant assemblies.[3] While some of the assembled DNA-NPs formed structures approaching 500 nm in size, Assembly System II they did not form large assemblies spanning several microns in size and containing many thousands of DNA-NPs, as reported for Assembly System I.[15]

Having confirmed that DNA-NPs assembled, we proceeded to mix Assembly System II with adenosine (Figure 3.2b), and characterized the resultant solution using UV-visible spectroscopy and TEM. Assembly System II's SPR peak did not change after

adding adenosine (Figure 3.2c). TEM micrographs confirmed that Assembly System II remained assembled after adding adenosine (Figure 3.2e).

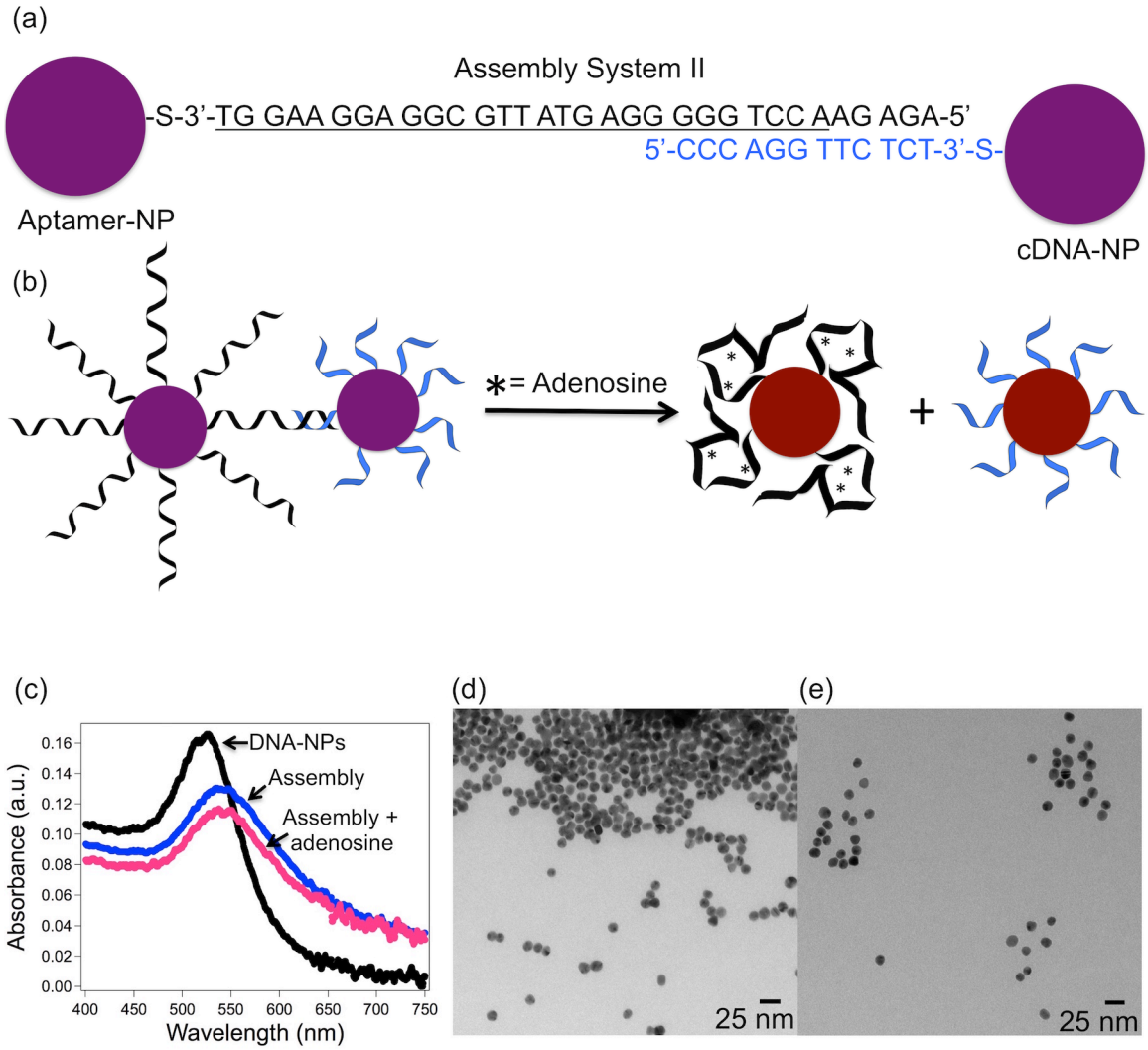

Figure 3.2: (a) Assembly System II DNA sequence binding arrangement, with aptamer portion of the sequence underlined. (b) Cartoon of assembled DNA-NPs reacting with adenosine. (c) Absorbance spectra of DNA-NPs before and after assembly, two minutes after mixing with 2mM adenosine. (d) Representative TEM micrograph of Assembly System II (e) Representative TEM micrograph of Assembly System II after adding adenosine.

These pieces of evidence, and the fact that the DNA-NPs readily assembled at room temperature, suggest that Assembly System II was too stable for the aptamer to de-hybridize and bind the analyte and provide the desired sensing response. In Assembly System III, the distance between DNA-NPs within the assemblies was decreased.

Characterization of Structure and Reactivity of Assembly System III

DNA-NPs designed to form Assembly System III (Figure 3.3) did not begin assembling at room temperature. They were incubated at 4°C for eight days before a pellet appeared to form. Approximately 8% of DNA-NPs designed to form System III appeared to be incorporated into assemblies. However, the SPR peak of these assemblies did not shift to longer wavelengths after this incubation or after adding adenosine (Figure 3.3c). This suggests that DNA-NPs designed to form Assembly System III merely settled out of solution at 4°C.

DNA-NPs designed to form Assembly System III exhibited much lower hybridization efficiency than those designed to form Assembly System II. Theoretical modeling predicts that DNA hybridization near DNA tethering sites proceed at much slower rates than DNA hybridization further away from the surface.[75] The distance between individual DNA strands bound to AuNPs is smaller near the AuNP surface, which increases the magnitude of the repulsive electrostatic forces they exert on one another.[71] We hypothesized that diminishing the electrostatic forces between DNA strands on the AuNPs could increase their hybridization efficiency.

Decreasing the number of DNA recognition strands on gold surfaces[76] and AuNPs[72] promotes DNA hybridization, but additional ligands are required to promote DNA-NPs stability[65] and prevent non-specific adsorption of DNA bases to the gold surface.[77] PEG3 was therefore used to reduce the number of recognition strands on the surface of the AuNPs when preparing Assembly System IV.

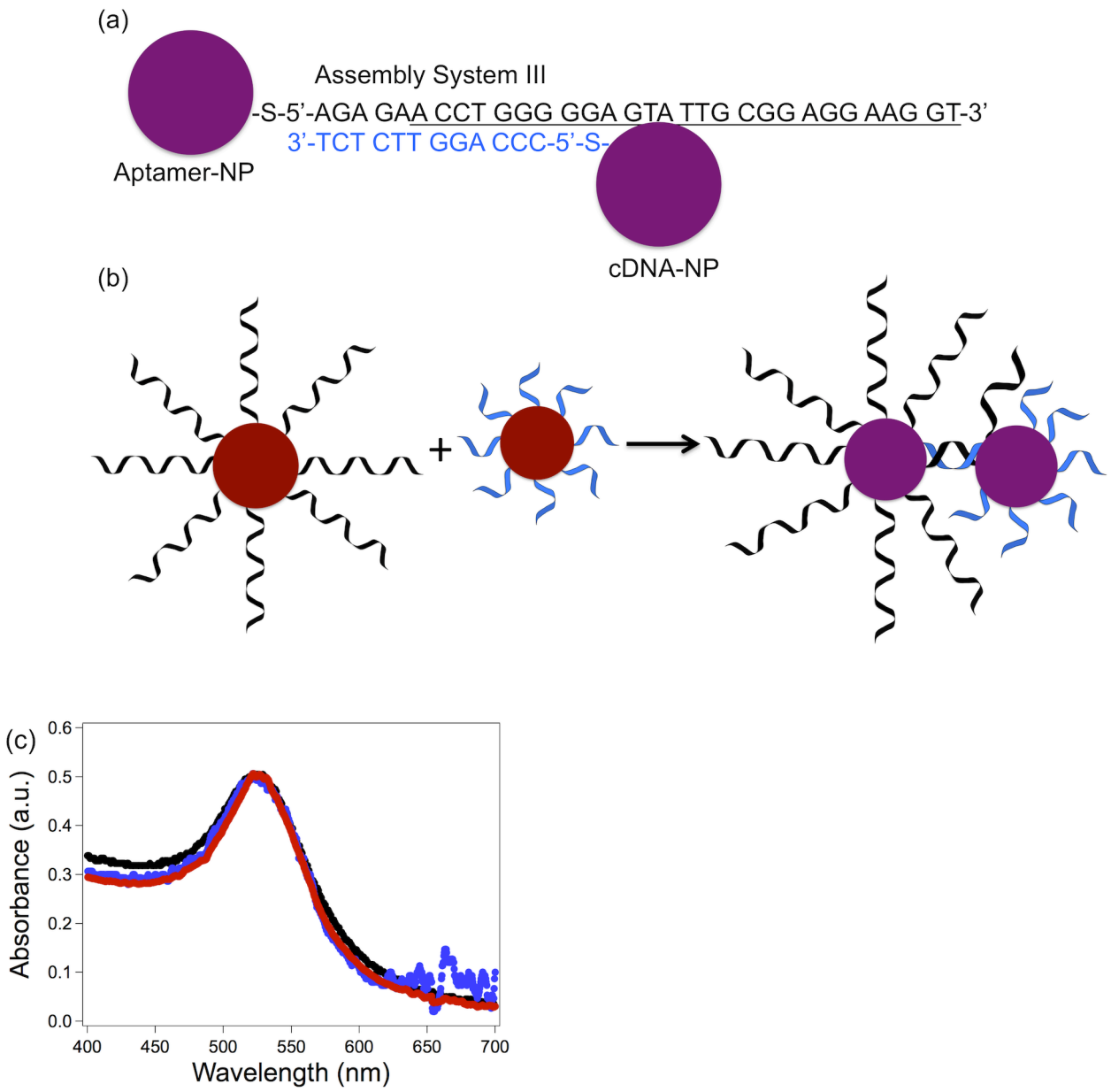

Figure 3.3: (a) Assembly System III DNA sequence binding arrangement, with aptamer portion of the sequence underlined. (b) Cartoon of DNA-NPs assembling. (c) Absorbance spectra (arbitrary units) of DNA-NP assembly before (black) and after assembly (blue), two minutes after mixing with 2 mM adenosine (red).

Characterization of Structure and Reactivity of Assembly System IV

Decreasing the number of recognition strands on the AuNPs produced DNA/PEG3-NPs (Figure 3.4a) that formed Assembly System IV at 4°C within three days in solutions containing 300 mM NaCl. The ligand shells of both the aptamer-NPs

and cDNA-NPs had to be diluted before they could form Assembly System IV. No assembly occurred as a result of diluting the ligand shell of either the aptamer-NPs or cDNA-NPs while keeping the other intact. Approximately 30% of DNA/PEG3-NPs designed to form System IV were incorporated into assemblies large enough to pellet when centrifuged after incubation.

The SPR peaks corresponding to DNA/PEG3-NPs in both the pellet and supernatant shifted to longer wavelengths broadened, though the SPR peak of AuNPs in the pellet exhibited a significantly larger increase in their full width half maximum absorbance (Figure B2; see Appendix B for all B Figures and Tables). This suggests that Assembly System IV formed smaller assemblies, less effectively separated by centrifugation. For this study, only assemblies incorporated into the pellet were reacted with adenosine.

DNA/PEG3-NPs assembled at a slower rate than fully passivated DNA-NPs. DNA binding in solution is promoted by attractions between fluctuating counterions associated with individual DNA strands.[78] One possible explanation for the difference in assembly rate is that AuNPs functionalized by fewer DNA strands experience a lower counterion attraction between DNA-NPs. This explanation is supported by our observation that DNA-NPs with ligand shells diluted by short oligonucleotide sequences (i.e. A_5) readily assemble overnight (data not shown).

The SPR absorbance peak of DNA-NPs designed to form Assembly System IV shifted 15nm to longer wavelengths, and broadened by 130 nm (Figure 3.4c). These spectral changes indicated the successful formation of AuNP assemblies.[79]

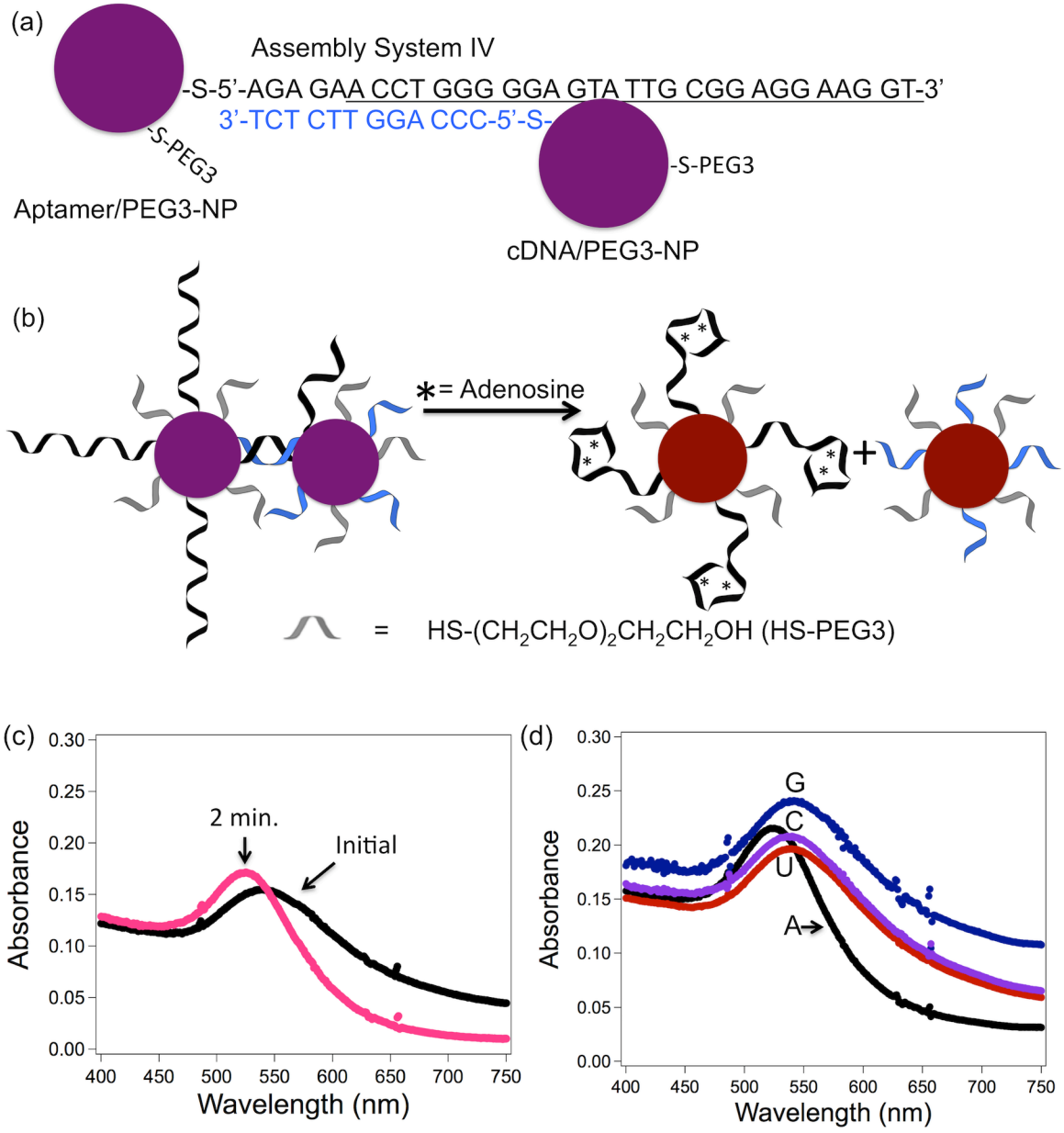

Figure 3.4: (a) Assembly System IV DNA sequence binding arrangement, with aptamer portion of the sequence underlined. (b) Cartoon of assembled DNA/PEG3-NPs reacting with adenosine. (c) Absorbance spectra of DNA/PEG3-NP assembly before and after assembly, two minutes after mixing with 2mM adenosine (d) Results from mixing DNA/PEG3-NP assemblies with 2 mM adenosine (A), cytosine (C), uridine (U) or 1 mM guanosine (G)

Assembly System IV's SPR peak (Figure 3.4c) shifted and broadened more than System II's SPR peak (Figure 3.2c). This is unsurprising, since plasmon coupling between AuNPs is distance dependent.[29–31]

Assembly System IV appeared as dimers, trimers and small groups of DNA/PEG3-NPs in TEM micrographs (Figure 3.5a). The appearance of Assembly IV in TEM micrographs therefore confirmed assembly formation, and revealed that System IV assemblies are much smaller than System II assemblies.

Assembly System IV was then mixed with adenosine (Figure 3.4b). Within two minutes of mixing the assembly with 2 mM adenosine, the AuNP SPR peak returned to 520 nm, the λmax corresponding to the individual DNA/PEG3-NPs prior to assembly (Figure 3.4c). This confirmed that Assembly System IV successfully reacted with adenosine.

To test the specificity of System IV's disassembly in the presence of adenosine, we reacted System IV with other biomolecules with structures similar to adenosine, specifically guanosine, cytosine and uridine. No spectral changes occurred when System IV was mixed with guanosine, cytosine or uridine (Figure 3.4d), which demonstrated that the sensing reaction was specific to adenosine.

Based on their appearance in TEM micrographs, DNA/PEG3-NPs retained their size and shape while assembling into System IV (Figure 3.5a). DNA/PEG3-NPs within System IV were initially bound to one another in dimers, trimers and small groups (Figure 3.5a). After reacting with 2 mM adenosine, DNA/PEG3-NPs appeared as monomers or dimers in TEM micrographs (Figure 3.5b). This confirmed that the majority of System IV assemblies successfully reacted with adenosine, thereby disassembling.

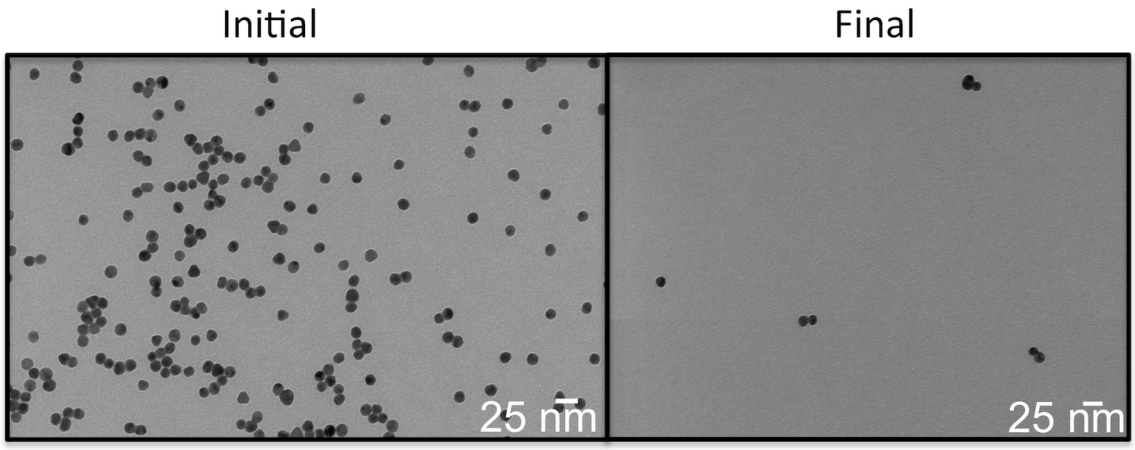

Figure 3.5: Representative TEM micrographs of (a) DNA/PEG3-NP assemblies (b) DNA/PEG3-NP assemblies after reacting with adenosine.

Having confirmed that System IV could disassemble in the presence of a large concentration of adenosine, it was then reacted with biologically relevant adenosine concentrations. To do so, a series of buffered reaction solutions containing System IV assemblies, 150 mM NaCl and various amounts of adenosine were mixed. UV-visible spectroscopy was used to measure the absorbance spectrum of the resultant solution after two minutes. A ratiometric method was used to evaluate the resultant UV-visible data, as has been done for other sensors.[15,80] Ratiometric methods use the ratio of an analyte's absorbance or fluorescent emission at two different wavelengths to assess the analyte concentration.

Our corroborative UV-visible and TEM data, and that reported by others who have prepared DNA-NP assemblies,[3,15,29] show that the A_{520}/A_{550} value of DNA-NPs decreases upon assembly and increases upon disassembly. Because the A_{520}/A_{550} value varies based on the extent of nanoparticle assembly, we thought it was reasonable to use this ratio to gauge the extent of aptamer-mediated disassembly response.

Previous research suggests that the plasmon absorbance modes of dimers can be viewed as the linear combinations of the plasmon absorbance modes for individual AgNPs, analogous to atomic orbitals in molecular orbital theory.[81] The analogy was further extended to explain the plasmon absorbance modes of trimers and quadrumers using "group theory", describing the plasmon modes of the aggregate in terms of the structure-symmetric combinations of the plasmon modes of individual AgNPs.[82] Other theoretical work demonstrated a systematic shift in the plasmon resonance absorbance as a function of the number of AuNPs assembled in a line formation.[83] Based on these findings, we would predict the plasmon absorbance of our AuNP assemblies (and the relative absorbance at each wavelength) to vary systematically as a function of the number of AuNPs in the assembly and their position relative to one another.

The A_{520} or A_{700} of System IV could have been plotted to try and assess the relative proportions of individual vs. assembled AuNPs over a range of adenosine concentrations. Since the absorbance of individual AuNPs varies at each wavelength according to the overall nanoparticle concentration, examining a ratio of absorbance values minimizes the potential error introduced by variations in the number of AuNPs found in the light path during a given measurement.

Therefore, the A_{520}/A_{550} was plotted as a function of the adenosine concentration (Figure 3.6), and used to assess the relative degree of AuNP assembly. One limitation to this analysis is that there is a distribution of AuNP assemblies containing different numbers of AuNPs, and we can only view the global average plasmon absorbance. From the absorbance ratio, we can tell the relative number of AuNPs that are assembled, but could not possibly make conclusions about individual

assembly sizes or their proportion of the overall nanoparticle population from this analysis.

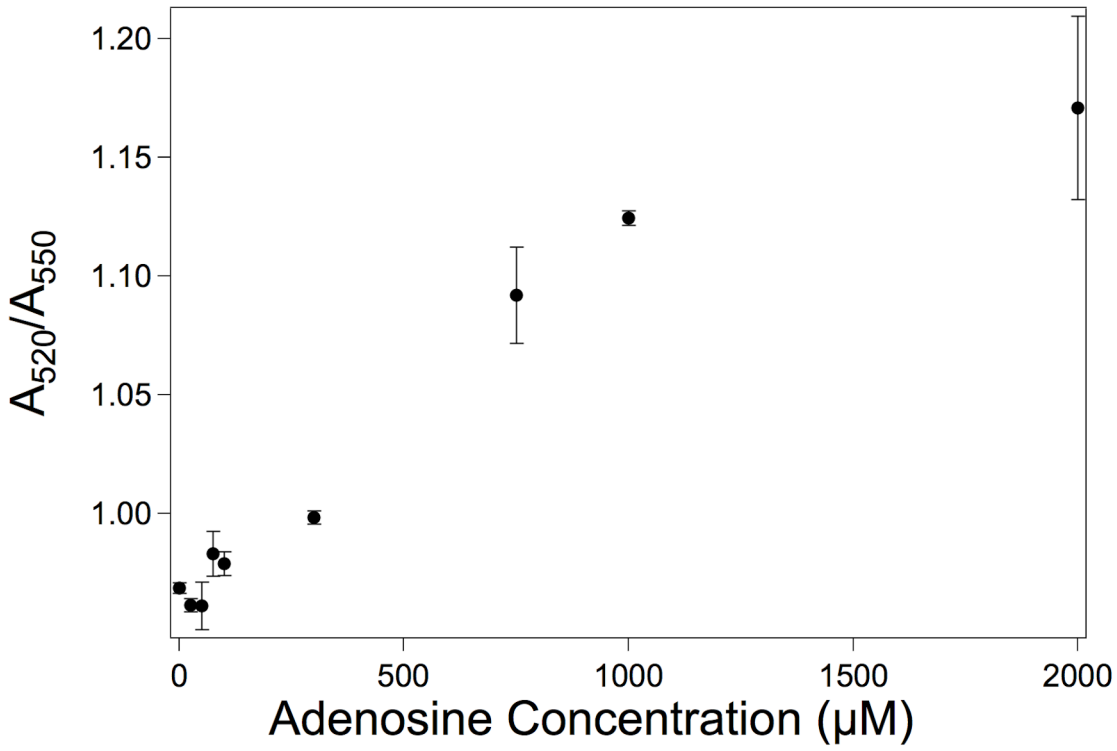

Figure 3.6: Analysis of the extent of AuNP disassembly during reaction between Assembly System IV and various amounts of adenosine. Error bars represent the standard deviation for three replicates.

As expected, reaction solutions containing the lowest concentrations of adenosine had the lowest A_{520}/A_{550} values and reaction solutions containing the highest concentrations of adenosine had the highest A_{520}/A_{550} value (Figure 3.6). 75μM was the lowest concentration of adenosine at which the A_{520}/A_{550} value significantly increased over the control sample, and is therefore the detection limit for Assembly System IV. This detection limit is a 4-fold improvement over that of the linker-mediated colorimetric disassembly-based adenosine sensor previously reported (300 μM).[15]

Assembly System IV exhibited a linear response to adenosine concentrations of 75μM-1mM. The linear regression line corresponding to the 75μM-1mM region of the sensing response curve (Figure 3.6) had an R^2 value of 0.966, indicating it is reasonably linear. It is preferable to use the quasi-linear region of a calibration curve to quantify analytes to avoid introducing analytical errors.[84] Therefore, our sensor's large linear response range is a significant advantage for quantifying analytes.

Decreasing the size of the DNA-NP assemblies and the number of linkages between DNA-NPs produced a highly reactive colorimetric disassembly-based sensor with a lower detection limit and greater quantification range than existing disassembly-based sensors. This sensor responded to biologically relevant adenosine concentrations.

In this paper, we learned that the arrangement of DNA sequences and AuNPs within assembly systems has a profound impact on their stability to assemble and sense adenosine. Assembly System II, designed to have large inter-particle spacings, was so stable that the aptamer sequence was unable to change conformation and bind its analyte. Assembly System III, designed to have short inter-particle spacings, was not stable enough to form assemblies. Diluting the ligand shell of these AuNPs, thereby decreasing the electrostatic repulsion between DNA ligands on the AuNP surfaces, increased their hybridization efficiency and allowed Assembly System IV to form. The assembly arrangement and number of DNA recognition strands per AuNPs were therefore identified as key criteria for designing functional biosensors.

Our sensing platform is broadly applicable, because it can be used to detect any analyte for which a DNA or RNA sequence has been identified. The development of nuclease resistant aptamer sequences (L-DNA),[85,86] and two new functional DNA

bases,[87,88] will continue to expand the utility of aptamers as sensing reagents. By marrying existing SELEX techniques and these new technologies, robust aptamers with high binding affinities and with highly specific reactivity may be isolated.

CONCLUSION

DNA-NPs directly hybridized to one another (Assembly Systems II and IV) formed much smaller assemblies than those reported for DNA-NPs linked together by hybridizing a crosslinking strand (Assembly System I). The sensor created by directly hybridizing DNA/PEG3-NPs (Assembly System IV) exhibited rapid, specific and sensitive detection of adenosine. It has a lower detection limit (75μM) and larger quantification range (75μM-1mM) than existing colorimetric disassembly-based sensors, and responds to biologically relevant adenosine concentrations.

The distance between DNA-NPs within the assembly systems had a profound impact on their stability. The assembly system with large inter-particle spacings (Assembly System II) was so stable that the aptamer sequence was unable to change conformation and bind its analyte. The assembly system with short inter-particle spacings (Assembly System III) was not stable enough to assemble when the density of recognition strands on their surfaces was maximized. Decreasing the density of recognition sequences on the DNA-NPs using a neutral ligand permitted AuNP assembly formation and sensing, presumably by decreasing the electrostatic repulsion between DNA strands on the surface of the AuNPs.

This sensing platform is broadly applicable, because it can be used to detect any analyte for which a DNA, RNA or L-DNA aptamer sequence has been identified. The insights we gained regarding the importance of arrangement of DNA sequences and

AuNPs within the assembly system and the impact of diluting the DNA ligand shell are important considerations for technologies involving disassembly of DNA-NPs from DNA-functionalized surfaces. Our results will therefore have a broad impact on the design of aptamer-based sensors.

EXPERIMENTAL

All details regarding materials used and instrumentation are available in Appendix B.

Preparation of DNA-NPs and DNA/PEG3-NPs

12 nm AuNPs were synthesized and characterized using UV-Visible spectroscopy, transmission electron microscopy and small angle x-ray scattering, as previously described.[64] Characterization methods and data are available in Appendix A (Figure A1 and Figure A2).

DNA-NPs were prepared as previously described,[64,65] with modifications. Briefly: The concentration of DNA and AuNP solutions was determined based on their A_{520} and A_{260}, using their predicted extinction coefficients.[64] AuNPs and DNA were mixed. The reaction solution contained 16 uM DNA and 16 nM AuNPs. pH 3 citric acid buffer (10 mM) was added, followed by NaCl (70 mM),[65,66] and being incubated overnight, as previously described.[64]Disulfide-terminated DNA was mixed with AuNP solutions

The PEG3 diluent ligand ($NaSO_3S(CH_2CH_2O)_2CH_2CH_2OH$) was prepared as previously described.[69] A description of the synthesis and purification of this ligand is provided in Appendix B. To prepare DNA/PEG3-NPs, disulfide-terminated DNA sequences were mixed with PEG3 and then added to AuNPs. The ligand exchange

mixture contained 8 nM AuNPs, 8 uM DNA and either 500 uM (aptamer-NPs) or 750 uM (cDNA-NPs) PEG3. 1000 DNA ligands were present per AuNP.

All DNA-NP and DNA/PEG3-NP ligand exchange reaction solutions were incubated 5 minutes after initial mixing before adding 100 uL pH 3 citric acid buffer. After 10 minutes. NaCl was added (70 mM) and reaction solutions were incubated for 18 hours before being purified. Performing the ligand exchange at this pH and salt concentration promotes DNA adsorption to the surface of the AuNPs.[65,66]

DNA-NPs and DNA/PEG3-NPs were purified by centrifuging 4 times for 20 minutes at 20 000g, resuspending in buffer containing 1mM pH 8.2 Tris Acetate and 100 mM NaCl after each centrifugation step. DNA-NPs and DNA/PEG3-NPs were stored in nanopure water for 2-3 days before assembly.

DNA-NPs and DNA/PEG3-NPs were characterized using TEM, Small Angle X-ray Scattering (SAXS), UV-visible and fluorescence spectroscopy. Based on the UV-visible absorbance, TEM and SAXS data, the DNA/PEG3-NPs do not change size and shape during functionalization. The number of DNA strands per AuNP were determined using UV-visible and fluorescence spectroscopy, with modifications.[64] Because the PEG3 ligand absorbed light at 260 nm, DNA concentrations were determined using fluorescence spectroscopy. When the same concentrations of DNA and AuNPs were mixed with and without PEG3, PEG3 significantly reduced the number of strands per AuNPs.

Preparation of DNA-NP and DNA/PEG3-NP Assemblies

The concentration of purified DNA-NPs was determined using UV-visible spectroscopy,[64,89] and equimolar amounts of DNA-NPs (1.5 nM each) were incubated overnight in solutions containing 25 mM Tris acetate buffer and 300 mM NaCl. This assembly was performed at 4°C, as NPs with overhangs need to be incubated at lower temperatures[15–17] to decrease DNA-NP disassembly rate.[90]

UV-visible spectroscopy was used to confirm that the DNA-NPs and DNA/PEG3-NPs maintained their overall size and shape (Figure B1) and SAXS was used to confirm that DNA-NPs retained their core size and polydispersity during assembly (Table B1). UV-visible spectroscopy and a commercially available fluorescent dye based assay were used to confirm that the AuNPs maintained the same ligand shell during assembly (Table B2).[64,91] Complete descriptions of TEM, SAXS, UV-visible and fluorescence spectroscopy methods used to characterize DNA-NPs before and after incubation and sensing are provided in Appendix B.

Sensing Adenosine using DNA-NP and DNA/PEG3-NP Assemblies

Assemblies were separated from individual AuNPs by centrifuging 30 seconds at 1000g and removing the supernatant. UV-visible spectroscopy (Figure B2) was used to confirm the separation of individual AuNPs from assemblies. Aliquots of DNA-NP or DNA/PEG3-NP assemblies were transferred to each tube, followed by the correct amount of buffer, NaCl and adenosine solutions prepare solutions containing 12.5 mM pH 8.2 tris acetate buffer, 150 mM NaCl and the appropriate concentration of adenosine. The UV-visible spectra of these solutions were measured two minutes after they were mixed.

The solubility of DNA/PEG3-NP assemblies is inversely proportional to their size, and large assemblies slowly precipitate at room temperature. To avoid experimental artifacts introduced by solution inhomogeneity, each reaction solution was pipetted up and down just prior to measuring its UV-visible spectrum.

Preparation of DNA-NP and DNA/PEG3 Samples for TEM Analysis

TEM microscopy was used to assess the extent of DNA-NP assembly, and the size of the assemblies before and after reacting with adenosine. 10 uL of reaction solutions containing 0 mM adenosine (initial) or 2 mM adenosine (final) were transferred onto amine-functionalized TEM grids, and incubated for 1 minute. 200 uL water was then added, and each grid was transferred to a new water droplet for additional rinsing. The water rinses during TEM grid preparation were very important to avoid introducing experimental artifacts, because drying effects can make AuNPs look like they are assembled when they are not (Figure B3). TEM grids were dried by wicking the solution using a kimwipe.

BRIDGE

The sensing system formed from directly hybridizing nanoparticles with dilute ligand shells detects adenosine at a lower detection limit and over a larger quantification range than existing colorimetric disassembly-based AuNP sensors. In Chapter 4, we systematically test the effect of varying the number of aptamers per AuNP on the resulting assembly/disassembly chemistry.

CHAPTER IV

IMPACT OF POLYVALENCY ON STRUCTURE AND REACTIVITY OF DNA APTAMER-LINKED GOLD NANOPARTICLE ASSEMBLIES

Note: Portions of Chapter IV are expected to appear in an upcoming publication co-authored with James E. Hutchison. I designed and performed the experiments and composed the manuscript corresponding to Chapter IV. James E. Hutchison was the principle investigator for this work and provided experimental and editorial guidance.

INTRODUCTION

Aptamer-functionalized gold nanoparticles (aptamer-NPs) have enormous potential as building blocks for sensors because they exploit both the specific and sensitive molecular recognition properties of aptamers[1,2] and the colorimetric sensing properties of AuNPs.[3,4] Aptamers are short (<100 nucleotide) single-stranded DNA or RNA sequences that fold into well-defined three dimensional structures that bind target analytes with a sensitivity and selectivity that equals or exceeds that of antibodies.[2,5,6] An increasing number of sensing and therapeutic applications exploit the ability of DNA aptamers to adopt different conformations and bind either complementary DNA sequences or analyte molecules.[1,2,7,8]

Many sensors use aptamer-mediated nanoparticle assembly[9–12] or disassembly[13–17] to respond to target analytes, yet the impact of their ligand shell architecture on their sensing response has largely remained unexplored. In most cases, a single example of each functional material is presented, without elucidating the design rules for creating materials with improved detection limits and quantification ranges. Those papers that have assessed the impact of the DNA binding environment upon aptamer-mediated

assembly and disassembly[15,17] focused on the impact of the assembly arrangement, not the number of binding groups (polyvalency).

DNA aptamer-mediated AuNP assembly and disassembly is dependent the DNA primary sequence,[15,18] assembly arrangement[15,17] and ligand shell density[17]. We recently[17] demonstrated that it is necessary to dilute the ligand shells of aptamer-functionalized AuNPs for them to assemble by direct hybridization at small inter-particle spacings. We demonstrated that these assemblies sense adenosine with lower detection limits and larger quantification ranges than existing AuNP disassembly-based sensors. We did not systematically vary the aptamer strand density to test its effect on aptamer-mediated AuNP disassembly. The number of bonds between AuNPs and the electrostatic repulsion between them should be proportional to the number of aptamers on the AuNPs, and thereby have a large impact on the sensor's detection limit and quantification range. To the best of our knowledge, no one has quantified the impact of diluting the DNA-NP ligand shell on the sensing properties of AuNP assemblies.

DNA hybridization to DNA-functionalized nanoparticles (DNA-NPs) is sensitive to the recognition sequence density on the NP surface.[19,20] It is an anti-cooperative process, in which each successful binding event inhibits subsequent binding events due to the large enthalpy and entropy costs introduced by nearby charged ligands.[20] Randeria and coworkers showed that the penalties resulting from multiple DNA hybridization events increase greatly after 10 or more linkages are attached to the DNA-functionalized AuNPs.[20]

Thermal melting[21,22] and aptamer-mediated disassembly[14] of DNA-linked AuNPs have been described as cooperative processes. DNA strands that reside within the interior

of DNA-NP assemblies are in close proximity to multiple neighboring DNA strands, and therefore experience large enthalpy and entropy costs from interacting with them. As aptamers within sensing assemblies switch conformation to bind adenosine instead of their complementary DNA sequence (cDNA), there are fewer connections between AuNPs, but similar electrostatic repulsion forces between neighboring ligands. As the aptamer strands dehybridize to interact with the analyte, the assemblies become less stable until they rapidly disassemble. The disassembly reaction is therefore cooperative, because each adenosine binding event promotes disassembly. The slope at the inflection point of the sensing response curve describes the cooperativity of the sensor.

Our initial prediction was that AuNPs functionalized with greater numbers of aptamers would form more bonds to other AuNPs, leading to higher apparent disassociation constants (K_D values) and greater cooperativity.

In this paper, we examined the impact of the number of aptamers per AuNP on their assembly/disassembly chemistry. Introducing bunte salt-protected polyethylene glycol ligands during DNA ligand exchange onto citrate-stabilized AuNPs was a convenient method to vary the number of aptamer strands on DNA-NPs. Assemblies were prepared by reacting the aptamer-NPs with cDNA-functionalized AuNPs (cDNA-NPs). AuNPs with the lowest aptamer ligand density exhibited the lowest detection limit and widest range of detection of the sensors we prepared. The number of aptamer strands per AuNP determined the cooperativity and K_D value of each assembly. These results have important implications for designing the binding environment for DNA-NP assembly in solution and on surfaces, because they suggest different strategies are

appropriate for creating sensors to act as "on-off" detectors and those for quantifying analytes.

RESULTS AND DISCUSSION

Preparation of DNA/PEG3-NPs

DNA/PEG3-NPs were prepared by co-conjugating AuNPs with the aptamer sequence or cDNA sequence and a bunte salt-terminated ligand composed of 3 polyethylene glycol units ($NaSO_3S(CH_2CH_2O)_2CH_2CH_2OH$, PEG3), as previously described (Figure 4.1).[17] To investigate the effect of diluting the DNA aptamer ligand shell on the properties of the assemblies they form, cDNA/PEG3-NPs and a series of aptamer/PEG3-NPs functionalized with different numbers of aptamer strands were prepared.

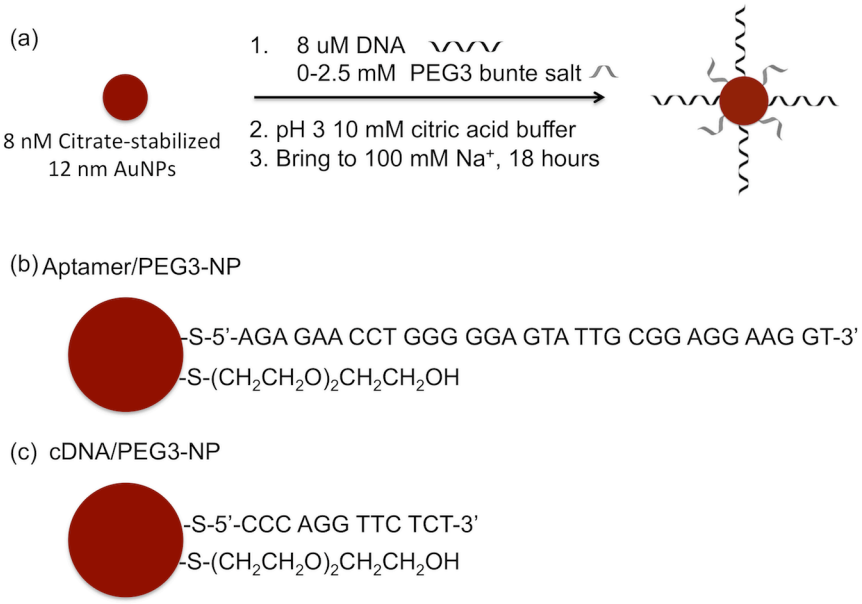

Figure 4.1: (a) Preparation of aptamer/PEG3-NPs and cDNA/PEG3-NPs. 12 nm citrate-stabilized AuNPs are mixed with disulfide-terminated DNA ($HO(CH_2)_6S$-S-5'-DNA-3'and bunte-salt terminated PEG3 ($NaSO_3S(CH_2CH_2O)_2CH_2CH_2OH$) ligands, which bind to AuNPs via thiolate linkages (b) Aptamer/PEG3-NPs and (c) cDNA/PEG3-NPs

Citrate-stabilized AuNPs (8 nM) were mixed with the same concentration of disulfide-terminated DNA aptamers (8 uM) and various concentrations (0-2.5 mM) of bunte salt-terminated PEG3 ligand (Figure 4.2). The disulfide at the end of the DNA strand forms a thiolate bond with the surface of the AuNPs without being reduced beforehand.[23–26] The number of DNA aptamer strands per AuNP was lower when higher concentrations of PEG3 were used, indicating that PEG3 competed with the DNA aptamers for binding sites on the AuNPs. The PEG3 ligand was also used to prepare cDNA/PEG3-NPs.

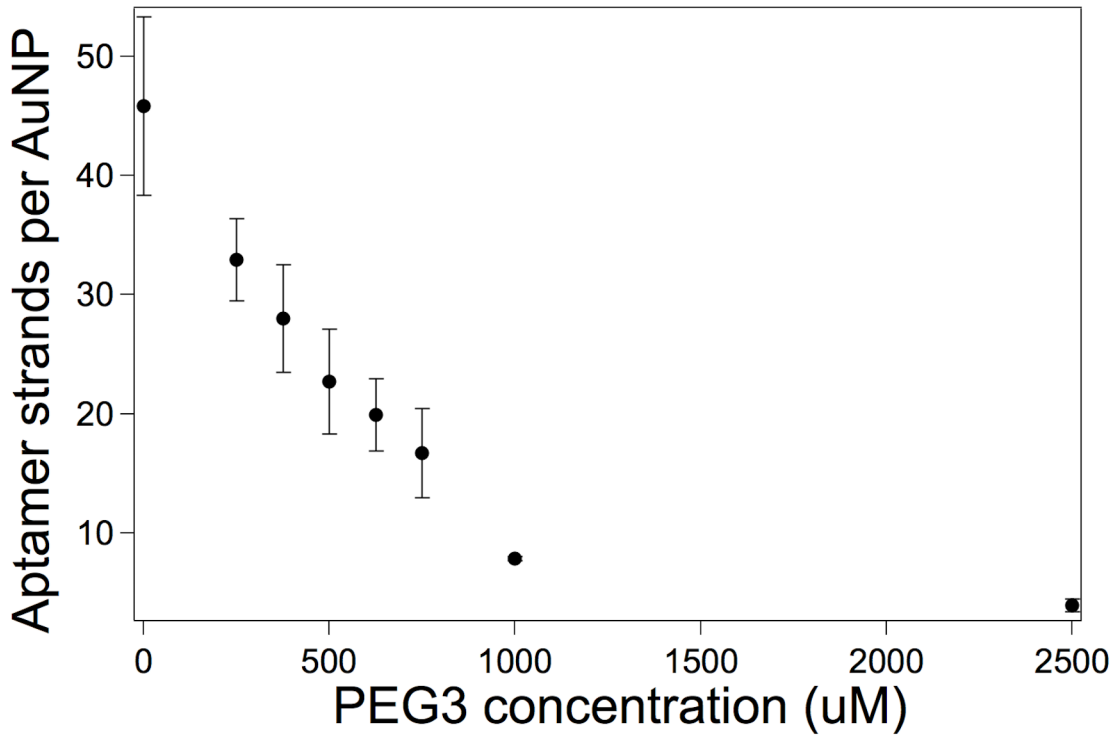

Figure 4.2: Aptamer/PEG3-NPs with a range of aptamer surface coverages, prepared by holding the AuNP concentration (8 nM) and DNA concentration (8 uM) constant while varying the PEG3 concentration during ligand exchange.

Assembly of DNA/PEG3-NPs

Having developed a method to prepare both aptamer/PEG3-NPs (Figure 4.2) and cDNA/PEG3-NPs, the impact of diluting the aptamer-np ligand shell on the assembly

reaction between aptamer/PEG3-NPs and cDNA/PEG3-NPs was investigated. Initially, we tried assembling aptamer/PEG3-NPs (Figure 4.1a) and cDNA/PEG3-NPs (Figure 4.1b) functionalized with low numbers of recognition strands. Decreasing both the number of aptamer strands and the number of cDNA strands to very low numbers inhibited DNA-NP assembly (see Appendix C). Instead, the number of aptamer sequences per AuNP was varied, and they were assembled by mixing them with cDNA/PEG3-NPs functionalized with an intermediate number (55±7) of ligands (Figure 4.3a).

DNA/PEG3-NPs were assembled by mixing equimolar amounts (1.5 nM each) of aptamer/PEG3-NPs and cDNA/PEG3-NPs, and allowing them to react in buffered (pH 8.2) solutions containing 600 mM NaCl for 4 days at 4°C.

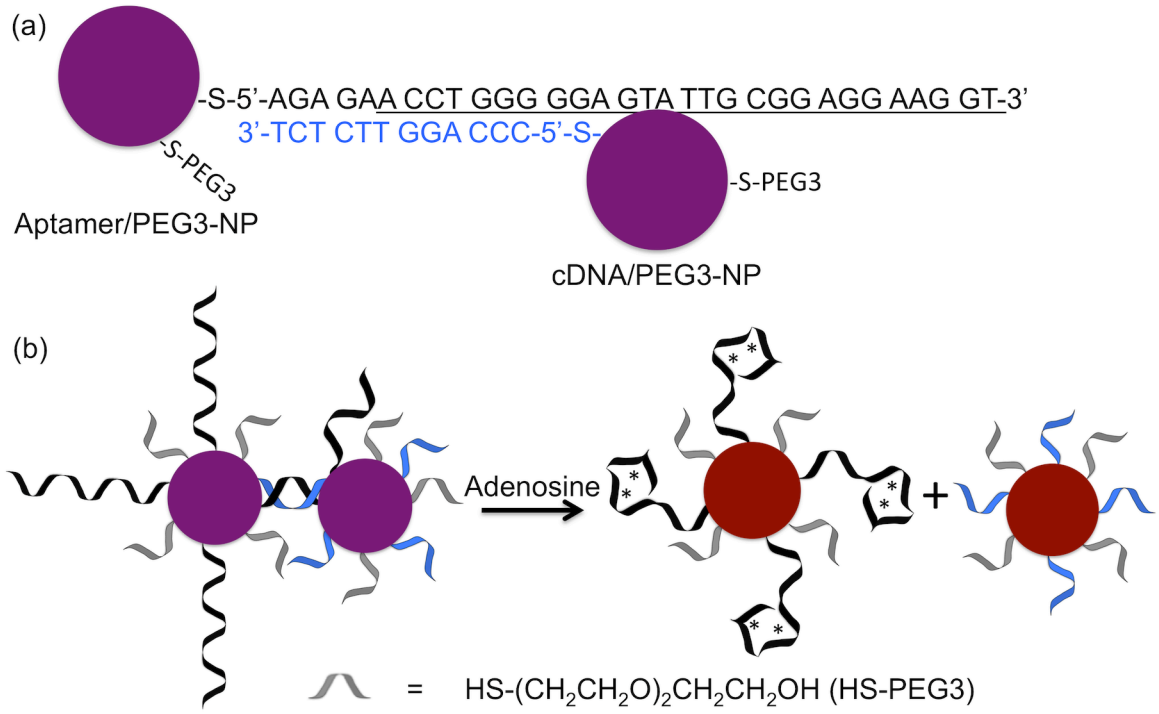

Figure 4.3: (a) Assembly arrangement for reaction between cDNA/PEG3-NPs and aptamer/PEG3-NPs functionalized with 20, 24, 30 or 35 aptamers (adenosine aptamer sequence underlined). (b) Cartoon of DNA/PEG3-NP assemblies reacting with adenosine, causing disassembly.

The assemblies were separated from individual DNA/PEG3-NPs by centrifuging for 30 seconds at 1000 rcf, then redispersing them in solutions containing 25 mM pH 8.2 Tris acetate buffer and 600 mM NaCl.[17] Solutions containing DNA/PEG3-NP assemblies were brought to 300 mM NaCl before being characterized.

Characterization of DNA/PEG3-NP Assemblies

DNA/PEG3-NP assembly was confirmed using UV-visible spectroscopy (Figure 4.4) and TEM (Figure 4.5). The DNA-NPs did not change shape, size or ligand shell composition during assembly, as determined by TEM (Figure 4.5), SAXS (Table C1; see Appendix C for all C Figures and Tables), UV-visible (Figure C1) and fluorescence spectroscopy (Table C2).

Assembling the aptamer/PEG3-NPs with cDNA/PEG3-NPs shifted the SPR peak of the AuNPs to longer wavelengths and broadened it (Figure 4.4). As reported for DNA-NP assemblies formed from 12 nm AuNPs, [14,21,27] the absorbance value of the assembled DNA/PEG3-NPs decreased compared to that of the individual nanoparticles. These spectral changes were expected based on theory and previous reports on optical properties of AuNP assemblies.[28,29]

The shifts in λmax for the DNA/PEG3-NP assemblies prepared at 600 mM NaCl were larger than when they were assembled at 300 mM NaCl,[17] indicating that the nanoparticles formed larger assemblies at the higher salt concentration.[27] Increasing the salt concentration favors AuNP assembly by decreasing the electrostatic repulsion between DNA strands. As expected, the assembled DNA/PEG3-NPs exhibited smaller λmax shifts than those reported for DNA-NPs with undiluted ligand shells,[14,21,27] suggesting that DNA/PEG3-NP assemblies contain fewer nanoparticles. This makes

sense because DNA hybridization proceeds more slowly in dilute solutions, and DNA-NPs with diluted ligand shells have fewer reactive groups, so are capable of forming fewer bonds with neighboring nanoparticles.

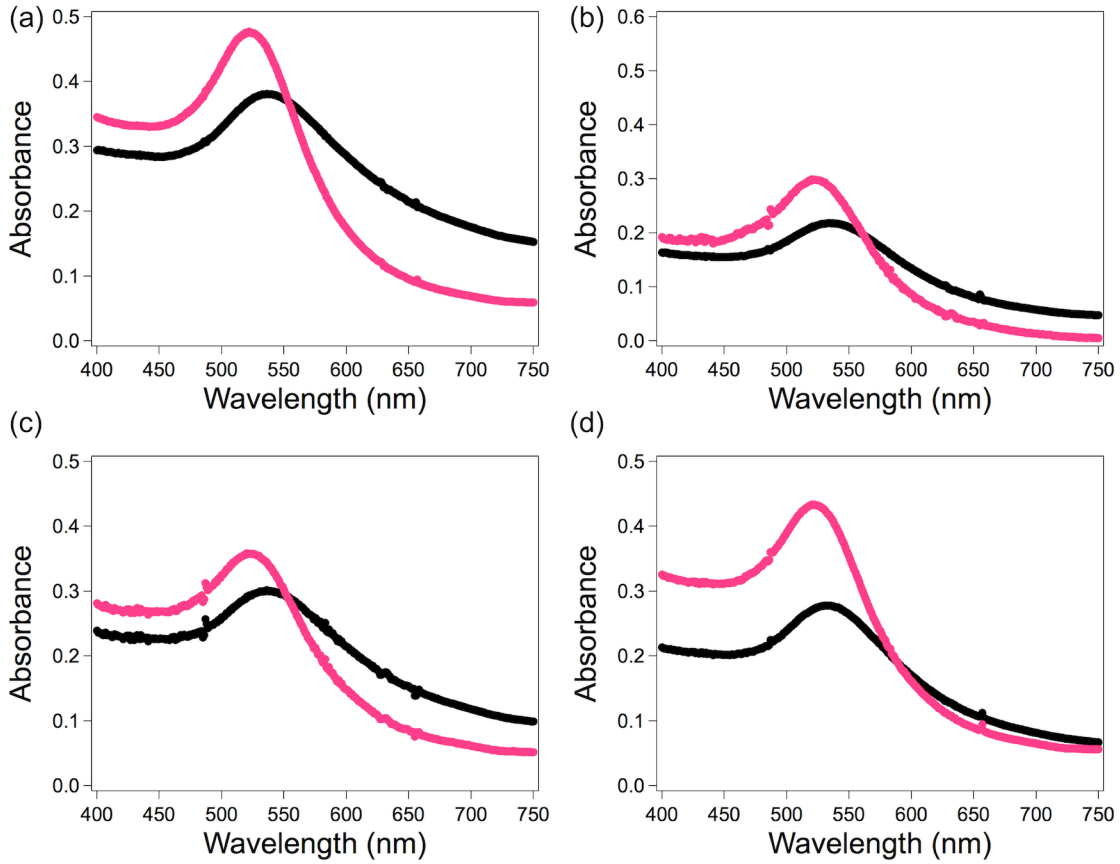

Figure 4.4: UV-visible spectra of DNA/PEG3-NP assemblies (black) formed by reacting cDNA/PEG3-NPs with aptamer/PEG3-NPs functionalized with (a) 20 (b) 24, (c) 30 or (d) 35 aptamer strands, and their subsequent reaction with 2 mM adenosine (pink).

Transmission electron microscopy (TEM) was used to determine whether the number of aptamers bound to the AuNPs affected the size of the DNA/PEG3-NP assemblies. Sample preparation artifacts were avoided as described previously,[17] and individual DNA/PEG3-NPs remained dispersed during TEM deposition (Appendix B, Figure B3). Based on the TEM data, each equilibrium mixture of assembled DNA/PEG3-NPs was composed of a mixture of individual DNA/PEG3-NPs, dimers, trimers and

small groups of DNA/PEG3-NPs (Figure 4.5). Additional TEM micrographs are available in Appendix C (Figure C3).

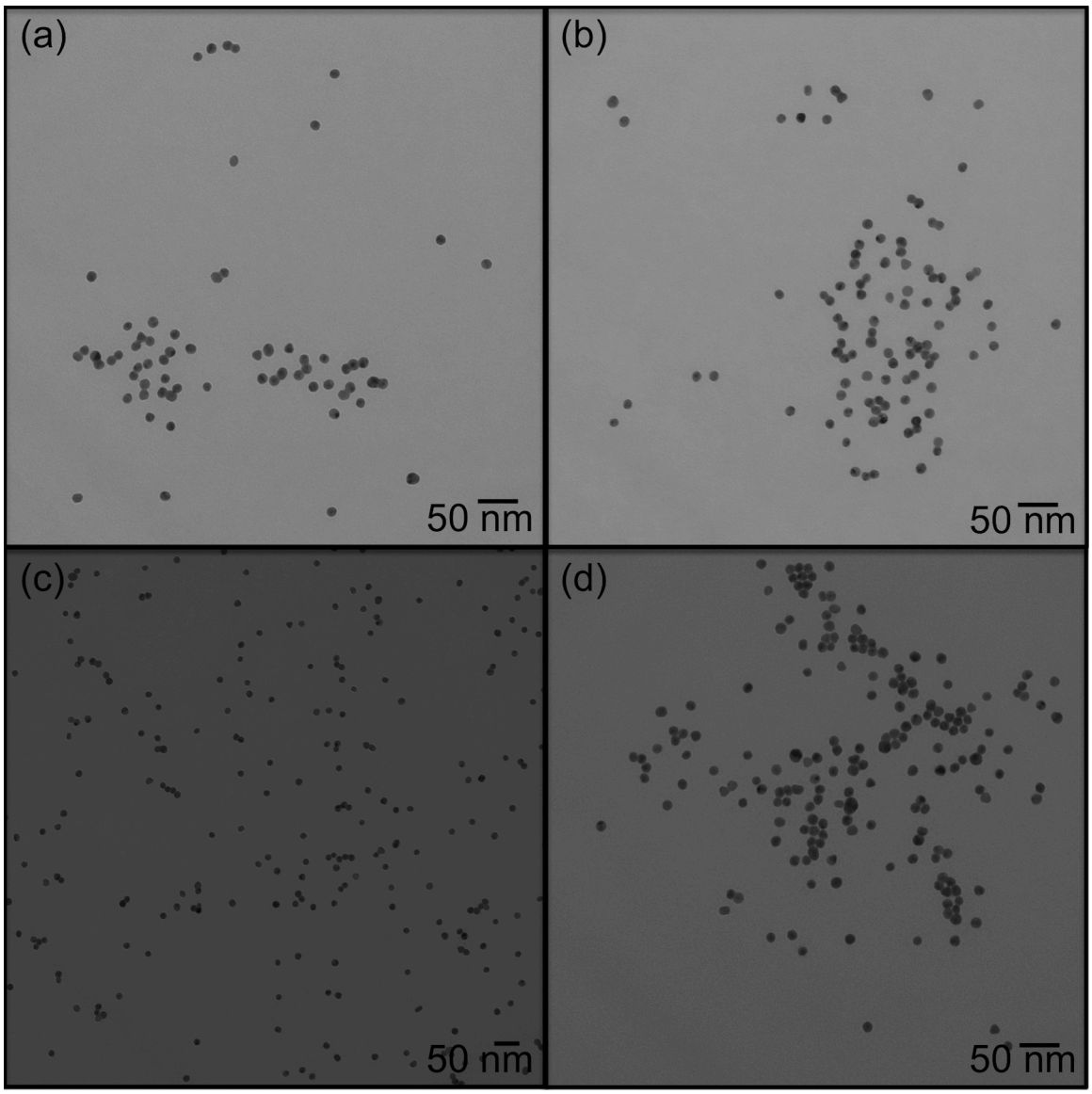

Figure 4.5: Representative TEM micrographs of DNA/PEG3-NP assemblies formed by reacting cDNA/PEG3-NPs with aptamer/PEG3-NPs functionalized with (a) 20 (b) 24 (c) 30 or (d) 35 aptamer strands.

The size of the DNA/PEG3-NP assemblies appeared to modestly increase according to the number of aptamer strands. The absence of the large micron-sized AuNP assemblies reported for assemblies of DNA-NPs with undiluted ligand shells[14,30] was

consistent with the relatively small λmax shifts we observed after nanoparticle assembly (Figure 4.4).

Characterization of Reactions between DNA/PEG3-NP Assemblies and Adenosine

Having confirmed the assembly of cDNA/PEG3-NPs with aptamer/PEG3-NPs, we proceeded to react the assemblies with adenosine. All DNA/PEG3-NP assemblies exhibited a colorimetric response to adenosine (Figure 4.4), with their UV-visible absorbance spectra returning to a λmax of 520 nm within 2 minutes after adding 2 mM adenosine. The DNA/PEG3-NPs appeared as monomers and dimers in TEM micrographs prepared from these solutions (Figure C2). This confirmed the successful reaction between the assemblies and adenosine. Since all DNA/PEG3-NP assemblies reacted to high adenosine concentrations, we proceeded to examine their reactivity towards a range of more physiologically relevant adenosine concentrations.

To do this, a series of buffered reaction solutions containing assembled DNA/PEG3-NPs, 150 mM NaCl and various concentrations of adenosine were prepared. After two minutes, the UV-visible absorbance of each resultant solution was measured. Because the position and shape of the SPR peak of the DNA/PEG3-NPs shifts as they assemble and disassemble, we can extract information regarding the equilibrium concentrations of individual and assembled DNA/PEG3-NPs from them.

The A_{520}/ A_{550} ratio decreases during AuNP assembly,[14,21,27] and increases upon nanoparticle disassembly.[14,21] This ratio was therefore used to quantify the extent of DNA/PEG3-NP disassembly in response to adenosine. The A_{520}/A_{550} values for each reaction between assembled AuNPs and adenosine were normalized according to the reaction starting points and endpoint, where "0" is the A_{520}/A_{550} ratio at the starting point

(0 uM adenosine), and "1" is the A_{520}/A_{550} ratio at the end point (2 mM adenosine) of the reaction between the assembled DNA/PEG3-NPs and adenosine. The A_{520}/A_{550} ratio for the reaction between DNA/PEG3-NP assemblies and 2 mM adenosine was considered the endpoint because their λmax (520 nm) indicated the solution contained mostly individual nanoparticles. These values were plotted as a function of the adenosine concentration (Figure 4.6).

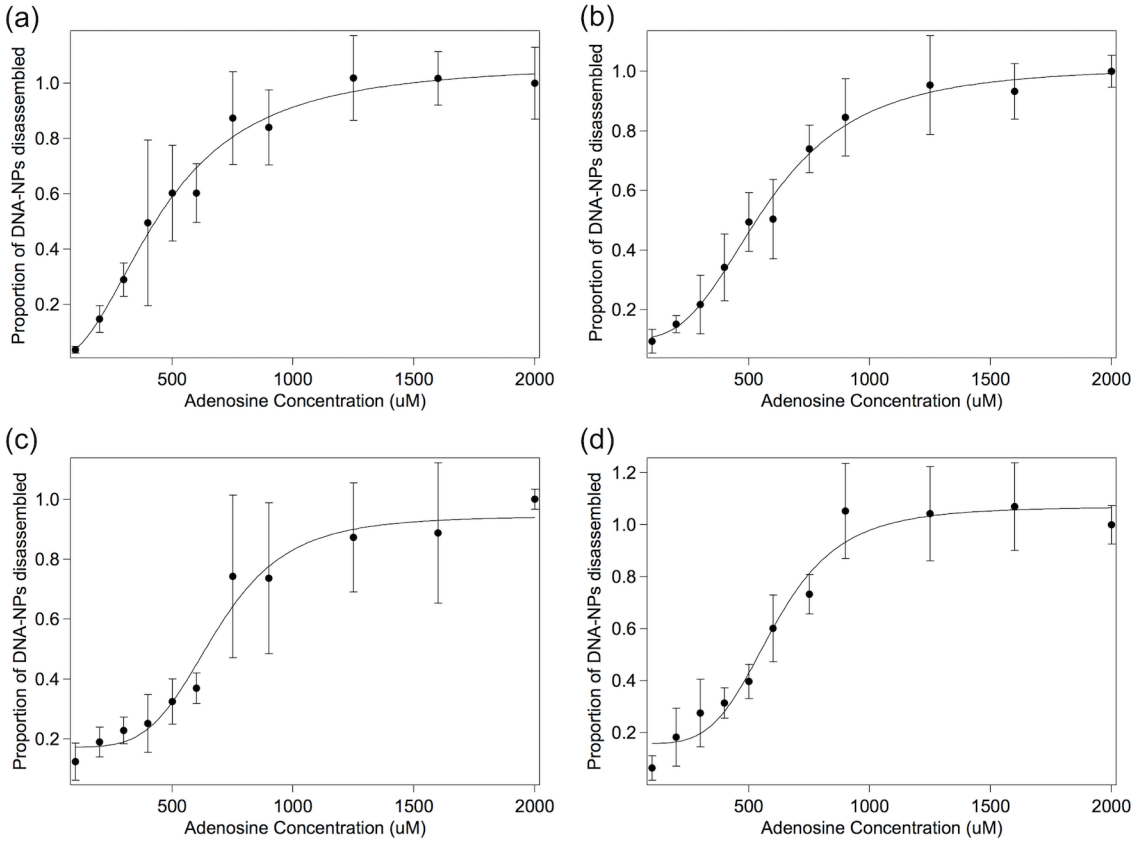

Figure 4.6: UV-visible ratiometric data describing reactions between adenosine and DNA/PEG3-NP assemblies prepared from aptamer/PEG3-NPs functionalized with (a) 20 (b) 24, (c) 30 or (d) 35 aptamer strands.

It is clear from inspecting Figure 4.6 that the number of aptamers per AuNP had a profound effect on the length of the initial plateau, the length of the quasi-linear region of

the response curve, and the adenosine concentration and slope of each curve at its inflection point.

DNA/PEG3-NP assemblies formed from aptamer/PEG3-NPs functionalized with 20 aptamers per AuNP had the shortest initial plateau, and therefore the lowest limit of detection. This curve also had the longest quasi-linear region, and therefore the largest range of quantification. Quantifying the analyte in the quasi-linear region of a response curve is preferable because it introduces the smallest analytical error.[31] The obvious qualitative differences between the responses of our sensors to adenosine prompted us to examine our data more quantitatively by modeling our data using the Hill Equation.

The Hill equation is commonly used to assess the cooperativity of protein binding,[31,32] and more recently been used to assess the cooperativity of biosensors.[17,31] It is a sigmoidal function used to describe analyte binding by proteins (or other nanoparticles) that possess more than one analyte recognition site. This model makes the following assumptions: (1) binding subunits are identical and (2) occupy equivalent positions, (3) the conformation of each subunit is constrained by interactions with other subunits, (4) transitions between these conformations is reversible, (5) if a subunit changes conformation, it affects the affinity of at least one other subunit and (6) when transitioning from one state to the other, molecular symmetry is conserved.[33,34]

By modeling our sensing data using the Hill equation, we assumed that (1) at the reaction starting point, all aptamer/PEG3-NPs have formed the same number of bonds to neighboring cDNA/PEG3-NPs (2) these aptamers have equivalent affinity for adenosine, (3) aptamer strands impose entropy and enthalpy costs on neighboring DNA strands, (4) aptamers bound to cDNA on other AuNPs are able to change conformation to bind

adenosine, (5) the successful dehybridization of one AuNP from the assembly will affect the stability of the overall assembly and (6) all AuNPs disassemble by the endpoint of the reaction. One likely source of error generated by our data modeling is our assumption that all aptamer/PEG3-NPs formed the same number of bonds to neighboring AuNPs, and therefore have the same affinity for the analyte. TEM micrographs prepared from the assemblies (Figure 4.5) show a distribution of assembly sizes. Therefore, our response curves will reflect the average number of bonds between AuNPs and average influence that each DNA-NP dehybridization event has on the stability of the AuNP assemblies.

The magnitude and direction of the Hill coefficient describes the extent to which a binding event at one recognition site affects binding events at other recognition sites. A Hill coefficient greater than one indicates a positive cooperative response, a coefficient of one indicates a non-cooperative response and a Hill coefficient less than one indicates negative cooperativity. Assemblies from DNA-NPs with undiluted ligand shells have exhibited positive cooperative melting properties,[21] so we expected our DNA/PEG3-NPs to exhibit positive cooperative disassembly.

Equations generated from modeling our data that described the response of the assembled DNA/PEG3-NPs to adenosine had positive apparent Hill coefficients, indicating that the reactions were cooperative (Figure 4.7a).

Initially, we predicted that both the apparent Hill coefficients and K_D values for the reactions between our assemblies and adenosine would be directly proportional to the number of aptamers per AuNP

The apparent Hill coefficient for our sensing curves increased as a function of the number of aptamers on the AuNPs until it reached a certain DNA surface coverage (30 per AuNP), then appears to plateau (Figure 4.7a).

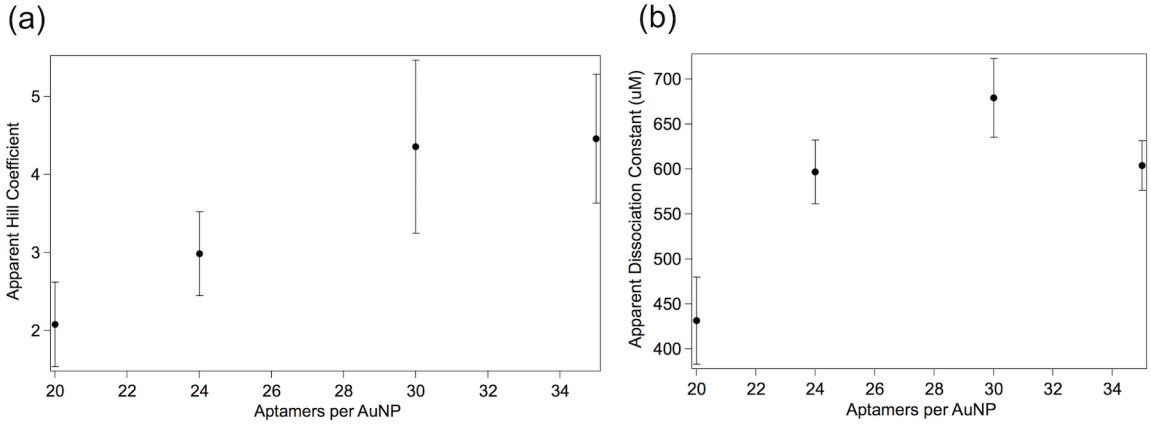

Figure 4.7: (a) Apparent Hill coefficients and (b) Apparent dissociation constants for the reaction between DNA/PEG3-NP assemblies and adenosine

The assembly formed from AuNPs functionalized with 35 aptamers statistically had the same apparent Hill coefficient as the assembly formed from AuNPs functionalized with 30 aptamers. This suggests that either the number or total strengths of bonds and electrostatic repulsion between AuNPs stayed the same, or increased proportionally. However, the large error bar associated with the apparent Hill coefficient calculated for the assembly formed from aptamers/PEG3-NPs functionalized with 30 aptamers per AuNP makes it difficult to draw definitive conclusions from comparing it to assemblies formed from aptamer/PEG3-NPs functionalized with 24 or 35 aptamers per AuNP. The magnitude of the error associated with this apparent Hill coefficient arises from the lack of reproducible sensing at intermediate adenosine concentrations (Figure 4.6c). Excluding this data point, the apparent Hill coefficients for our reaction solutions did follow the expected trend, increasing as a function of the number of aptamers per AuNP.

The K_D values for our nanoparticle assemblies increased as a function of the aptamer surface coverage until reaching 30 aptamers per AuNP, then decreased when there were 35 aptamers per AuNP (Figure 4.7b). The error bars associated with our K_D values likely arise from errors associated with individual data points near the inflection points on our sensor response curves (Figure 4.6). These data are likely scattered due to variance in the equilibrium position of our DNA/PEG3-NP assembly solutions from batch to batch, which could affect the average number of bonds between AuNPs.

The assembly formed from AuNPs functionalized with 35 aptamers had a lower K_D value than the AuNPs functionalized with 30 aptamers. This suggests that fewer linkages formed between DNA/PEG3-NPs or the linkages that did form were less stable; either such possibility would be expected to affect the balance of attractive and repulsive forces between AuNPs. It seems more likely that the additional aptamers changed the ligand shell structure in a way that prevented some aptamers from binding adenosine. Increasing the number of DNA ligands on gold nanoparticles causes them to extend more vertically from surfaces,[3,35,36] and molecular crowding on surfaces can inhibit DNA hybridization.[37,38] Perhaps having too many aptamer sequences on the AuNPs sterically hindered aptamer-adenosine interactions, leading to the lower K_D value.

Introducing bunte salt-protected PEG3 ligands during DNA-NP preparation was a convenient and effective way to dilute the number of DNA recognition strands bound to AuNPs, while maintaining their ability to assemble into clusters and perform disassembly-based sensing. DNA/PEG3-NPs functionalized with fewer than 20 aptamer ligands were not stable at elevated salt concentrations required for DNA/PEG3-NP assembly. (e.g. 600 mM NaCl). DNA/PEG3-NPs functionalized with 8 or fewer DNA

strands were not stable in 300 mM NaCl (data not shown), suggesting the PEG3 diluent ligand is not sufficiently bulky to sterically stabilize 12 nm AuNPs. Using a bulkier PEG diluent ligand could facilitate preparation of stable DNA/PEG-NPs functionalized with even fewer DNA recognition strands, thereby producing nanoparticle assemblies with lower disassociation constants and a wider analyte quantification range.

Our results have important implications for designing the binding environment for DNA-NP structures in solution and on surfaces, because they demonstrate that diluting the aptamer ligand shell produces sensors with lower detection limits, dissociation constants and larger quantification ranges than sensors made from assembling DNA-NPs with undiluted ligand shells. DNA-NPs with undiluted ligand shells are therefore preferable for applications for which a simple "on/off" response is desired, where cooperative reactions are advantageous. DNA-NPs with diluted ligand shells are preferable for more quantitative applications in which non-cooperative target binding is preferred.

CONCLUSION

The number of aptamer strands attached to DNA/PEG3-NPs has a significant impact on the detection limit, quantification range, dissociation constant and cooperativity of the sensing response of nanoparticle assemblies prepared from them. The K_D values for our nanoparticle assemblies increased as a function of the aptamer surface coverage until an intermediate surface coverage was reached, then decreased, presumably due to molecular crowding. The cooperativity of the disassembly-based sensing response increased according to the number of aptamers on the AuNPs until it reached a certain DNA surface coverage before plateauing.

Assemblies formed from DNA/PEG3-NPs with the lowest number of aptamers had the lowest detection limit and the largest quantification range, and are therefore preferable for more quantitative applications in which it is preferable to precisely determine the analyte concentration. DNA-NPs with less diluted ligand shells are preferable for applications for which a simple "on/off" response is desired, because a highly cooperative reaction will generate the largest visible response over the shortest concentration range.

EXPERIMENTAL

All details regarding materials used and instrumentation are available in Appendix C. A description of the synthesis and purification of the PEG3 ligand is provided in Appendix B.

Preparation of DNA/PEG3-NPs

12 nm AuNPs (12.2 ± 1.8 nm) were synthesized, and characterized using UV-Visible spectroscopy, transmission electron microscopy and small angle x-ray scattering, as previously described.[26] The PEG3 diluent ligand was synthesized and purified as described previously.[39] A description of AuNP synthesis and characterization is available in Appendix A.

To prepare DNA/PEG3-NPs, disulfide-terminated DNA sequences were mixed with PEG3 and then added to AuNPs. The ligand exchange mixture contained 8 nM AuNPs, 8 uM DNA and either 750 uM PEG3 (cDNA/PEG3-NPs) or 0-750 uM PEG3 (aptamer/PEG3-NPs). 1000 DNA ligands were present per AuNP. After 5 minutes, pH 3 citric acid buffer (10mM) was added. After 10 minutes, NaCl was added (70 mM). The

reaction mixture was then incubated for approximately 18 hours before being purified by 4 rounds of centrifugation, as described previously.[17,26]

DNA/PEG3-NPs were characterized using TEM, Small Angle X-ray Scattering (SAXS), UV-visible and fluorescence spectroscopy. Based on the UV-visible absorbance, TEM and SAXS data, the DNA/PEG3-NPs do not change size and shape during functionalization. The number of DNA strands per AuNP were determined using UV-visible and fluorescence spectroscopy, with modifications.[26] Because the PEG3 ligand absorbed light at 260 nm, DNA concentrations were determined using fluorescence spectroscopy.

Preparation of DNA/PEG3-NP Assemblies

The concentration of purified DNA/PEG3-NPs was determined using UV-visible spectroscopy,[40] and equimolar amounts of DNA/PEG3-NPs functionalized with 20, 24, 30 or 35 aptamer strands per AuNP and cDNA/PEG3-NPs (1.5 nM each) were incubated for 4 days in solutions containing 25 mM Tris acetate buffer and 600 mM NaCl. This assembly was performed at 4°C, as NPs with overhangs need to be incubated at lower temperatures[14,15] to decrease DNA-NP disassembly rate.[41]

TEM and UV-visible spectroscopy (Figure C1) were used to confirm that DNA/PEG3-NPs retained their size and shape during assembly. SAXS was used to confirm that DNA/PEG3-NPs retained their size and polydispersity during assembly (Table S-1). UV-visible spectroscopy and a commercially available fluorescent dye based assay[26] were used to confirm that the ligand shell remained in tact (Table S-2). Complete descriptions of TEM and SAXS, UV-visible and fluorescence spectroscopy methods used

to characterize DNA-NPs before and after incubation and sensing are available in Appendix A.

Sensing Adenosine using DNA/PEG3-NP Assemblies

Supernatants containing unassembled DNA-NPs were removed by centrifuging 30 seconds at 1000g. Based on their resultant UV-visible spectra and TEM micrographs, DNA-NPs in the pellet were considered assembled. DNA-NPs in the supernatant were individual AuNPs, The extent of DNA-NP assembly was assessed by determining the relative amounts of DNA-NPs in the pellet and supernatant from A_{520} of each solution. DNA-NPs were mixed with the appropriate concentration of adenosine solution to bring each reaction mixture to the same final volume, containing 150 mM NaCl, 12.5 mM tris acetate pH 8.2, and the desired adenosine concentration. The UV-visible spectra of these solutions were measured two minutes after being mixed.

Preparation of DNA/PEG3-NP Samples for TEM Analysis

TEM microscopy was used to analyze the size of DNA-NP assemblies found in solutions resulting from the reaction of assembled DNA-NPs with adenosine. 10 uL of solutions containing assembled DNA-NPs with and without adenosine were transferred onto amine-functionalized TEM grids, and incubated for 1 minute. Approximately 500 uL water was then added, and each grid was transferred to a new water droplet for additional rinsing. TEM grids were dried by wicking the solution using a kimwipe.

BRIDGE

In Chapter IV, the recognition strand density on DNA/PEG3-NPs was found to significantly influence their assembly/disassembly chemistry. Its impact on disassembly-based sensing was evaluated qualitatively and quantitatively. Several key design rules

pertaining to the creation of new aptamer-based biosensors have now been elucidated. In Chapter V, I will reflect on how these insights will impact the design of nanomaterials and future avenues of research.

CHAPTER V

CONCLUDING SUMMARY

OVERVIEW

The intent of this dissertation was to develop a framework for understanding the impact of the DNA–NP ligand shell architecture on the structure and reactivity of DNA aptamer-linked gold nanoparticle assemblies. Challenges associated with characterizing the ligand shell of DNA-NPs, designing their assembly arrangement and the ligand shell composition were identified. Systematically investigating the variables that govern interactions at the nanoparticle-DNA interface and their impact upon the properties of the resulting sensors lead to elucidation of several design rules for creating new materials with enhanced properties.

In Chapter II, a method for determining the ligand shell composition of DNA-NPs was developed. Using this method, we were able to explore nanoparticle structure-property relationships in Chapter III and Chapter IV. In Chapter III, the effect of the assembly arrangement upon the ability of DNA-NPs to assemble and sense adenosine was explored, and an effective sensor involving DNA aptamers and AuNPs was created. The influence of the ligand shell composition upon this sensor was systematically investigated in Chapter IV. The results of this study allowed us to identify design rules for preparing DNA-NP assemblies tailored to specific applications.

KEY RESULTS AND BROADER IMPACTS

Label-free Quantification of DNA Bound to Gold Nanoparticles

In Chapter II, a rapid, convenient and inexpensive method to quantify the number of label-free DNA strands attached to AuNPs was developed. The number of label-free

DNA sequences bound to AuNPs can now be rapidly and conveniently determined using UV-visible spectroscopy. Our technique is broadly applicable, as it can be used to easily determine the number of DNA strands of any base composition attached to AuNPs of any size.

UV-visible spectroscopy and a conventional dye assay were used in tandem to determine two different label-free DNA sequences co-conjugated to AuNPs. The results from studying DNA-NPs with mixed ligand shells suggest that disulfide-terminated DNA sequences undergo rapid, non-specific adsorption onto AuNPs at pH 7, then rearrange to permit specific DNA binding at pH 3.

Using this approach, the ligand shell composition of a large of library of nanoparticles functionalized with mixed label-free DNA ligand shells can be precisely determined. This will deepen our understanding of nanoparticle ligand shell structure-property relationships, and lead to production of nucleic acid functionalized nanoparticles with precisely engineered assembly, sensing and gene regulation properties.

In principle, our method can be extended to determine the number of DNA or RNA strands bound to other noble metal nanoparticles or used to quantify the number of peptides bound to AuNPs. Our results will therefore have a broad impact on the characterization of biomolecule-functionalized nanoparticles.

Effect of Assembly Arrangement on Structure and Reactivity of DNA Aptamer-Linked Gold Nanoparticle Systems

In Chapter III, it was found that DNA-NPs directly hybridized to one another formed much smaller assemblies than those reported for DNA-NP assemblies formed by linker-mediated assembly. A sensor created by directly hybridizing DNA-NPs with

diluted ligand shells at short inter-particle distances exhibited a rapid, specific and sensitive response to adenosine. It had a lower detection limit (75μM) and larger quantification range (75μM-1mM) than existing colorimetric disassembly-based sensors, and responded to biologically relevant adenosine concentrations.

The position of the AuNPs and DNA strands within the assemblies had a profound impact on the extent of AuNP assembly and the ability of DNA-NP assemblies to sense adenosine. Designing the AuNPs to assemble with large inter-particle spacings within the assembly made the assemblies too stable to allow the aptamers to dehybridize and sense adenosine. When the complementary DNA binding site was positioned near the aptamer sequence's anchor to the AuNPs and the inter-particle spacing was small, the DNA-NP recognition strands had to be diluted before assembly and sensing could occur.

Our sensor is broadly applicable, because it can be used to produce colorimetric sensors for detecting any analyte for which an aptamer sequence has been identified. The insights we gained regarding the importance of designing the ligand shell architecture to precisely tune the stability of AuNP assemblies are important considerations for technologies involving disassembly of DNA-NPs from DNA-functionalized surfaces. Our results will therefore have a broad impact on the design of aptamer-based sensors.

Impact of Polyvalency on Structure and Reactivity of DNA Aptamer-Linked Gold Nanoparticle Assemblies

In Chapter IV, we discovered that the number of aptamer strands attached to DNA/PEG3-NPs had a significant impact on the detection limit, quantification range, dissociation constant and cooperativity of the sensing response of nanoparticle assemblies prepared from them. The apparent K_D values for our nanoparticle assemblies increased as

a function of the aptamer surface coverage until an intermediate surface coverage was reached, then decreased. The cooperativity of the disassembly-based sensing response increased according to the number of aptamers on the AuNPs until it reached a certain DNA surface coverage before appearing to plateau.

Assemblies formed from DNA/PEG3-NPs functionalized with the lowest number of aptamers had the lowest detection limit and the largest quantification range, and are therefore preferable for more quantitative applications in which it is preferable to precisely determine the analyte concentration. For this study, we used a very short diluent ligand that was unable to stabilize the AuNPs at very low recognition sequence densities and the elevated salt concentrations required for DNA-NP assembly. The properties of our sensor could be further improved by diluting the ligand shell using a slightly bulkier PEG ligand capable of sterically stabilizing the AuNPs.

DNA-NPs with less diluted ligand shells are preferable for applications for which a simple "on/off" response is desired, because a highly cooperative reaction will generate the largest visible response over the shortest concentration range.

Our results have wide-reaching implications, because they suggest that the properties of other materials composed of polyvalent building blocks that experience considerable attractive and repulsive forces can be tailored for specific applications by diluting the number of reactive groups.

The insights we gained from studying the ligand shell composition of DNA-functionalized nanoparticles, and the impact of their assembly arrangement and recognition strand density upon the structure and reactivity of the resulting nanoparticle assemblies will significantly impact the future design and development of biomolecule-

functionalized nanoparticles, leading to production of materials with precisely defined properties.

APPENDIX A

CHAPTER II SUPPLEMENTARY INFORMATION

Determination of AuNP Size Distribution using SAXS

The size distribution of purchased and prepared AuNPs were determined using small angle X-ray scattering (SAXS). AuNP samples were exposed to monochromated X-rays from a Long Fine Focal spot (LFF) sealed X-ray tube (Cu 1.54 Å) powered by a generator at 2 kW focused by multilayer optics, measured with a Roper CCD in a Kratky camera. The Anton Paar SAXSess, in line collimation mode, was set to average 50 x10s scans (large NPs) or 45s scans (small AuNPs). Dark current and background solution scans were collected for the same exposure times, and subtracted from the data before desmearing using the beam profile in Anton Paar SAXSQuant software. This data was imported into IGOR Pro, and reduced to 200 points, matching the number of bins to be fit. The size distribution of the synthesized (12.3 ± 1.9 nm) and purchased AuNPs (5.0 ± 0.5 nm) used in our study were determined (Figure A1) using the Modeling II macro in the IRENA package[1–4].

Determination of AuNP Shape using TEM

TEM analysis of AuNP shape was performed using an FEI Technai G2 Spirit TEM operating at 120 kV. Amine-functionalized TEM grids were purchased from Dune Sciences (Eugene, Oregon), and floated on 10 uL AuNPs for 1 minute, before being rinsed with water and dried by wicking. Data confirmed that AuNPs were spherical (Figure A2).

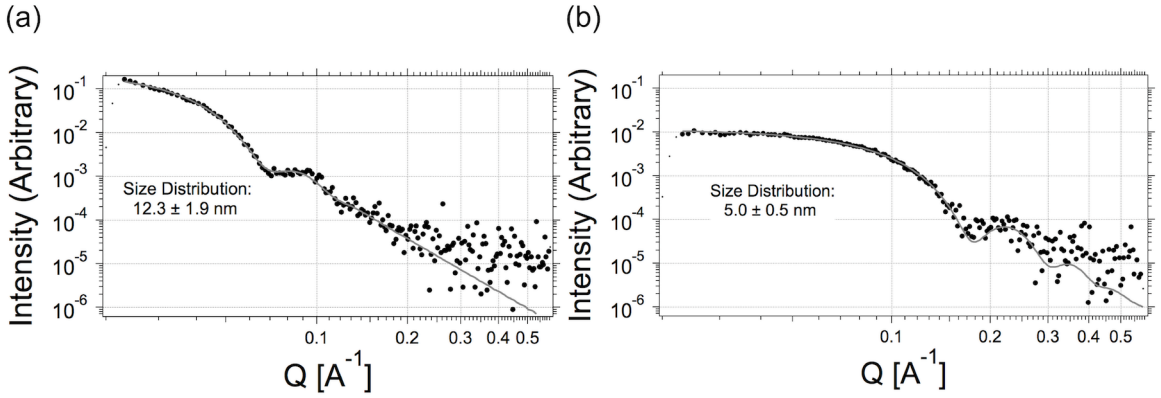

Figure A1: SAXS scattering data and corresponding model fits for aliquots of different sized AuNPs used to prepare DNA-NPs The size distribution of the synthesized (12.3 ± 1.9 nm) and purchased AuNPs (5.0 ± 0.5 nm) used in our study were determined using the IgorPro's Irena Modeling II macro.

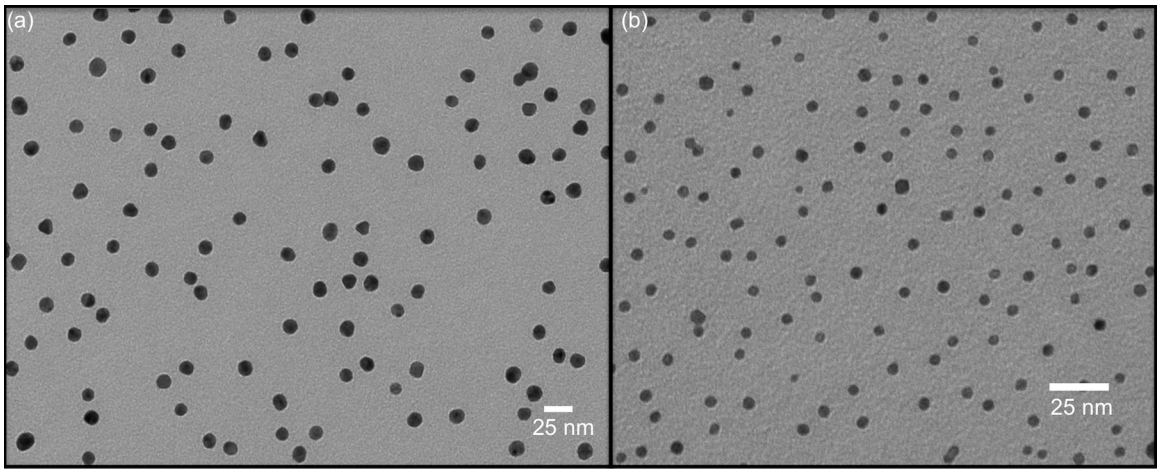

Figure A2: TEM micrographs of a) 12nm citrate-stabilized AuNPs prepared by sodium citrate reduction of $HAuCl_4$ and b) 5nm AuNPs purchased from Nanocomposix

Analysis of Excess Ligand Removal using Fluorescence Spectroscopy

15 nm AuNPs were functionalized using a fluorescently tagged ligand (TYE_{563}-5'-T_{24}-3'-S-S-$(CH_2)_3OH$, ε = 205 000 L/(mole·cm)), as described in the Experimental section. 1400 strands/NP were added during functionalization. DNA-NP samples were stored in amber tubes before and after purification to prevent photobleaching. Standard

solutions of fluorescently tagged DNA were also stored in amber tubes prior to measurement. DNA-NPs were purified by performing a series of centrifugation steps (20 000 rcf, 15 min.), adding sufficient 1 mM tris acetate 100 mM NaCl buffer to the sample to adjust it to its original mass after each spin. The fluorescent emission of each supernatant was measured using an SPEX Fluoromax-3 instrument (Jobin Yvon Inc., Horiba Group, New Jersey) (Figure A3a) in Emission Acquisition mode, and used to assess removal of the excess DNA. Steady state measurements were made by exciting samples at 548 nm and collecting emission counts from 552-650 nm (1 nm increments, 1s integration times). After two spins, very little free ligand remains in solution. To ensure the AuNPs were purified prior to quantification, 4 spins were used to remove excess ligand from each 12 nm DNA-NP sample.

5 nm AuNPs were functionalized using a fluorescently tagged ligand (TYE_{563}-5′-A_{12}-3′-S-S-$(CH_2)_3OH$, ε = 157 400), as described in the Experimental section. DNA-NPs were purified by performing a series of centrifugation steps above a 50 kDa filter membrane (13 500 rcf, 9 min.), adding 500 uL 1 mM tris acetate 100 mM NaCl buffer to the sample to adjust it to its original mass after each spin. The fluorescent emission (Ex. 549 nm, Em. 563 nm) of each flowthrough was measured using the SPEX Fluoromax-3 instrument (Figure A3b), as described above. After 4 spins, very little free ligand remains in solution. To ensure nanoparticles were purified prior to quantification, 5 spins were used to remove excess ligand from each 5 nm DNA-NP sample.

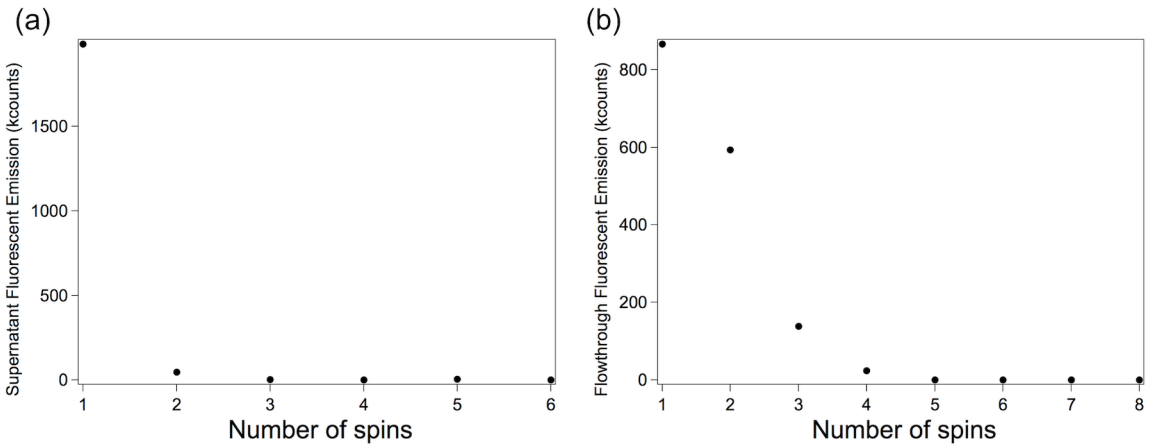

Figure A3: Fluorescence emission of solution containing excess fluorophore-tagged DNA removed from DNA-NP samples by centrifugation during AuNP purification. (a) DNA present in supernatant after each centrifugation step during purification of 12 nm DNA-NPs. (b) DNA present in flowthrough after each centrifugation step during purification of 5 nm DNA-NPs.

During initial development of our UV-visible spectroscopy based quantification method, we noticed that our analytical method was producing inconsistent values for the number of DNA strands bound to each NP during replicate measurements performed on the same sample. We hypothesized that there may be another component in the reaction mixture (other than the DNA and decomposed NPs) that may be absorbing light at 260 nm, which would mean a term was missing from Equation 3. We found that some buffers commonly used for purifying DNA-NPs absorb at 260 nm (Figure A4), and the centrifugation process would therefore cause systematic errors. Reducing the concentration of Tris acetate from 25 mM to 1 mM in the buffer solution and resuspending the nanoparticles in nanopure after purification eliminated this source of error from our calculations.

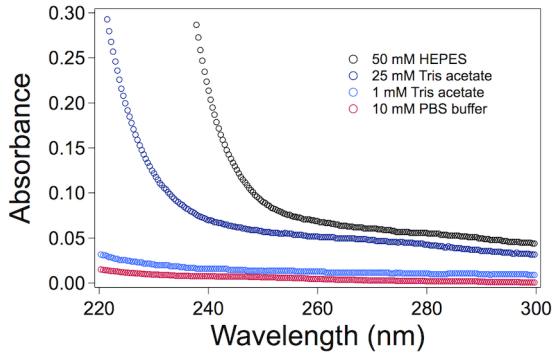

Figure A4: UV-visible absorbance of buffers used during DNA-NP purification

The presence of DNA_2 introduced an average error of 0.2% when determining the DNA_1 concentration. The presence of DNA_3 introduced an average error of 6% when determining the DNA_1 concentration. A similar experiment was preformed using DNA_4, determining its concentration with and without DNA_2 (total DNA concentration in mixtures = 100 nM). The presence of DNA_2 introduced 9% error when determining the concentration of DNA_4, when DNA_4:DNA_2 molar ratio was greater than 10:90 (Figure A5c). The presence of DNA_3 introduced substantial error in determining the concentration of DNA_4, when the DNA_4:DNA_3 molar ratio was less than 50:50 (data not shown).

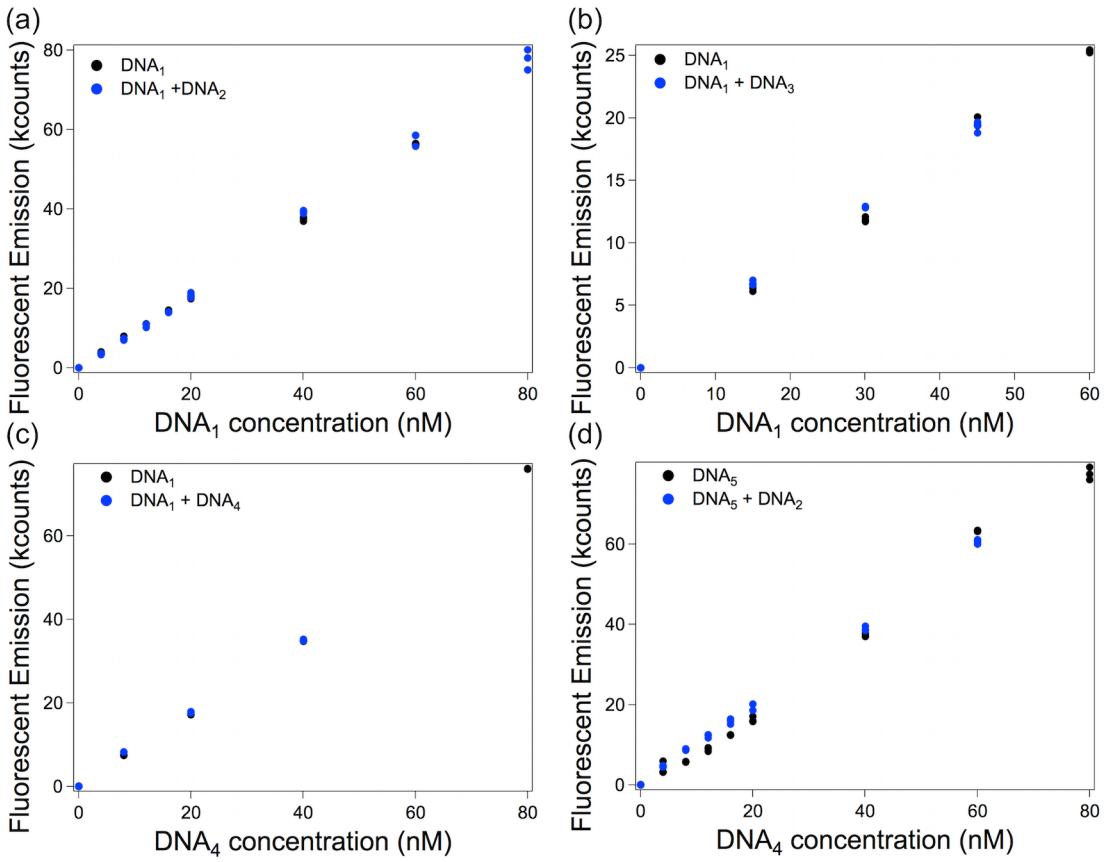

Figure A5: Fluorescent dye assay emission data collected from solutions containing known concentrations of DNA. (a) DNA_1 with and without DNA_2 (b) DNA_1 with and without DNA_3 (c) DNA_1 with and without DNA_4 (d) DNA_5 with and without DNA_2.

APPENDIX B

CHAPTER III SUPPLEMENTARY INFORMATION

Materials

All DNA samples were purchased from Integrated DNA Technologies (Coralville, Iowa). DNA sequences were purified by either the standard desalting method or HPLC. A "Quant-It" OliGreen ssDNA Assay kit was purchased from Thermo Fisher Scientific (Grand Island, NY). Clear 1.5 mL microcentrifuge tubes were purchased from VWR (Radnor, PA). DNA sequences were purified by either the standard desalting method or HPLC. A "Quant-It" OliGreen ssDNA Assay kit was purchased from Thermo Fisher Scientific (Grand Island, NY). Clear and amber 1.5 mL microcentrifuge tubes and opaque polypropylene black 96 well plates (Costar) were purchased from VWR (Radnor, PA). Sodium citrate dehydrate and hydrogen tetrachloroaurate hydrate were purchased from Sigma Aldrich (St. Louis, Missouri). Amine-functionalized TEM grids were purchased from Dune Sciences (Eugene, Oregon).

Synthesis of PEG3 Ligand

The protected thiol MEEE-BS ligand (PEG3) was synthesized and purified as described previously.[1] Briefly: 2-[2-(2-chloroethoxy)- ethoxy]ethanol (2.0 g, 11.9 mmol) was dissolved in 150 mL nanopure water. Sodium thiosulfate (0.8 molar equivalents) was added and the solution was refluxed for 3 hours. Water was removed *in vacuo*, then the crude product was dissolved in ethanol and gravity filtered. Ethanol was removed by rotary evaporation, yielding the colorless, viscous oil product.

Instrumentation

UV-visible absorbance spectra of AuNP and DNA solutions, DNA-NPs, DNA/PEG3-NPs and assemblies were obtained using either a BioTek Synergy 2 instrument or a Mikropack DH-2000 UV-vis-NIR light source equipped with an Ocean Optics USB2000 spectrophotometer or or a Hewlett Packard 8453 spectrophotometer with HP ChemStation. UV-visible spectra of DNA were obtained using these or a Thermo Scientific Nanodrop 2000 spectrophotometer path length (10mm) and baseline corrected at 340nm.

The endpoint (after 5-15 minutes) fluorescent emission of solutions used to quantify DNA were measured in 96-well opaque black well plates (Costar) using a Biotek Synergy 2 instrument equipped with a tungsten lamp and filters (EX 485/20 nm, EM 528/20 nm). The data collection time was autoscaled, so that 80,000 counts were emitted from the well containing the highest concentration of DNA.

Determination of DNA-NP and DNA/PEG3-NP Size, Shape, and Ligand Shell Composition before and after Incubation in 300 mM NaCl

UV-visible spectroscopy (Figure B1) was used to confirm that the DNA-NPs and DNA/PEG3-NPs maintained their overall size and shape during assembly. The UV-visible absorbance peaks collected after incubating the samples for 3 days in 300 mM NaCl had the same λmax and FWHM as before the incubation, which indicates that the DNA-NPs and DNA/PEG3-NPs maintained their core size and shape (Figure B1).

SAXS patterns were obtained as described in Appendix A, and used to determine the size and polydispersity of DNA-NP samples before and after incubation in 300 mM

NaCl solution (Table B1). While the core size of some AuNPs (originally 12.2 ±1.2 nm) had slightly increased during DNA functionalization, their size and polydispersity did not change appreciably as the result of incubating the AuNPs in buffered solutions containing 300 mM NaCl.

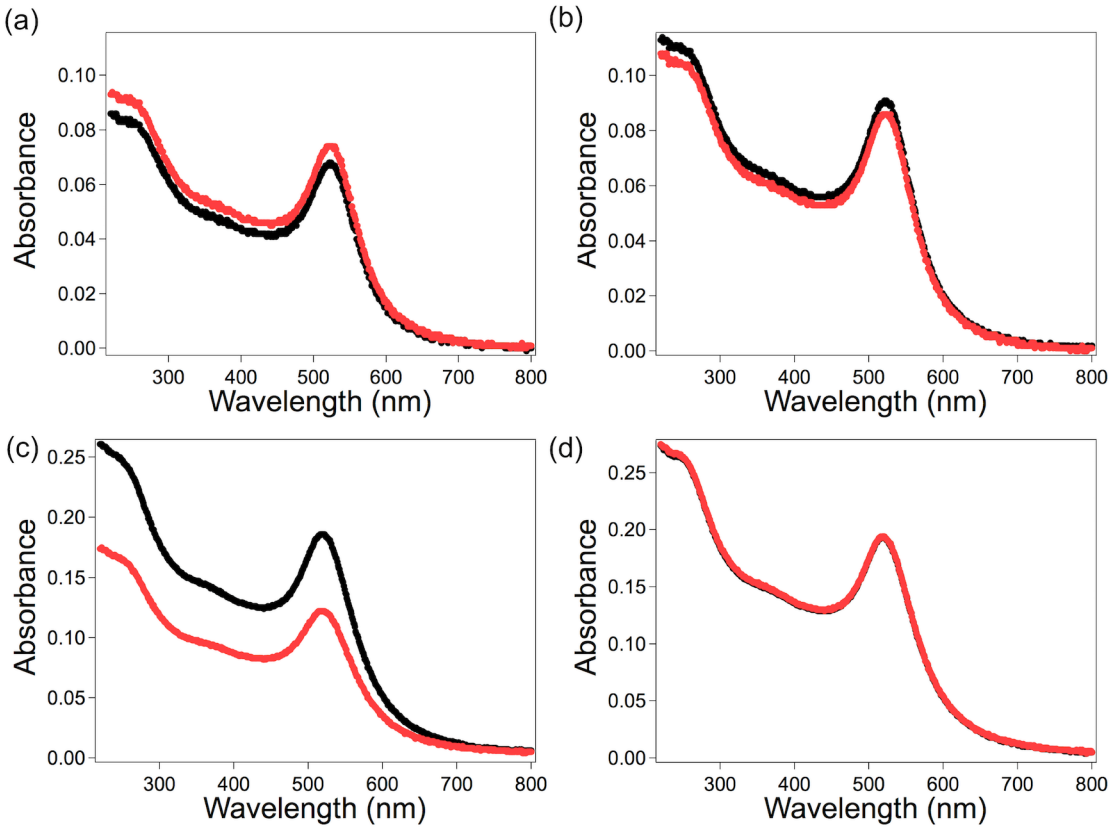

Figure B1: UV-visible spectra of DNA-NPs and DNA/PEG3-NPs before (black) and after (red) 300 mM NaCl incubation. Assembly System II: (a) Aptamer-NPs (b) cDNA-NPs. Assembly System IV: (c) Aptamer-NPs (d) cDNA-NPs

Table B1: Characterization of DNA-NP and DNA/PEG3-NP core size and polydispersity before and after 300 mM NaCl incubation

Assembly System (Figure 3.1)	DNA sequence	Core size/ polydispersity	Core size/ polydispersity
II	Aptamer	12.6±1.2	12.5±1.3
II	cDNA	12.7±1.2	12.6±1.0
IV	Aptamer	12.2±1.6	12.2±1.7
IV	cDNA	12.4±1.3	12.4±1.2

Determination of the Number of DNA Strands per AuNP using UV-visible Spectroscopy

UV-visible spectroscopy and fluorescence spectroscopy were used to determine the number of DNA strands per AuNP before and after incubation in 300 mM NaCl (Table B2). The number of DNA strands per AuNP was calculated by dividing the DNA concentration by the AuNP concentration. The concentration of AuNPs in each sample was determined using the A_{520} and calculated extinction coefficient of AuNPs of the same core size. The concentration of DNA was determined by decomposing the DNA-NPs using cyanide, mixing the resultant solution with Oligreen dye, and comparing the fluorescence of the resultant solution to a calibration curve prepared using pure DNA[2]. The PEG3 ligand absorbs light strongly at 260 nm, so UV-visible spectroscopy could not be used to quantify the ligand shell directly.

Table B2: Number of DNA strands per AuNP for DNA-NPs and DNA/PEG3-NPs before and after 300 mM NaCl incubation

Assembly System (Figure 3.1)	DNA sequence	Before incubation	After incubation
II	Aptamer	27±1	26±1
II	cDNA	124±1	122±1
IV	Aptamer	21±1	20±1
IV	cDNA	59±4	61±2

These results indicate that the ligand shell composition of the DNA-NPs and DNA/PEG3-NPs did not change as a result of being incubated in solutions containing 300 mM NaCl for 3 days during AuNP assembly.

Separation of Assemblies from Individual DNA/PEG3-NPs

Almost all DNA-NPs assembled into Assembly System II, and none of the DNA-NPs assembled into Assembly System III. Some, but not all, of the DNA/PEG3-NPs were incorporated into the pellet during centrifugation after incubation (Figure B2). Interestingly, the DNA/PEG3-NPs in the supernatant indicated exhibited changes in their UV-visible absorbance spectrum indicating that they partially assembled. In particular, their SPR peak shifted to longer wavelengths and their FWHM increased, but not as much as those DNA/PEG3-NPs in the pellet. This suggests a more nuanced assembly behavior. In future investigations, adding additional NaCl during DNA/PEG3-NP assembly may increase the proportion of the AuNPs that assemble.

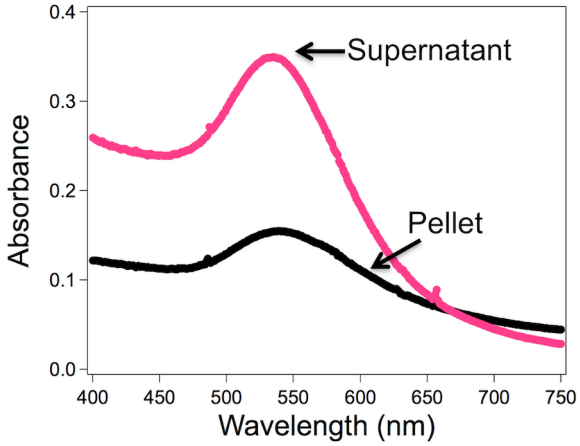

Figure B2: UV-visible spectra of DNA/PEG3-NPs in pellet and supernatant after centrifugation.

Preparation of DNA-NP and DNA/PEG3-NP Samples for TEM Analysis

To confirm that our TEM grid preparation method did not introduce experimental artifacts caused by drying effects, the same sample was prepared for TEM analysis with and without diluting the 10 uL droplet containing unassembled DNA/PEG3-NPs with water prior to transferring the grid to the rinse solution. It is clear from our TEM results that simply transferring the grid to the water rinse droplet causes the DNA/PEG3-NPs to stick together on the TEM grid, giving the appearance of assembly formation (Figure B3a). Diluting the droplet with 200 uL nanopure before transferring the grid to more water for a static rinse (float on water) allowed the DNA/PEG3-NPs to remain dispersed on the TEM grids (Figure B3b).

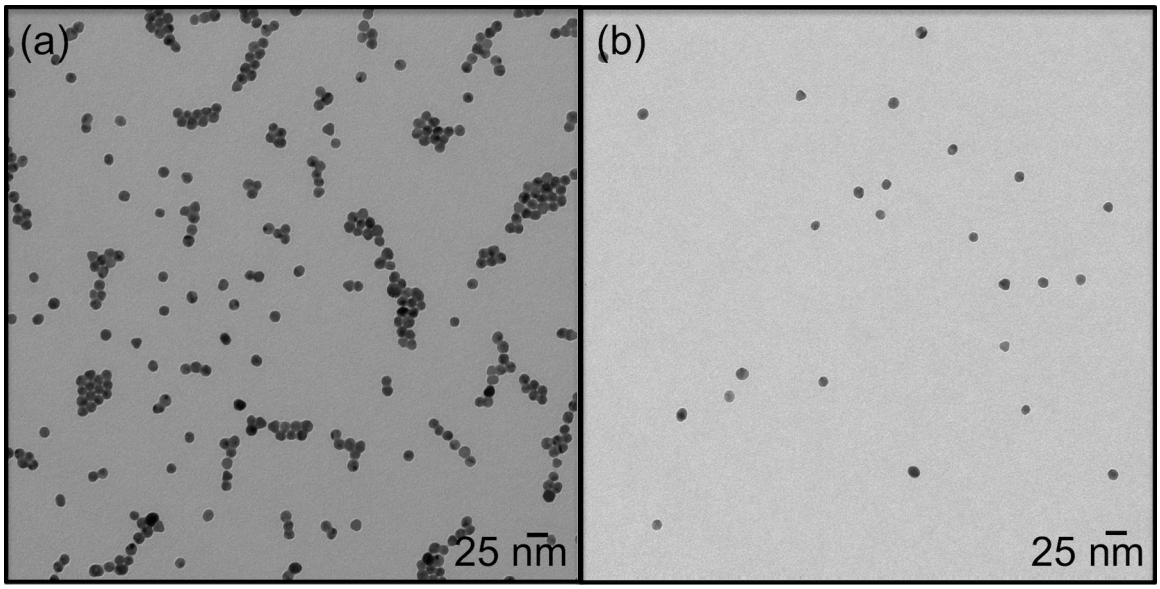

Figure B3: Representative TEM micrographs of individual DNA/PEG3-NPs from samples prepared (a) with and (b) without diluting the DNA/PEG3-NP solution with 200 uL nanopure water before transferring the grid to the rinse solution.

APPENDIX C

CHAPTER IV SUPPLEMENTARY INFORMATION

Materials and Methods

All DNA samples were purchased from Integrated DNA Technologies (Coralville, Iowa). DNA sequences were purified by either the standard desalting method or HPLC. A "Quant-It" OliGreen ssDNA Assay kit was purchased from Thermo Fisher Scientific (Grand Island, NY). Clear 1.5 mL microcentrifuge tubes and opaque polypropylene black 96 well plates (Costar) were purchased from VWR (Radnor, PA). Sodium citrate dihydrate, hydrogen tetrachloroaurate hydrate and UV-transparent 96 well plates (Corning) were purchased from Sigma Aldrich (St. Louis, Missouri). 2-[2-(2-chloroethoxy)- ethoxy]ethanol (99%) was purchased from Aldrich. Amine-functionalized TEM grids were purchased from Dune Sciences (Eugene, Oregon). A complete description of the synthetic method for producing the PEG3 ligand is available in Appendix C.

Instrumentation

UV-visible absorbance spectra of AuNP, DNA and DNA-NP solutions were obtained using either a BioTek Synergy 2 instrument, a Mikropack DH-2000 UV-vis-NIR light source equipped with an Ocean Optics USB2000 spectrophotometer or a Hewlett Packard 8453 spectrophotometer with HP ChemStation. UV-visible spectra of DNA were obtained using these or a Thermo Scientific Nanodrop 2000 spectrophotometer path length (10mm) and baseline corrected at 340nm.

The endpoint (after 5-15 minutes) fluorescent emission of the solutions were measured in 96-well opaque black well plates (Costar) using a Biotek Synergy 2 instument equipped with a tungsten lamp and filters (EX 485/20 nm, EM 528/20 nm). The data collection time was autoscaled, so that 80,000 counts were emitted from the well containing the highest concentration of DNA.

Designing Reaction Conditions for Preparing DNA/PEG3-NP Assemblies

Initially, we tried diluting the aptamer and cDNA ligand shells to the same extent using PEG3. Decreasing the number of recognition strands on each AuNP to below ~30% of their maximum surface coverage inhibited DNA-NP assembly.

Given that DNA/PEG3-NPs functionalized with a range of different aptamer surface coverages were able to assemble with AuNPs functionalized with an intermediate number of cDNA ligands (55 cDNA strands per AuNP), we were surprised that our DNA/PEG3-NPs functionalized with diluted cDNA ligand shells (below approximately 45 per AuNP) could not bind aptamer-functionalized AuNPs over any reasonable time frame. Decreasing the number of DNA recognition strands is expected to lower the enthalpy and entropy costs of assembling DNA-NPs that arise from electrostatic repulsion, while providing greater accessibility for binding.[2] DNA-NP assembly may be inhibited when the recognition strand coverage on both sets of AuNPs is diluted because (i) there is a lower probability that multiple DNA bonds between DNA-NP will form, and (ii) individual bonds between DNA strands on AuNP surfaces will be less enduring due to the reversible nature of the AuNP hybridization process.

DNA strand hybridization to DNA-functionalized surfaces is reversible, and DNA strands have a large probability of desorbing and performing a brief search for another

binding ligand in the near vicinity.[3] Successful (e.g. enduring) DNA-NP hybridization may therefore require the availability of multiple unhybridized DNA strands nearby the initial binding strand, which may not be the case for DNA-NPs with significantly diluted ligand shells.

Assessing DNA/PEG3-NP Stability during Assembly and Reaction with Adenosine

UV-visible spectroscopy (Figure C1) and SAXS (Table C1) were used to confirm that DNA/PEG3-NPs retained their size and shape during assembly in solutions containing 600 mM NaCl.

The TEM micrographs of the DNA/PEG3-NP assemblies (Figure 4.5) confirmed that the AuNPs remained spherical and maintained a similar core size before and after the incubation. The UV-visible absorbance spectra of DNA/PEG3-NPs incubated individually in 600 mM NaCl confirmed that the AuNPs retained roughly the same size and shape, as their λmax did not shift to longer wavelengths and their FWHM stayed the same (Figure C1).

SAXS patterns were obtained as described in Appendix A, and used to determine the size and polydispersity of DNA-NP samples before and after incubation in 600 mM NaCl solution (Table C1). While the core size of some AuNPs (originally 12.2 ±1.2 nm) had slightly increased during DNA functionalization, their size and polydispersity did not change appreciably as the result of incubating the AuNPs in buffered solutions containing 600 mM NaCl (Table C1). Their core size and polydispersity remained the same for at least 3 weeks after ligand exchange (data not shown).

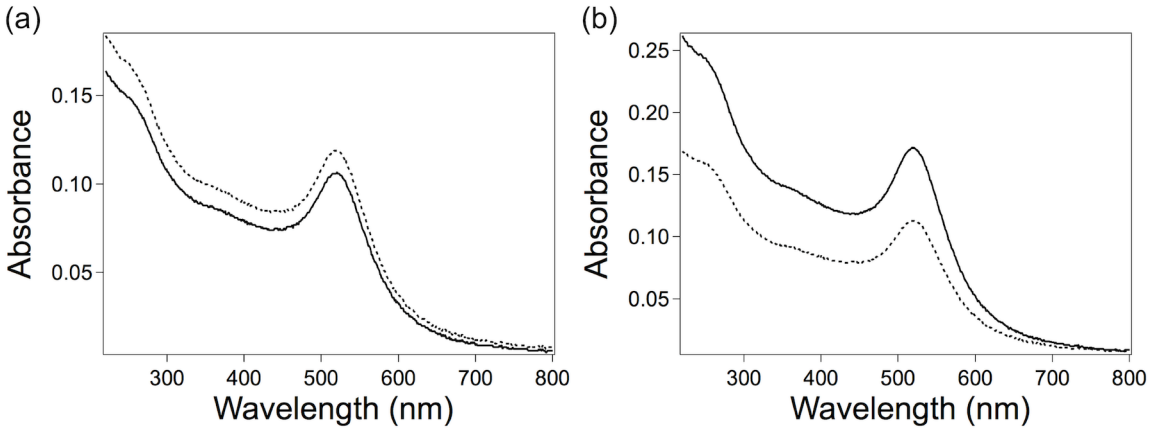

Figure C1: UV-visible spectra of DNA/PEG3-NPs before (solid line) and after (dashed line) 600 mM NaCl incubation. (a) Aptamer/PEG3-NPs functionalized with 24 aptamers per AuNP (b) cDNA/PEG3-NPs

Table C1: Characterization of DNA/PEG3-NP core size and polydispersity before and after 600 mM NaCl incubation

DNA strands per AuNP	DNA sequence	Core size/ polydispersity	Core size/ polydispersity
20	Aptamer	12.2±1.6	12.2±1.7
24	Aptamer	11.8±1.5	12.2±1.2
55	cDNA	12.4±1.3	12.4±1.2

UV-visible and fluorescence spectroscopy quantification of the DNA/PEG3-NP ligand shell confirmed that the number of DNA strands per AuNP did not change appreciably as a result of the DNA/PEG3-NPs being incubated in solutions containing 600 mM NaCl (Table C2).

Table C2: Number of DNA strands per AuNP for DNA/PEG3-NPs before and after 600 mM NaCl incubation

Target # DNA strands per AuNP	DNA sequence	Before incubation	After incubation
20	Aptamer	19.8±0.6	18±3
24	Aptamer	25.5±0.6	26±3
55	cDNA	59±4	61±2

The ligand shell of our DNA/PEG3-NPs did begin to decompose in water within 20 days after completing the ligand exchange, as reported by others.[4] They did not experience ligand loss as a result of being incubated in 600 mM NaCl for 4 days, but it would be unsurprising if they also began to decompose if stored in our assembly conditions over long time intervals. We therefore recommend that these nanoparticles be used soon after being prepared (as we did in our study). Alternately, AuNP samples can also be formulated to remain in tact when freeze-dried[5], and sucrose has been identified as a method to preserve assembled the reactivity of assembled DNA-NPs[6] during this procedure.

TEM Analysis of Reaction between DNA/PEG3-NPs and Adenosine

TEM analysis confirmed that the DNA/PEG3-NPs separated in solution after their reaction with adenosine, because no DNA/PEG3-NP assemblies were present on TEM grids prepared from those samples (Figure C2).

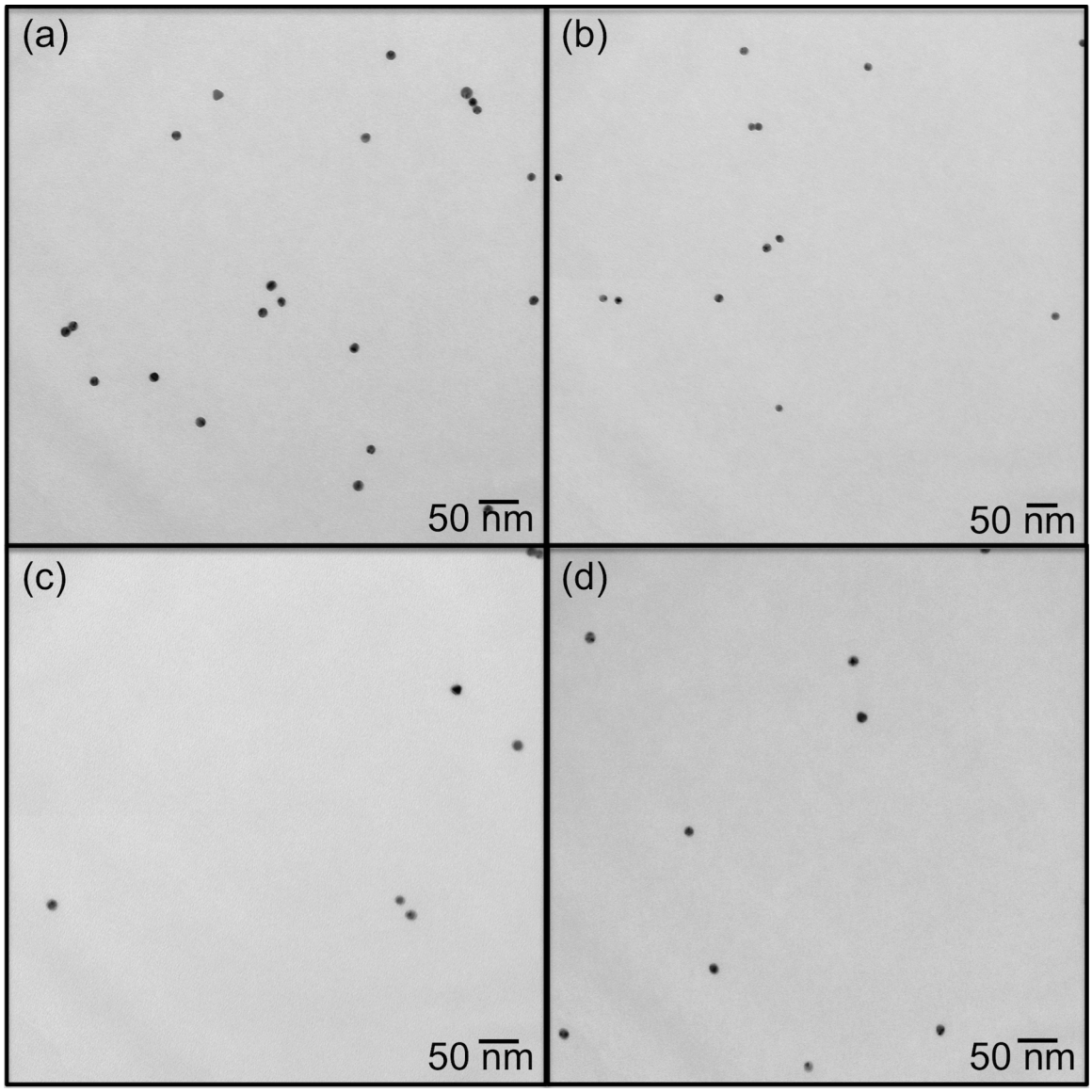

Figure C2: Representative TEM micrographs of DNA/PEG3-NPs after reacting with adenosine

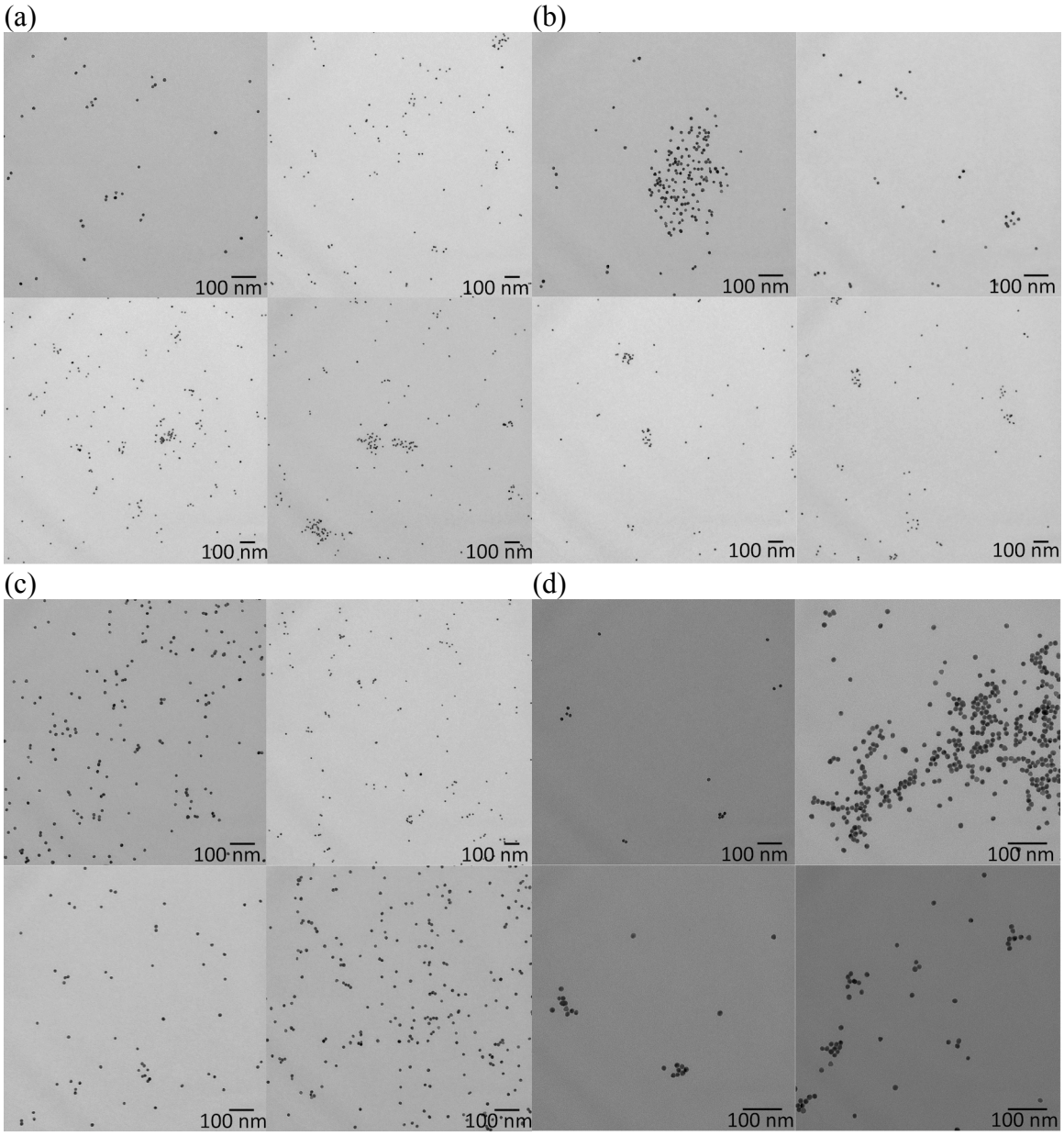

Figure C3: Additional TEM micrographs of AuNP assemblies formed from reacting cDNA/PEG3-NPs with apt/PEG3-NPs functionalized with (a) 20 (b) 24 (c) 30 or (d) 35 aptamers per AuNP

REFERENCES CITED

CHAPTER I

(1) Anker, J. N.; Hall, W. P.; Lyandres, O.; Shah, N. C.; Zhao, J.; Van Duyne, R. P. Biosensing with Plasmonic Nanosensors. *Nat. Mater.* **2008**, *7*, 442–453.

(2) Saha, K.; Agasti, S. S.; Kim, C.; Li, X.; Rotello, V. M. Gold Nanoparticles in Chemical and Biological Sensing. *Chem. Rev.* **2012**, *112*, 2739–2779.

(3) Zhao, W.; Brook, M. A.; Li, Y. Design of Gold Nanoparticle-Based Colorimetric Biosensing Assays. *ChemBioChem* **2008**, *9*, 2363–2371.

(4) He, Q.; Shi, J. Mesoporous Silica Nanoparticle Based Nano Drug Delivery Systems: Synthesis, Controlled Drug Release and Delivery, Pharmacokinetics and Biocompatibility. *J. Mater. Chem.* **2011**, *21*, 5845.

(5) Tang, F.; Li, L.; Chen, D. Mesoporous Silica Nanoparticles: Synthesis, Biocompatibility and Drug Delivery. *Adv. Mater.* **2012**, *24*, 1504–1534.

(6) Dreaden, E. C.; Alkilany, A. M.; Huang, X.; Murphy, C. J.; El-Sayed, M. A. The Golden Age: Gold Nanoparticles for Biomedicine. *Chem. Soc. Rev.* **2012**, *41*, 2740.

(7) Ghosh, P.; Han, G.; De, M.; Kim, C. K.; Rotello, V. M. Gold Nanoparticles in Delivery Applications. *Adv. Drug Deliv. Rev.* **2008**, *60*, 1307–1315.

(8) Chithrani, B. D.; Ghazani, A. A.; Chan, W. C. W. Determining the Size and Shape Dependence of Gold Nanoparticle Uptake into Mammalian Cells. *Nano Lett.* **2006**, *6*, 662–668.

(9) Lal, S.; Clare, S. E.; Halas, N. J. Nanoshell-Enabled Photothermal Cancer Therapy: Impending Clinical Impact. *Acc. Chem. Res.* **2008**, *41*, 1842–1851.

(10) Huang, X.; El-Sayed, M. A. Gold Nanoparticles: Optical Properties and Implementations in Cancer Diagnosis and Photothermal Therapy. *J. Adv. Res.* **2010**, *1*, 13–28.

(11) Rosi, N. L.; Mirkin, C. A. Nanostructures in Biodiagnostics. *Chem. Rev.* **2005**, *105*, 1547–1562.

(12) Smith, A. M.; Nie, S. Semiconductor Nanocrystals: Structure, Properties, and Band Gap Engineering. *Acc. Chem. Res.* **2010**, *43*, 190–200.

(13) Daniel, M. C.; Astruc, D. Gold Nanoparticles: Assembly, Supramolecular Chemistry, Quantum-Size-Related Properties, and Applications Toward Biology, Catalysis, and Nanotechnology. *Chem. Rev.* **2004**, *104*, 293–346.

(14) Lohse, S. E.; Murphy, C. J. Applications of Colloidal Inorganic Nanoparticles: From Medicine to Energy. *J. Am. Chem. Soc.* **2012**, *134*, 15607–15620.

(15) Eustis, S.; el-Sayed, M. A. Why Gold Nanoparticles Are More Precious than Pretty Gold: Noble Metal Surface Plasmon Resonance and Its Enhancement of the Radiative and Nonradiative Properties of Nanocrystals of Different Shapes. *Chem. Soc. Rev.* **2006**, *35*, 209–217.

(16) Mok, W.; Li, Y. Recent Progress in Nucleic Acid Aptamer-Based Biosensors and Bioassays. *Sensors* **2008**, *8*, 7050–7084.

(17) Chiu, T.-C.; Huang, C.-C. *Aptamer-Functionalized Nano-Biosensors*; 2009; Vol. 9.

(18) E. Wang, R.; Zhang, Y.; Cai, J.; Cai, W.; Gao, T. Aptamer-Based Fluorescent Biosensors. *Curr. Med. Chem.* **2011**, *18*, 4175–4184.

(19) Song, S.; Wang, L.; Li, J.; Fan, C.; Zhao, J. Aptamer-Based Biosensors. *TrAC Trends Anal. Chem.* **2008**, *27*, 108–117.

(20) Han, K.; Liang, Z.; Zhou, N. Design Strategies for Aptamer-Based Biosensors. *Sensors* **2010**, *10*, 4541–4557.

(21) Liu, J.; Cao, Z.; Lu, Y. *Functional Nucleic Acid Sensors Functional Nucleic Acid Sensors*; 2009; Vol. 109.

(22) Navani, N. K.; Li, Y. Nucleic Acid Aptamers and Enzymes as Sensors. *Curr. Opin. Chem. Biol.* **2006**, *10*, 272–281.

(23) Strehlitz, B.; Nikolaus, N.; Stoltenburg, R. Protein Detection with Aptamer Biosensors. *Sensors* **2008**, *8*, 4296–4307.

(24) Lee, J. O.; So, H. M.; Jeon, E. K.; Chang, H.; Won, K.; Kim, Y. H. Aptamers as Molecular Recognition Elements for Electrical Nanobiosensors. *Anal. Bioanal. Chem.* **2008**, *390*, 1023–1032.

(25) Song, S.; Qin, Y.; He, Y.; Huang, Q.; Fan, C.; Chen, H.-Y. Functional Nanoprobes for Ultrasensitive Detection of Biomolecules. *Chem. Soc. Rev.* **2010**, *39*, 4234.

(26) Rana, S.; Bajaj, A.; Mout, R.; Rotello, V. M. Monolayer Coated Gold Nanoparticles for Delivery Applications. *Adv. Drug Deliv. Rev.* **2012**, *64*, 200–216.

(27) Paliwoda, R. E.; Li, F.; Reid, M. S.; Lin, Y.; Le, X. C. Sequential Strand Displacement Beacon for Detection of DNA Coverage on Functionalized Gold Nanoparticles Sequential Strand Displacement Beacon for Detection of DNA Coverage on Functionalized Gold Nanoparticles. **2014**.

(28) Anderson, B. J.; Larkin, C.; Guja, K.; Schildbach, J. F. *Chapter 12 Using Fluorophore-Labeled Oligonucleotides to Measure Affinities of Protein-DNA Interactions*; 1st ed.; Elsevier Inc., 2008; Vol. 450.

(29) Knutson, T. R.; Knutson, C. M.; Mozzetti, A. R.; Campos, A. R.; Haynes, C. L.; Penn, R. L. A Fresh Look at the Crystal Violet Lab with Handheld Camera Colorimetry. *J. Chem. Educ.* **2015**, 150407093912003.

(30) Askim, J. R.; Suslick, K. S. Hand-Held Reader for Colorimetric Sensor Arrays. *Anal. Chem.* **2015**, 150715155014002.

(31) Moores, A.; Goettmann, F. The Plasmon Band in Noble Metal Nanoparticles: An Introduction to Theory and Applications. *New J. Chem.* **2006**, *30*, 1121.

(32) Prigodich, A. E.; Randeria, P. S.; Briley, W. E.; Kim, N. J.; Daniel, W. L.; Giljohann, D. a.; Mirkin, C. a. Multiplexed Nanoflares: MRNA Detection in Live Cells. *Anal. Chem.* **2012**, *84*, 2062–2066.

(33) Li, X.; Guo, J.; Asong, J.; Wolfert, M. A.; Boons, G. J. Multifunctional Surface Modification of Gold-Stabilized Nanoparticles by Bioorthogonal Reactions. *J. Am. Chem. Soc.* **2011**, *133*, 11147–11153.

(34) Pellegrino, T.; Kudera, S.; Liedl, T.; Javier, A. M.; Manna, L.; Parak, W. J. On the Development of Colloidal Nanoparticles towards Multifunctional Structures and Their Possible Use for Biological Applications. *Small* **2005**, *1*, 48–63.

(35) Rechberger, W.; Hohenau, A.; Leitner, A.; Krenn, J. R.; Lamprecht, B.; Aussenegg, F. R. Optical Properties of Two Interacting Gold Nanoparticles. *Opt. Commun.* **2003**, *220*, 137–141.

(36) Ghosh, S. K.; Pal, T. Interparticle Coupling Effect on the Surface Plasmon Resonance of Gold Nanoparticles: From Theory to Applications. *Chem. Rev.* **2007**, *107*, 4797–4862.

(37) Pei, H.; Li, F.; Wan, Y.; Wei, M.; Liu, H.; Su, Y.; Chen, N.; Huang, Q.; Fan, C. Designed Diblock Oligonucleotide for the Synthesis of Spatially Isolated and Highly Hybridizable Functionalization of DNA-Gold Nanoparticle Nanoconjugates. *J. Am. Chem. Soc.* **2012**, *134*, 11876–11879.

(38) Garrett, R. H.; Grisham, C. M. *Biochemistry*; Kiselica, S.; Williams, P., Eds.; 3rd ed.; Thomson Learning, Brooks/Cole, 2005.

(39) Ostblom, M.; Liedberg, B.; Demers, L.; Mirkin, C. On the Structure and Desorption Dynamics of DNA Bases Adsorbed on Gold: A Temperature-Programmed Study. *J Phys Chem B* **2005**, *109*, 15150–15160.

(40) Wolf, L. K.; Gao, Y.; Georgiadis, R. M. Sequence-Dependent DNA Immobilization: Specific versus Nonspecific Contributions. *Langmuir* **2004**, *20*, 3357–3361.

(41) Steel, A. B.; Levicky, R. L.; Herne, T. M.; Tarlov, M. J. Immobilization of Nucleic Acids at Solid Surfaces: Effect of Oligonucleotide Length on Layer Assembly. *Biophys. J.* **2000**, *79*, 975–981.

(42) Hurst, S. J.; Lytton-Jean, A. K. R.; Mirkin, C. A. Maximizing DNA Loading on a Range of Gold Nanoparticle Sizes. *Anal. Chem.* **2006**, *78*, 8313–8318.

(43) Zhang, X.; Servos, M. R.; Liu, J. Instantaneous and Quantitative Functionalization of Gold Nanoparticles with Thiolated DNA Using a pH-Assisted and Surfactant-Free Route. *J. Am. Chem. Soc.* **2012**, *134*, 7266–7269.

(44) Zhang, X.; Gouriye, T.; Göeken, K.; Servos, M. R.; Gill, R.; Liu, J. Toward Fast and Quantitative Modification of Large Gold Nanoparticles by Thiolated DNA: Scaling of Nanoscale Forces, Kinetics, and the Need for Thiol Reduction. *J. Phys. Chem. C* **2013**, *117*, 15677–15684.

(45) Zhang, X.; Servos, M. R.; Liu, J. Surface Science of DNA Adsorption onto Citrate-Capped Gold Nanoparticles. *Langmuir* **2012**, *28*, 3896–3902.

(46) Sandström, P.; Boncheva, M.; Åkerman, B. Nonspecific and Thiol-Specific Binding of DNA to Gold Nanoparticles. *Langmuir* **2003**, *19*, 7537–7543.

(47) Nassef, H. M.; Bermudo Redondo, M. C.; Ciclitira, P. J.; Ellis, H. J.; Fragoso, A.; O'Sullivan, C. K. Electrochemical Immunosensor for Detection of Celiac Disease Toxic Gliadin in Foodstuff. *Anal. Chem.* **2008**, *80*, 9265–9271.

(48) Peterson, A. W.; Heaton, R. J.; Georgiadis, R. M. The Effect of Surface Probe Density on DNA Hybridization. *Nucleic Acids Res.* **2001**, *29*, 5163–5168.

(49) Herne, T. M.; Tarlov, M. J. Characterization of DNA Probes Immobilized on Gold Surfaces. *J. Am. Chem. Soc.* **1997**, *119*, 8916–8920.

(50) Demers, L. M.; Mirkin, C. A; Mucic, R. C.; Reynolds, R. A.; Letsinger, R. L.; Elghanian, R.; Viswanadham, G. A Fluorescence-Based Method for Determining the Surface Coverage and Hybridization Efficiency of Thiol-Capped Oligonucleotides Bound to Gold Thin Films and Nanoparticles. *Anal. Chem.* **2000**, *72*, 5535–5541.

(51) Park, S.; Brown, K. A.; Hamad-Schifferli, K. Changes in Oligonucleotide Conformation on Nanoparticle Surfaces by Modification with Mercaptohexanol. *Nano Lett.* **2004**, *4*, 1925–1929.

(52) Brown, K. A.; Park, S.; Hamad-Schifferli, K. Nucleotide-Surface Interactions in DNA-Modified Au-Nanoparticle Conjugates: Sequence Effects on Reactivity and Hybridization. *J. Phys. Chem. C* **2008**, *112*, 7517–7521.

(53) Randeria, P. S.; Jones, M. R.; Kohlstedt, K. L.; Banga, R. J.; Olvera de la Cruz, M.; Schatz, G. C.; Mirkin, C. a. What Controls the Hybridization Thermodynamics of Spherical Nucleic Acids? *J. Am. Chem. Soc.* **2015**, 150304145409002.

(54) Das, P.; Zafar, S. Mechanistic In Fl Uence of Nanometer Length-Scale Surface Chemistry on DNA Hybridization. **2015**.

(55) Jones, M. R.; Seeman, N. C.; Mirkin, C. A. Programmable Materials and the Nature of the DNA Bond. *Science (80-.).* **2015**, *347*, 1260901–1260901.

(56) Kang, B.; Mackey, M. A.; El-Sayed, M. A. Nuclear Targeting of Gold Nanoparticles in Cancer Cells Induces DNA Damage, Causing Cytokinesis Arrest and Apoptosis. *J. Am. Chem. Soc.* **2010**, *132*, 1517–1519.

(57) Park, K.; Lee, S.; Kang, E.; Kim, K.; Choi, K.; Kwon, I. C. New Generation of Multifunctional Nanoparticles for Cancer Imaging and Therapy. *Adv. Funct. Mater.* **2009**, *19*, 1553–1566.

(58) Storhoff, J. J.; Elghanian, R.; Mucic, R. C.; Mirkin, C. A.; Letsinger, R. L. Article One-Pot Colorimetric Differentiation of Polynucleotides with Single Base Imperfections Using Gold Nanoparticle Probes One-Pot Colorimetric Differentiation of Polynucleotides with Single Base Imperfections Using Gold Nanoparticle Probes. **1998**, *7863*, 1959–1964.

(59) Rosi, N. L.; Giljohann, D. A.; Thaxton, C. S.; Lytton-Jean, A. K. R.; Han, M. S.; Mirkin, C. A. Oligonucleotide-Modified Gold Nanoparticles for Intracellular Gene Regulation. *Science* **2006**, *312*, 1027–1030.

(60) Mirkin, C. A.; Letsinger, R. L.; Mucic, R. C.; Storhoff, J. J. A DNA-Based Method for Rationally Assembling Nanoparticles into Macroscopic Materials. *Nature*, 1996, *382*, 607–609.

(61) Elghanian, R. Selective Colorimetric Detection of Polynucleotides Based on the Distance-Dependent Optical Properties of Gold Nanoparticles. *Science (80-.).* **1997**, *277*, 1078–1081.

(62) Jin, R.; Wu, G.; Li, Z.; Mirkin, C. A.; Schatz, G. C. What Controls the Melting Properties of DNA-Linked Gold Nanoparticle Assemblies? *J. Am. Chem. Soc.* **2003**, *125*, 1643–1654.

(63) Lytton-Jean, A. K. R.; Mirkin, C. A. A Thermodynamic Investigation into the Binding Properties of DNA Functionalized Gold Nanoparticle Probes and Molecular Fluorophore Probes. *J. Am. Chem. Soc.* **2005**, *127*, 12754–12755.

(64) Nykypanchuk, D.; Maye, M. M.; van der Lelie, D.; Gang, O. DNA-Guided Crystallization of Colloidal Nanoparticles. *Nature* **2008**, *451*, 549–552.

(65) Maye, M. M.; Nykypanchuk, D.; Van Der Lelie, D.; Gang, O. A Simple Method for Kinetic Control of DNA-Induced Nanoparticle Assembly. *J. Am. Chem. Soc.* **2006**, *128*, 14020–14021.

(66) Macfarlane, R. J.; Lee, B.; Hill, H. D.; Senesi, A. J.; Seifert, S.; Mirkin, C. A. Molecular Recognition and Self-Assembly Special Feature: Assembly and Organization Processes in DNA-Directed Colloidal Crystallization. *Proc. Natl. Acad. Sci. U. S. A.* **2009**, *106*, 10493–10498.

(67) Park, S. Y.; Lytton-Jean, A. K. R.; Lee, B.; Weigand, S.; Schatz, G. C.; Mirkin, C. A. DNA-Programmable Nanoparticle Crystallization. *Nature* **2008**, *451*, 553–556.

(68) Macfarlane, R. J.; Lee, B.; Jones, M. R.; Harris, N.; Schatz, G. C.; Mirkin, C. A. Nanoparticle Superlattice Engineering with DNA. *Science (80-.).* **2011**, *334*, 204–208.

(69) Angioletti-Uberti, S.; Varilly, P.; Mognetti, B. M.; Frenkel, D. Mobile Linkers on DNA-Coated Colloids: Valency without Patches. *arXiv Prepr. arXiv ...* **2014**, *1*, 1–14.

(70) Smith, B. D.; Dave, N.; Huang, P.-J. J. J.; Liu, J. Assembly of DNA-Functionalized Gold Nanoparticles with Gaps and Overhangs in Linker DNA. *J. Phys. Chem. C* **2011**, *115*, 7851–7857.

(71) Gan, S. D.; Patel, K. R. Enzyme Immunoassay and Enzyme-Linked Immunosorbent Assay. *J. Invest. Dermatol.* **2013**, *133*, e12.

(72) Posthuma-Trumpie, G. A.; Korf, J.; Van Amerongen, A. Lateral Flow (immuno)assay: Its Strengths, Weaknesses, Opportunities and Threats. A Literature Survey. *Anal. Bioanal. Chem.* **2009**, *393*, 569–582.

(73) Nicholas, M. W.; Nelson, K. North, South, or East? Blotting Techniques. *J. Invest. Dermatol.* **2013**, *133*, e10.

(74) O'Sullivan, C. K. Aptasensors--the Future of Biosensing? *Anal. Bioanal. Chem.* **2002**, *372*, 44–48.

(75) Hermann, T.; Patel, D. J. Adaptive Recognition by Nucleic Acid Aptamers. *Science* **2000**, *287*, 820–825.

(76) Ding, J.; Gu, Y.; Li, F.; Zhang, H.; Qin, W. DNA Nanostructure-Based Magnetic Beads for Potentiometric Aptasensing. *Anal. Chem.* **2015**, *87*, 6465–6469.

(77) Lao, Y.-H.; Phua, K. K. L.; Leong, K. W. Aptamer Nanomedicine for Cancer Therapeutics: Barriers and Potential for Translation. *ACS Nano* **2015**, *9*, 2235–2254.

(78) Famulok, M. Oligonucleotide Aptamers That Recognize Small Molecules. *Curr. Opin. Struct. Biol.* **1999**, *9*, 324–329.

(79) Tombelli, S.; Mascini, M. Aptamers Biosensors for Pharmaceutical Compounds. *Comb. Chem. High Throughput Screen.* **2010**, *13*, 641–649.

(80) Liu, J.; Lu, Y. Adenosine-Dependent Assembly of Aptazyme-Functionalized Gold Nanoparticles and Its Application as a Colorimetric Biosensor. *Anal. Chem.* **2004**, *76*, 1627–1632.

(81) Lehrer, S. B.; Ayuso, R.; Reese, G. Seafood Allergy and Allergens: A Review. *Mar. Biotechnol.* **2003**, *5*, 339–348.

(82) Liu, H.; Malhotra, R.; Peczuh, M. W.; Rusling, J. F. Electrochemical Immunosensors for Antibodies to Peanut Allergen Ara h2 Using Gold Nanoparticle-Peptide Films. *Anal. Chem.* **2010**, *82*, 5865–5871.

(83) Wang, Z.; Zhang, J.; Ekman, J. M.; Kenis, P. J. A.; Lu, Y. DNA-Mediated Control of Metal Nanoparticle Shape: One-Pot Synthesis and Cellular Uptake of Highly Stable and Functional Gold Nanoflowers. *Nano Lett.* **2010**, *10*, 1886–1891.

(84) Wang, W.; Han, J.; Wu, Y.; Yuan, F.; Chen, Y.; Ge, Y. Simultaneous Detection of Eight Food Allergens Using Optical Thin-Film Biosensor Chips. *J. Agric. Food Chem.* **2011**, *59*, 6889–6894.

(85) Torres-Chavolla, E.; Alocilja, E. C. Aptasensors for Detection of Microbial and Viral Pathogens. *Biosens. Bioelectron.* **2009**, *24*, 3175–3182.

(86) Fischer, N. O.; Tarasow, T. M.; Tok, J. B. H. Aptasensors for Biosecurity Applications. *Curr. Opin. Chem. Biol.* **2007**, *11*, 316–328.

(87) Chen, Y. M.; Yu, C. J.; Cheng, T. L.; Tseng, W. L. Colorimetric Detection of Lysozyme Based on Electrostatic Interaction with Human Serum Albumin-Modified Gold Nanoparticles. *Langmuir* **2008**, *24*, 3654–3660.

(88) He, L. L.; Rodda, T.; Haynes, C. L.; Deschaines, T.; Strother, T.; Diez-Gonzalez, F.; Labuza, T. P. Detection of a Foreign Protein in Milk Using Surface-Enhanced Raman Spectroscopy Coupled with Antibody-Modified Silver Dendrites. *Anal. Chem.* **2011**, *83*, 1510–1513.

(89) Kirby, R.; Cho, E. J.; Gehrke, B.; Bayer, T.; Park, Y. S.; Neikirk, D. P.; McDevitt, J. T.; Ellington, A. D. Aptamer-Based Sensor Arrays for the Detection and Quantitation of Proteins. *Anal. Chem.* **2004**, *76*, 4066–4075.

(90) Medley, C. D.; Smith, J. E.; Tang, Z.; Wu, Y.; Bamrungsap, S.; Tan, W. Gold Nanoparticle-Based Colorimetric Assay for the Direct Detection of Cancerous Cells. *Anal. Chem.* **2008**, *80*, 1067–1072.

(91) Pavlov, V.; Xiao, Y.; Shlyahovsky, B.; Willner, I. Aptamer-Functionalized Au Nanoparticles for the Amplified Optical Detection of Thrombin. *J. Am. Chem. Soc.* **2004**, *126*, 11768–11769.

(92) Huang, C.-C.; Huang, Y.-F.; Cao, Z.; Tan, W.; Chang, H.-T. Aptamer-Modified Gold Nanoparticles for Colorimetric Determination of Platelet-Derived Growth Factors and Their Receptors. *Anal. Chem.* **2005**, *77*, 5735–5741.

(93) Lee, J. S.; Han, M. S.; Mirkin, C. A. Colorimetric Detection of Mercuric Ion (Hg2+) in Aqueous Media Using DNA-Functionalized Gold Nanoparticles. *Angew. Chemie - Int. Ed.* **2007**, *46*, 4093–4096.

(94) Sun, D.; Lu, J.; Chen, Z.; Yu, Y.; Mo, M. A Repeatable Assembling and Disassembling Electrochemical Aptamer Cytosensor for Ultrasensitive and Highly Selective Detection of Human Liver Cancer Cells. *Anal Chim Acta* **2015**, *885*, 166–173.

(95) Liu, J.; Lu, Y. Fast Colorimetric Sensing of Adenosine and Cocaine Based on a General Sensor Design Involving Aptamers and Nanoparticles. *Angew. Chemie - Int. Ed.* **2005**, *45*, 90–94.

(96) Liu, J.; Lu, Y. Non-Base Pairing DNA Provides a New Dimension for Controlling Aptamer-Linked Nanoparticles and Sensors. *J. Am. Chem. Soc.* **2007**, *129*, 8634–8643.

(97) Xiao, R.; Wang, D.; Lin, Z.; Qiu, B.; Liu, M.; Guo, L.; Chen, G. Disassembly of Gold Nanoparticle Dimers for Colorimetric Detection of Ochratoxin A. *Anal. Methods* **2015**, *7*, 842–845.

(98) Li, L.; Li, B.; Qi, Y.; Jin, Y. Label-Free Aptamer-Based Colorimetric Detection of Mercury Ions in Aqueous Media Using Unmodified Gold Nanoparticles as Colorimetric Probe. *Anal. Bioanal. Chem.* **2009**, *393*, 2051–2057.

(99) Liu, J.; Lu, Y. Preparation of Aptamer-Linked Gold Nanoparticle Purple Aggregates for Colorimetric Sensing of Analytes. *Nat. Protoc.* **2006**, *1*, 246–252.

(100) Gopinath, S. C. B.; Lakshmipriya, T.; Awazu, K. Colorimetric Detection of Controlled Assembly and Disassembly of Aptamers on Unmodified Gold Nanoparticles. *Biosens. Bioelectron.* **2014**, *51*, 115–123.

(101) Soh, J. H.; Lin, Y.; Rana, S.; Ying, J. Y.; Stevens, M. M. Colorimetric Detection of Small Molecules in Complex Matrixes via Target-Mediated Growth of Aptamer-Functionalized Gold Nanoparticles. *Anal. Chem.* **2015**, 150721144153000.

(102) Zhao, W.; Ali, M. M.; Aguirre, S. D.; Brook, M. A.; Li, Y. Paper-Based Bioassays Using Gold Nanoparticle Colorimetric Probes. *Anal. Chem.* **2008**, *80*, 8431–8437.

(103) Liu, J.; Mazumdar, D.; Lu, Y. A Simple and Sensitive "Dipstick" Test in Serum Based on Lateral Flow Separation of Aptamer-Linked Nanostructures. *Angew. Chemie - Int. Ed.* **2006**, *45*, 7955–7959.

(104) Sivaraman, S. K.; Kumar, S.; Santhanam, V. Monodisperse Sub-10nm Gold Nanoparticles by Reversing the Order of Addition in Turkevich Method - The Role of Chloroauric Acid. *J. Colloid Interface Sci.* **2011**, *361*, 543–547.

(105) Frens, G. Controlled Nucleation for the Regulation of the Particle Size in Monodisperse Gold Suspensions. *Nat. Phys. Sci.* **1973**, *241*, 20–22.

(106) Wuithschick, M.; Birnbaum, A.; Witte, S.; Sztucki, M.; Vainio, U.; Pinna, N.; Rademann, K.; Emmerling, F.; Kraehnert, R. Turkevich in New Robes : Key Questions Answered for the Most Common Gold Nanoparticle Synthesis. **2015**, 7052–7071.

(107) Richman, E. K.; Hutchison, J. E. Bottleneck. **2009**, *3*, 2441–2446.

(108) Haiss, W.; Thanh, N. T. K.; Aveyard, J.; Fernig, D. G. Determination of Size and Concentration of Gold Nanoparticles from UV - Vis Spectra. **2007**, *79*, 4215–4221.

(109) Liu, X.; Atwater, M.; Wang, J.; Huo, Q. Extinction Coefficient of Gold Nanoparticles with Different Sizes and Different Capping Ligands. *Colloids Surfaces B Biointerfaces* **2007**, *58*, 3–7.

(110) Hendel, T.; Wuithschick, M.; Kettemann, F.; Birnbaum, A.; Rademann, K. In-Situ Determination of Colloidal Gold Concentrations with UV-Vis Spectroscopy : Limitations and Perspectives. *4*.

(111) Jain, P. K.; Huang, W.; El-sayed, M. A. On the Universal Scaling Behavior of the Distance Decay of Plasmon Coupling in Metal Nanoparticle Pairs : A Plasmon Ruler Equation On the Universal Scaling Behavior of the Distance Decay of Plasmon Coupling in Metal Nanoparticle Pairs : A Plasmon Ruler Eq. *Nano* **2007**.

(112) Storhoff, J. J.; Lazarides, A. A.; Mucic, R. C.; Mirkin, C. A.; Letsinger, R. L.; Schatz, G. C. What Controls the Optical Properties of DNA-Linked Gold Nanoparticle Assemblies? *J. Am. Chem. Soc.* **2000**, *122*, 4640–4650.

(113) Wang, Z. Transmission Electron Microscopy of Shape-Controlled Nanocrystals and Their Assemblies. *J. Phys. Chem. B* **2000**, *104*, 1153–1175.

(114) Pyrz, W. D.; Buttrey, D. J. Particle Size Determination Using TEM: A Discussion of Image Acquisition and Analysis for the Novice Microscopist. *Langmuir* **2008**, *24*, 11350–11360.

(115) McKenzie, L. C.; Haben, P. M.; Kevan, S. D.; Hutchison, J. E. Determining Nanoparticle Size in Real Time by Small-Angle X-Ray Scattering in a Microscale Flow System. *J. Phys. Chem. C* **2010**, *114*, 22055–22063.

(116) Pauw, B. R. Everything SAXS: Small-Angle Scattering Pattern Collection and Correction. *J. Phys. Condens. Matter* **2013**, *25*, 383201.

(117) Nelson, A. Co-Refinement of Multiple-Contrast neutron/X-Ray Reflectivity Data Using MOTOFIT. *J. Appl. Crystallogr.* **2006**, *39*, 273–276.

(118) Simms, G. A.; Padmos, J. D.; Zhang, P. Structural and Electronic Properties of Protein/thiolate-Protected Gold Nanocluster with "Staple" Motif: A XAS, L-DOS, and XPS Study. *J. Chem. Phys.* **2009**, *131*, 0–9.

(119) Ilavsky, J.; Jemian, P. R. Irena: Tool Suite for Modeling and Analysis of Small-Angle Scattering. *J. Appl. Crystallogr.* **2009**, *42*, 347–353.

(120) Beaucage, G. Approximations Leading to a Unified Exponential/Power-Law Approach to Small-Angle Scattering. *J. Appl. Crystallogr.* **1995**, *28*, 717–728.

(121) Holden, M. J.; Haynes, R. J.; Rabb, S. A.; Satija, N.; Yang, K.; Blasic, J. R. Factors Affecting Quantification of Total DNA by UV Spectroscopy and PicoGreen Fluorescence. *J. Agric. Food Chem.* **2009**, *57*, 7221–7226.

(122) Cavaluzzi, M. J.; Borer, P. N. Revised UV Extinction Coefficients for Nucleoside-5'-Monophosphates and Unpaired DNA and RNA. *Nucleic Acids Res.* **2004**, *32*, e13.

(123) Sambrook, J.; Russell, D. *Molecular Cloning, 3rd Edition*; Cold Spring Harbor Laboratory Press: New York, USA, 2001.

(124) Jana, N. R.; Gearheart, L.; Obare, S. O.; Murphy, C. J. Anisotropic Chemical Reactivity of Gold Spheroids and Nanorods. *Langmuir* **2002**, *18*, 922–927.

(125) Resch-Genger, U.; Grabolle, M.; Cavaliere-Jaricot, S.; Nitschke, R.; Nann, T. Quantum Dots versus Organic Dyes as Fluorescent Labels. *Nat. Methods* **2008**, *5*, 763–775.

(126) Dulkeith, E.; Morteani, A. C.; Niedereichholz, T.; Klar, T. A.; Feldmann, J.; Levi, S. A.; van Veggel, F. C. J. M.; Reinhoudt, D. N.; Möller, M.; Gittins, D. I. Fluorescence Quenching of Dye Molecules near Gold Nanoparticles: Radiative and Nonradiative Effects. *Phys. Rev. Lett.* **2002**, *89*, 203002.

(127) Demers, L. M.; Mirkin, C. A.; Mucic, R. C.; Reynolds, R. A.; Letsinger, R. L.; Elghanian, R.; Viswanadham, G. Based Method for Determining the Surface Coverage and Hybridization Efficiency of Thiol - Capped Oligonucleotides Bound to Gold Thin Films and Nanoparticles. **2000**, *72*, 5535–5541.

(128) Paliwoda, R. E.; Li, F.; Reid, M. S.; Lin, Y.; Le, X. C. Coverage on Functionalized Gold Nanoparticles. **2014**.

(129) MolecularProbes. *Quant-iT ™ OliGreen ® ssDNA Reagent and Kit*; 2008.

CHAPTER II

(1) Liu, J.; Cao, Z.; Lu, Y. *Functional Nucleic Acid Sensors Functional Nucleic Acid Sensors*; 2009; Vol. 109.

(2) Jones, M. R.; Seeman, N. C.; Mirkin, C. A. *Science (80-.).* **2015**, *347* (6224), 1260901–1260901.

(3) Mirkin, C. A.; Letsinger, R. L.; Mucic, R. C.; Storhoff, J. J. *Nature*. 1996, pp 607–609.

(4) Liu, J.; Lu, Y. *Anal. Chem.* **2004**, *76* (6), 1627–1632.

(5) Liu, J.; Lu, Y. *Angew. Chemie - Int. Ed.* **2005**, *45* (1), 90–94.

(6) Storhoff, J. J.; Lazarides, A. A.; Mucic, R. C.; Mirkin, C. A.; Letsinger, R. L.; Schatz, G. C. *J. Am. Chem. Soc.* **2000**, *122* (19), 4640–4650.

(7) De, B. M.; Ghosh, P. S.; Rotello, V. M. **2008**, *01003*, 4225–4241.

(8) Dreaden, E. C.; Alkilany, A. M.; Huang, X.; Murphy, C. J.; El-Sayed, M. A. *Chem. Soc. Rev.* **2012**, *41* (7), 2740.

(9) Prigodich, A. E.; Randeria, P. S.; Briley, W. E.; Kim, N. J.; Daniel, W. L.; Giljohann, D. A.; Mirkin, C. A. *Anal. Chem.* **2012**, *84* (4), 2062–2066.

(10) Rosi, N. L.; Giljohann, D. a; Thaxton, C. S.; Lytton-Jean, A. K. R.; Han, M. S.; Mirkin, C. A. *Science* **2006**, *312* (5776), 1027–1030.

(11) Park, S. Y.; Lytton-Jean, A. K. R.; Lee, B.; Weigand, S.; Schatz, G. C.; Mirkin, C. A. *Nature* **2008**, *451* (7178), 553–556.

(12) Macfarlane, R. J.; Lee, B.; Jones, M. R.; Harris, N.; Schatz, G. C.; Mirkin, C. A. *Science (80-.).* **2011**, *334* (6053), 204–208.

(13) Li, F.; Zhang, H.; Lai, C.; Li, X. F.; Le, X. C. *Angew. Chemie - Int. Ed.* **2012**, *51* (37), 9317–9320.

(14) Paliwoda, R. E.; Li, F.; Reid, M. S.; Lin, Y.; Le, X. C. **2014**.

(15) Giljohann, D. A.; Seferos, D. S.; Patel, P. C.; Millstone, J. E.; Rosi, N. L.; Mirkin, C. A. *Nano Lett.* **2007**, *7* (12), 3818–3821.

(16) Zhao, W.; Hsing, I.-M. *Chem. Commun. (Camb).* **2010**, *46* (8), 1314–1316.

(17) Seferos, D. S.; Prigodich, A. E.; Giljohann, D. A.; Patel, P. C.; Mirkin, C. A. *Nano Lett.* **2009**, *9* (1), 308–311.

(18) Demers, L. M.; Mirkin, C. A; Mucic, R. C.; Reynolds, R. A; Letsinger, R. L.; Elghanian, R.; Viswanadham, G. **2000**, *72* (22), 5535–5541.

(19) Jin, R.; Wu, G.; Li, Z.; Mirkin, C. A.; Schatz, G. C. *J. Am. Chem. Soc.* **2003**, *125* (6), 1643–1654.

(20) Randeria, P. S.; Jones, M. R.; Kohlstedt, K. L.; Banga, R. J.; Olvera de la Cruz, M.; Schatz, G. C.; Mirkin, C. A. *J. Am. Chem. Soc.* **2015**, 150304145409002.

(21) Zhang, X.; Servos, M. R.; Liu, J. *J. Am. Chem. Soc.* **2012**, *134* (17), 7266–7269.

(22) Zhang, X.; Servos, M. R.; Liu, J. *Langmuir* **2012**, *28* (8), 3896–3902.

(23) Paliwoda, R. E.; Li, F.; Reid, M. S.; Lin, Y.; Le, X. C. **2014**.

(24) Anderson, B. J.; Larkin, C.; Guja, K.; Schildbach, J. F. *Chapter 12 Using Fluorophore-Labeled Oligonucleotides to Measure Affinities of Protein-DNA Interactions*, 1st ed.; Elsevier Inc., 2008; Vol. 450.

(25) Woehrle, G. H.; Brown, L. O.; Hutchison, J. E. *J. Am. Chem. Soc.* **2005**, *127* (7), 2172–2183.

(26) Acuna, G. P.; Bucher, M.; Stein, I. H.; Steinhauer, C.; Kuzyk, A.; Holzmeister, P.; Schreiber, R.; Moroz, A.; Stefani, F. D.; Liedl, T.; Simmel, F. C.; Tinnefeld, P. *ACS Nano* **2012**, *6* (4), 3189–3195.

(27) MolecularProbes. *Quant-iT ™ OliGreen ® ssDNA Reagent and Kit*; 2008.

(28) Liu, X.; Atwater, M.; Wang, J.; Huo, Q. *Colloids Surfaces B Biointerfaces* **2007**, *58* (1), 3–7.

(29) Cavaluzzi, M. J.; Borer, P. N. *Nucleic Acids Res.* **2004**, *32* (1), e13.

(30) Jana, N. R.; Gearheart, L.; Obare, S. O.; Murphy, C. J. *Langmuir* **2002**, *18* (3), 922–927.

(31) Cutler, J. I.; Auyeung, E.; Mirkin, C. A. *J. Am. Chem. Soc.* **2012**, *134* (3), 1376–1391.

(32) Frens, G. *Nat. Phys. Sci.* **1973**, *241* (105), 20–22.

(33) Sivaraman, S. K.; Kumar, S.; Santhanam, V. *J. Colloid Interface Sci.* **2011**, *361* (2), 543–547.

(34) Zhang, X.; Gouriye, T.; Göeken, K.; Servos, M. R.; Gill, R.; Liu, J. *J. Phys. Chem. C* **2013**, *117* (30), 15677–15684.

(35) Rawashdeh-omary, M. A.; Omary, M. A.; Patterson, H. H.; May, R. *J. Am. Chem. Soc.* **2000**, *122* (11), 10371–10380.

(36) Steel, A. B.; Herne, T. M.; Tarlov, M. J. *Anal. Chem.* **1998**, *70* (22), 4670–4677.

(37) Hurst, S. J.; Lytton-Jean, A. K. R.; Mirkin, C. A. *Anal. Chem.* **2006**, *78* (24), 8313–8318.

(38) Claridge, S. A.; Williams, S. C.; Goh, S. L.; Micheel, C. M. **2004**, No. 7, 1628–1635.

(39) Wang, Y.; Wang, Y.; Breed, D. R.; Manoharan, V. N.; Feng, L.; Hollingsworth, A. D.; Weck, M.; Pine, D. J. *Nature* **2012**, *490* (7422), 51–55.

(40) Angioletti-Uberti, S.; Varilly, P.; Mognetti, B. M.; Frenkel, D. *arXiv Prepr. arXiv ...* **2014**, *1* (September), 1–14.

(41) Peterson, A. W.; Wolf, L. K.; Georgiadis, R. M. *J. Am. Chem. Soc.* **2002**, *124* (49), 14601–14607.

(42) Li, H.; Rothberg, L. J. *J. Am. Chem. Soc.* **2004**, *126* (35), 10958–10961.

(43) Wang, W.; Ding, X.; He, M.; Wang, J.; Lou, X. *Anal. Chem.* **2014**, *86* (20), 10186–10192.

(44) Nelson, E. M.; Rothberg, L. J. *Langmuir* **2011**, *27* (5), 1770–1777.

(45) Macfarlane, R. J.; Lee, B.; Hill, H. D.; Senesi, A. J.; Seifert, S.; Mirkin, C. A. *Proc. Natl. Acad. Sci. U. S. A.* **2009**, *106* (26), 10493–10498.

(46) Ghosh, P.; Han, G.; De, M.; Kim, C. K.; Rotello, V. M. *Adv. Drug Deliv. Rev.* **2008**, *60* (11), 1307–1315.

(47) Liu, J. *Phys. Chem. Chem. Phys.* **2012**, *14* (30), 10485.

(48) Sambrook, J.; Russell, D. *Molecular Cloning, 3rd Edition*; Cold Spring Harbor Laboratory Press: New York, USA, 2001.

(49) Edelhoch, H. *Biochemistry* **1967**, *6* (7), 1948–1954.

(50) Bencze, W.; Schmid, K. *Anal. Chem.* **1957**, *2* (8), 1193–1196.

(51) Lee, J. S.; Lytton-Jean, A. K. R.; Hurst, S. J.; Mirkin, C. A. *Nano Lett.* **2007**, *7* (7), 2112–2115.

(52) Sönnichsen, C.; Reinhard, B. M.; Liphardt, J.; Alivisatos, A. P. *Nat. Biotechnol.* **2005**, *23* (6), 741–745.

(53) Hajizadeh, S.; Farhadi, K.; Forough, M.; Sabzi, R. E. *Anal. Methods* **2011**, *3* (11), 2599.

CHAPTER III

[1] C. A. Mirkin, R. L. Letsinger, R. C. Mucic, J. J. Storhoff, *Nature* **1996**, *382*, 607–609.

[2] A. P. Alivisatos, K. P. Johnsson, X. Peng, T. E. Wilson, C. J. Loweth, M. P. Bruchez, P. G. Schultz, *Nature* **1996**, *382*, 609–11.

[3] J. J. Storhoff, A. A. Lazarides, R. C. Mucic, C. A. Mirkin, R. L. Letsinger, G. C. Schatz, *J. Am. Chem. Soc.* **2000**, *122*, 4640–4650.

[4] R. Jin, G. Wu, Z. Li, C. A. Mirkin, G. C. Schatz, *J. Am. Chem. Soc.* **2003**, *125*, 1643–1654.

[5] S. Y. Park, A. K. R. Lytton-Jean, B. Lee, S. Weigand, G. C. Schatz, C. A. Mirkin, *Nature* **2008**, *451*, 553–556.

[6] D. Nykypanchuk, M. M. Maye, D. van der Lelie, O. Gang, *Nature* **2008**, *451*, 549–552.

[7] R. J. Macfarlane, B. Lee, M. R. Jones, N. Harris, G. C. Schatz, C. A. Mirkin, *Science (80-.).* **2011**, *334*, 204–208.

[8] M. R. Jones, N. C. Seeman, C. A. Mirkin, *Science (80-.).* **2015**, *347*, 1260901–1260901.

[9] V. Pavlov, Y. Xiao, B. Shlyahovsky, I. Willner, *J. Am. Chem. Soc.* **2004**, *126*, 11768–11769.

[10] C.-C. Huang, Y.-F. Huang, Z. Cao, W. Tan, H.-T. Chang, *Anal. Chem.* **2005**, *77*, 5735–5741.

[11] J. S. Lee, M. S. Han, C. A. Mirkin, *Angew. Chemie - Int. Ed.* **2007**, *46*, 4093–4096.

[12] D. Sun, J. Lu, Z. Chen, Y. Yu, M. Mo, *Anal Chim Acta* **2015**, *885*, 166–173.

[13] R. Xiao, D. Wang, Z. Lin, B. Qiu, M. Liu, L. Guo, G. Chen, *Anal. Methods* **2015**, *7*, 842–845.

[14] J. Liu, Y. Lu, *Anal. Chem.* **2004**, *76*, 1627–1632.

[15] J. Liu, Y. Lu, *Angew. Chemie - Int. Ed.* **2005**, *45*, 90–94.

[16] J. Liu, Y. Lu, *Nat. Protoc.* **2006**, *1*, 246–252.

[17] J. Liu, Y. Lu, *J. Am. Chem. Soc.* **2007**, *129*, 8634–8643.

[18] J. Liu, D. Mazumdar, Y. Lu, *Angew. Chemie - Int. Ed.* **2006**, *45*, 7955–7959.

[19] T. Hermann, D. J. Patel, *Science* **2000**, *287*, 820–825.

[20] C. K. O'Sullivan, *Anal. Bioanal. Chem.* **2002**, *372*, 44–48.

[21] J. Liu, Z. Cao, Y. Lu, *Functional Nucleic Acid Sensors Functional Nucleic Acid Sensors*, **2009**.

[22] R. E. Wang, Y. Zhang, J. Cai, W. Cai, T. Gao, *Curr. Med. Chem.* **2011**, *18*, 4175–4184.

[23] Y.-H. Lao, K. K. L. Phua, K. W. Leong, *ACS Nano* **2015**, *9*, 2235–2254.

[24] T.-C. Chiu, C.-C. Huang, *Aptamer-Functionalized Nano-Biosensors*, **2009**.

[25] S. Eustis, M. A. El-Sayed, *Chem. Soc. Rev.* **2006**, *35*, 209–217.

[26] A. Moores, F. Goettmann, *New J. Chem.* **2006**, *30*, 1121.

[27] P. Ghosh, G. Han, M. De, C. K. Kim, V. M. Rotello, *Adv. Drug Deliv. Rev.* **2008**, *60*, 1307–1315.

[28] X. Huang, M. A. El-Sayed, *J. Adv. Res.* **2010**, *1*, 13–28.

[29] S. Ghosh, T. Pal, *Chem. Rev.* **2007**, *107*, 4797–4862.

[30] P. K. Jain, W. Huang, M. A. El-Sayed, *Nano* **2007**, DOI 10.1021/nl071008a.

[31] C. Sönnichsen, B. M. Reinhard, J. Liphardt, A. P. Alivisatos, *Nat. Biotechnol.* **2005**, *23*, 741–745.

[32] R. M. Berne, R. Rubio, R. R. Curnish, *Circ. Res.* **1974**, *35*, 262–271.

[33] D. G. Van Wylen, T. S. Park, R. Rubio, R. M. Berne, *J. Cereb. Blood Flow Metab.* **1986**, *6*, 522–528.

[34] S. Latini, F. Pedata, *J. Neurochem.* **2001**, *79*, 463–484.

[35] L. L. Ma, L. L. Ma, M. Su, Z. Wang, *Anal. Methods* **2014**, *6*, 4366.

[36] D. Han, H.-M. Kim, R. Chand, G. Kim, I.-S. Shin, Y.-S. Kim, *Appl. Biochem. Biotechnol.* **2015**, *177*, 812–820.

[37] S. Falzoni, G. Donvito, F. Di Virgilio, *Interface Focus* **2013**, *3*, 20120101.

[38] X. Zeng, X. Zhang, W. Yang, H. Jia, Y. Li, *Anal. Biochem.* **2012**, *424*, 8–11.

[39] X. Guan, H. J. Zhang, Y. N. Bi, L. Zhang, D. L. Hao, *Biomed. Microdevices* **2010**, *12*, 683–691.

[40] X. Zhu, Y. Zhang, W. Yang, Q. Liu, Z. Lin, B. Qiu, G. Chen, *Anal. Chim. Acta* **2011**, *684*, 121–125.

[41] D. Liao, H. Jiao, B. Wang, Q. Lin, C. Yu, *Analyst* **2012**, *137*, 978–82.

[42] R. Ren, Y. Zou, *Sensors Actuators B Chem.* **2011**, *156*, 298–303.

[43] C.-C. Nieh, W.-L. Tseng, *Biosens. Bioelectron.* **2014**, *61*, 404–409.

[44] V. Guieu, C. Ravelet, S. Perrier, Z. Zhu, S. Cayez, E. Peyrin, *Anal. Chim. Acta* **2011**, *706*, 349–353.

[45] H. Zhao, Y.-S. Wang, X. Tang, B. Zhou, J.-H. Xue, H. Liu, S.-D. Liu, J.-X. Cao, M.-H. Li, S.-H. Chen, *Anal. Chim. Acta* **2015**, *887*, -.

[46] F. Yan, F. Wang, Z. Chen, *Sensors Actuators, B Chem.* **2011**, *160*, 1380–1385.

[47] A. E. Ross, B. J. Venton, *Anal. Chem.* **2014**, *86*, 7486–93.

[48] K. Feng, C. Sun, Y. Kang, J. Chen, J. H. Jiang, G. L. Shen, R. Q. Yu, *Electrochem. commun.* **2008**, *10*, 531–535.

[49] S. Xie, G. Shafer, C. G. Wilson, H. B. Martin, *Diam. Relat. Mater.* **2006**, *15*, 225–228.

[50] X. Yang, J. Zhu, Q. Wang, K. Wang, L. Yang, H. Zhu, *Anal. Methods* **2012**, *4*, 2221.

[51] Z.-S. Wu, M.-M. Guo, S.-B. Zhang, C.-R. Chen, J.-H. Jiang, G.-L. Shen, R.-Q. Yu, *Anal. Chem.* **2007**, *79*, 2933–2939.

[52] F.-H. Ko, M. Tai, F.-K. Liu, Y.-C. Chang, *Sensors Actuators B Chem.* **2015**, *211*, 283–289.

[53] H. W. Qiu, S. C. Xu, P. X. Chen, S. S. Gao, Z. Li, C. Zhang, S. Z. Jiang, M. Liu, H. S. Li, D. J. Feng, *Appl. Surf. Sci.* **2015**, *332*, 614–619.

[54] D. a Yushchenko, O. B. Vadzyuk, S. O. Kosterin, G. Duportail, Y. Mély, V. G. Pivovarenko, *Anal. Biochem.* **2007**, *369*, 218–25.

[55] H. Urata, K. Nomura, S. Wada, M. Akagi, *Biochem. Biophys. Res. Commun.* **2007**, *360*, 459–63.

[56] W. Qiang, H. Liu, W. Li, X. Chen, D. Xu, *Anal. Chim. Acta* **2014**, *828*, 92–8.

[57] Y. Bai, F. Feng, L. Zhao, Z. Chen, H. Wang, Y. Duan, *Analyst* **2014**, *139*, 1843.

[58] S.-Y. Hung, Y.-C. Shih, W.-L. Tseng, *Anal. Chim. Acta* **2015**, *857*, 64–70.

[59] M. M. Carrozzo, L. Troisi, G. Cannazza, A. S. Cazzato, D. Braghiroli, C. Parenti, S. Guiducci, M. Zoli, *J. Pharm. Biomed. Anal.* **2012**, *70*, 563–6.

[60] P. J. J. Huang, J. Liu, *Anal. Chem.* **2010**, *82*, 4020–4026.

[61] F. Li, J. Zhang, X. Cao, L. Wang, D. Li, S. Song, B. Ye, C. Fan, *Analyst* **2009**, *134*, 1355–1360.

[62] B. Zheng, S. Cheng, W. Liu, M. H.-W. Lam, H. Liang, *Anal. Biochem.* **2013**, *438*, 144–9.

[63] D. E. Huizenga, J. W. Szostak, *Biochemistry* **1995**, *34*, 656–665.

[64] B. L. Baldock, J. E. Hutchison, *Anal. Chem.* **Prepared for submission.**

[65] X. Zhang, M. R. Servos, J. Liu, *J. Am. Chem. Soc.* **2012**, *134*, 7266–7269.

[66] X. Zhang, T. Gouriye, K. Göeken, M. R. Servos, R. Gill, J. Liu, *J. Phys. Chem. C* **2013**, *117*, 15677–15684.

[67] H. A. Biebuyck, G. M. Whitesides, *Langmuir* **1993**, *9*, 1766–1770.

[68] H. Biebuyck, C. Bain, G. Whitesides, *Langmuir* **1994**, 1825–1831.

[69] S. E. Lohse, J. A. Dahl, J. E. Hutchison, *Langmuir* **2010**, *26*, 7504–7511.

[70] J. Lukkari, M. Meretoja, I. Kartio, K. Laajalehto, M. Rajamäki, M. Lindström, J. Kankare, *Langmuir* **1999**, *15*, 3529–3537.

[71] H. D. Hill, J. E. Millstone, M. J. Banholzer, C. A. Mirkin, *ACS Nano* **2009**, *3*, 418–424.

[72] P. S. Randeria, M. R. Jones, K. L. Kohlstedt, R. J. Banga, M. Olvera de la Cruz, G. C. Schatz, C. A. Mirkin, *J. Am. Chem. Soc.* **2015**, 150304145409002.

[73] E. C. Dreaden, A. M. Alkilany, X. Huang, C. J. Murphy, M. A. El-Sayed, *Chem. Soc. Rev.* **2012**, *41*, 2740.

[74] S. J. Hurst, A. K. R. Lytton-Jean, C. A. Mirkin, *Anal. Chem.* **2006**, *78*, 8313–8318.

[75] M. F. Hagan, A. K. Chakraborty, *J. Chem. Phys.* **2004**, *120*, 4958.

[76] A. W. Peterson, L. K. Wolf, R. M. Georgiadis, *J. Am. Chem. Soc.* **2002**, *124*, 14601–14607.

[77] P. Das, S. Zafar, **2015**.

[78] I. Y. Wong, N. A. Melosh, *Biophys. J.* **2010**, *98*, 2954–2963.

[79] S. K. Ghosh, T. Pal, *Chem. Rev.* **2007**, *107*, 4797–4862.

[80] K. Asian, J. R. Lakowicz, C. D. Geddes, *Anal. Chem.* **2005**, *77*, 2007–2014.

[81] P. Nordlander, C. Oubre, E. Prodan, K. Li, M. I. Stockman, *Nano Lett.* **2004**, *4*, 899–903.

[82] D. W. Brandl, N. A. Mirin, P. Nordlander, *J. Phys. Chem. B* **2006**, *110*, 12302–12310.

[83] Z. Zhong, S. Patskovskyy, P. Bouvrette, J. H. T. Luong, A. Gedanken, *J. Phys. Chem. B* **2004**, *108*, 4046–4052.

[84] B. . Kurganov, A. . Lobanov, I. . Borisov, A. . Reshetilov, *Anal. Chim. Acta* **2001**, *427*, 11–19.

[85] D. Eulberg, S. Klussmann, *ChemBioChem* **2003**, *4*, 979–983.

[86] W. G. Purschke, D. Eulberg, K. Buchner, S. Vonhoff, S. Klussmann, *Proc. Natl. Acad. Sci. U. S. A.* **2006**, *103*, 5173–8.

[87] M. M. Georgiadis, I. Singh, W. F. Kellett, S. Hoshika, S. A. Benner, N. G. J. Richards, *J. Am. Chem. Soc.* **2015**, 150511170813006.

[88] L. Zhang, Z. Yang, K. Sefah, K. M. Bradley, S. Hoshika, M.-J. Kim, H.-J. Kim, G. Zhu, E. Jimenez, S. Cansiz, et al., *J. Am. Chem. Soc.* **2015**, 150512174152002.

[89] X. Liu, M. Atwater, J. Wang, Q. Huo, *Colloids Surfaces B Biointerfaces* **2007**, *58*, 3–7.

[90] Y. Okahata, M. Kawase, K. Niikura, F. Ohtake, H. Furusawa, Y. Ebara, *Anal. Chem.* **1998**, *70*, 1288–1296.

[91] MolecularProbes, *Quant-iT ™ OliGreen ® ssDNA Reagent and Kit*, **2008**.

CHAPTER IV

(1) Liu, J.; Cao, Z.; Lu, Y. *Functional Nucleic Acid Sensors Functional Nucleic Acid Sensors*; 2009; Vol. 109.

(2) O'Sullivan, C. K. Aptasensors--the Future of Biosensing? *Anal. Bioanal. Chem.* **2002**, *372*, 44–48.

(3) Jones, M. R.; Seeman, N. C.; Mirkin, C. A. Programmable Materials and the Nature of the DNA Bond. *Science (80-.).* **2015**, *347*, 1260901–1260901.

(4) Eustis, S.; El-Sayed, M. A. Why Gold Nanoparticles Are More Precious than Pretty Gold: Noble Metal Surface Plasmon Resonance and Its Enhancement of the Radiative and Nonradiative Properties of Nanocrystals of Different Shapes. *Chem. Soc. Rev.* **2006**, *35*, 209–217.

(5) Hermann, T.; Patel, D. J. Adaptive Recognition by Nucleic Acid Aptamers. *Science* **2000**, *287*, 820–825.

(6) Ding, J.; Gu, Y.; Li, F.; Zhang, H.; Qin, W. DNA Nanostructure-Based Magnetic Beads for Potentiometric Aptasensing. *Anal. Chem.* **2015**, *87*, 6465–6469.

(7) Lao, Y.-H.; Phua, K. K. L.; Leong, K. W. Aptamer Nanomedicine for Cancer Therapeutics: Barriers and Potential for Translation. *ACS Nano* **2015**, *9*, 2235–2254.

(8) E. Wang, R.; Zhang, Y.; Cai, J.; Cai, W.; Gao, T. Aptamer-Based Fluorescent Biosensors. *Curr. Med. Chem.* **2011**, *18*, 4175–4184.

(9) Pavlov, V.; Xiao, Y.; Shlyahovsky, B.; Willner, I. Aptamer-Functionalized Au Nanoparticles for the Amplified Optical Detection of Thrombin. *J. Am. Chem. Soc.* **2004**, *126*, 11768–11769.

(10) Huang, C.-C.; Huang, Y.-F.; Cao, Z.; Tan, W.; Chang, H.-T. Aptamer-Modified Gold Nanoparticles for Colorimetric Determination of Platelet-Derived Growth Factors and Their Receptors. *Anal. Chem.* **2005**, *77*, 5735–5741.

(11) Lee, J. S.; Han, M. S.; Mirkin, C. A. Colorimetric Detection of Mercuric Ion (Hg2+) in Aqueous Media Using DNA-Functionalized Gold Nanoparticles. *Angew. Chemie - Int. Ed.* **2007**, *46*, 4093–4096.

(12) Sun, D.; Lu, J.; Chen, Z.; Yu, Y.; Mo, M. A Repeatable Assembling and Disassembling Electrochemical Aptamer Cytosensor for Ultrasensitive and Highly Selective Detection of Human Liver Cancer Cells. *Anal Chim Acta* **2015**, *885*, 166–173.

(13) Liu, J.; Lu, Y. Adenosine-Dependent Assembly of Aptazyme-Functionalized Gold Nanoparticles and Its Application as a Colorimetric Biosensor. *Anal. Chem.* **2004**, *76*, 1627–1632.

(14) Liu, J.; Lu, Y. Fast Colorimetric Sensing of Adenosine and Cocaine Based on a General Sensor Design Involving Aptamers and Nanoparticles. *Angew. Chemie - Int. Ed.* **2005**, *45*, 90–94.

(15) Liu, J.; Lu, Y. Non-Base Pairing DNA Provides a New Dimension for Controlling Aptamer-Linked Nanoparticles and Sensors. *J. Am. Chem. Soc.* **2007**, *129*, 8634–8643.

(16) Xiao, R.; Wang, D.; Lin, Z.; Qiu, B.; Liu, M.; Guo, L.; Chen, G. Disassembly of Gold Nanoparticle Dimers for Colorimetric Detection of Ochratoxin A. *Anal. Methods* **2015**, *7*, 842–845.

(17) Baldock, B. L.; Hutchison, J. E. Effect of Assembly Arrangement on Reactivity of DNA Aptamer-Linker Gold Nanoparticle Assemblies. *Angew. Chemie (International ed. English) (Manuscript in Preparation)*

(18) Storhoff, J. J.; Elghanian, R.; Mucic, R. C.; Mirkin, C. A.; Letsinger, R. L. Article One-Pot Colorimetric Differentiation of Polynucleotides with Single Base Imperfections Using Gold Nanoparticle Probes One-Pot Colorimetric Differentiation of Polynucleotides with Single Base Imperfections Using Gold Nanoparticle Probes. **1998**, *7863*, 1959–1964.

(19) Demers, L. M.; Mirkin, C. A.; Mucic, R. C.; Reynolds, R. A.; Letsinger, R. L.; Elghanian, R.; Viswanadham, G. A Fluorescence-Based Method for Determining the Surface Coverage and Hybridization Efficiency of Thiol-Capped Oligonucleotides Bound to Gold Thin Films and Nanoparticles. *Anal. Chem.* **2000**, *72*, 5535–5541.

(20) Randeria, P. S.; Jones, M. R.; Kohlstedt, K. L.; Banga, R. J.; Olvera de la Cruz, M.; Schatz, G. C.; Mirkin, C. A. What Controls the Hybridization Thermodynamics of Spherical Nucleic Acids? *J. Am. Chem. Soc.* **2015**, 150304145409002.

(21) Jin, R.; Wu, G.; Li, Z.; Mirkin, C. A.; Schatz, G. C. What Controls the Melting Properties of DNA-Linked Gold Nanoparticle Assemblies? *J. Am. Chem. Soc.* **2003**, *125*, 1643–1654.

(22) Sikder, M. D. H.; Gibbs-Davis, J. M. The Influence of Gap Length on Cooperativity and Rate of Association in DNA-Modified Gold Nanoparticle Aggregates. *J. Phys. Chem. C* **2012**, *116*, 11694–11701.

(23) Biebuyck, H. A.; Whitesides, G. M. Interchange between Monolayers on Gold Formed from Unsymmetrical Disulfides and Solutions of Thiols: Evidence for Sulfur-Sulfur Bond Cleavage by Gold Metal. *Langmuir* **1993**, *9*, 1766–1770.

(24) Biebuyck, H.; Bain, C.; Whitesides, G. Comparison of Organic Monolayers on Polycrystalline Gold Spontaneously Assembled from Solutions Containing Dialkyl Disulfides or Alkanethiols. *Langmuir* **1994**, 1825–1831.

(25) Zhang, X.; Gouriye, T.; Göeken, K.; Servos, M. R.; Gill, R.; Liu, J. Toward Fast and Quantitative Modification of Large Gold Nanoparticles by Thiolated DNA: Scaling of Nanoscale Forces, Kinetics, and the Need for Thiol Reduction. *J. Phys. Chem. C* **2013**, *117*, 15677–15684.

(26) Baldock, B. L.; Hutchison, J. E. Label-Free UV-Visible Spectroscopy Based Method for Quantifying DNA Bound to Gold Nanoparticles. *Anal. Chem. Prepared for submission.*

(27) Storhoff, J. J.; Lazarides, A. A.; Mucic, R. C.; Mirkin, C. A.; Letsinger, R. L.; Schatz, G. C. What Controls the Optical Properties of DNA-Linked Gold Nanoparticle Assemblies? *J. Am. Chem. Soc.* **2000**, *122*, 4640–4650.

(28) Ghosh, S.; Pal, T. Interparticle Coupling Effect on the Surface Plasmon Resonance of Gold Nanoparticles: From Theory to Applications. *Chem. Rev.* **2007**, *107*, 4797–4862.

(29) Jain, P. K.; Huang, W.; El-Sayed, M. A. On the Universal Scaling Behavior of the Distance Decay of Plasmon Coupling in Metal Nanoparticle Pairs : A Plasmon Ruler Equation On the Universal Scaling Behavior of the Distance Decay of Plasmon Coupling in Metal Nanoparticle Pairs : A Plasmon Ruler Eq. *Nano* **2007**.

(30) Mirkin, C. A.; Letsinger, R. L.; Mucic, R. C.; Storhoff, J. J. A DNA-Based Method for Rationally Assembling Nanoparticles into Macroscopic Materials. *Nature*, 1996, *382*, 607–609.

(31) Kurganov, B. .; Lobanov, A. .; Borisov, I. .; Reshetilov, A. . Criterion for Hill Equation Validity for Description of Biosensor Calibration Curves. *Anal. Chim. Acta* **2001**, *427*, 11–19.

(32) Hill, A. V. The Possible Effects of the Aggregation of the Molecules of Haemoglobin on Its Dissociation Curves. *Proc. Physiol. Soc.* **1910**, *40*, iv – vii.

(33) Monod, J.; Wyman, J.; Changeux, J. P. On the Nature of Allosteric Transitions: A Plausible Model. *J Mol Biol* **1965**, *12*, 88–118.

(34) Weiss, J. N. The Hill Equation Revisited: Uses and Misuses. *FASEB J.* **1997**, *11*, 835–841.

(35) Parak, W. J.; Pellegrino, T.; Micheel, C. M.; Gerion, D.; Williams, S. C.; Alivisatos, a. P. Conformation of Oligonucleotides Attached to Gold Nanocrystals Probed by Gel Electrophoresis. *Nano Lett.* **2003**, *3*, 33–36.

(36) Hurst, S. J.; Lytton-Jean, A. K. R.; Mirkin, C. A. Maximizing DNA Loading on a Range of Gold Nanoparticle Sizes. *Anal. Chem.* **2006**, *78*, 8313–8318.

(37) Peterson, A. W.; Wolf, L. K.; Georgiadis, R. M. Hybridization of Mismatched or Partially Matched DNA at Surfaces. *J. Am. Chem. Soc.* **2002**, *124*, 14601–14607.

(38) Wong, I. Y.; Melosh, N. A. An Electrostatic Model for DNA Surface Hybridization. *Biophys. J.* **2010**, *98*, 2954–2963.

(39) Lohse, S. E.; Dahl, J. A.; Hutchison, J. E. Direct Synthesis of Large Water-Soluble Functionalized Gold Nanoparticles Using Bunte Salts as Ligand Precursors. *Langmuir* **2010**, *26*, 7504–7511.

(40) Liu, X.; Atwater, M.; Wang, J.; Huo, Q. Extinction Coefficient of Gold Nanoparticles with Different Sizes and Different Capping Ligands. *Colloids Surfaces B Biointerfaces* **2007**, *58*, 3–7.

(41) Okahata, Y.; Kawase, M.; Niikura, K.; Ohtake, F.; Furusawa, H.; Ebara, Y. Kinetic Measurements of DNA Hybridization on an Oligonucleotide-Immobilized 27-MHz Quartz Crystal Microbalance. *Anal. Chem.* **1998**, *70*, 1288–1296.

APPENDIX A

(1) Nelson, A. *J. Appl. Crystallogr.* **2006**, *39* (2), 273–276.

(2) Simms, G. A.; Padmos, J. D.; Zhang, P. *J. Chem. Phys.* **2009**, *131* (21), 0–9.

(3) Ilavsky, J.; Jemian, P. R. *J. Appl. Crystallogr.* **2009**, *42* (2), 347–353.

(4) Beaucage, G. *J. Appl. Crystallogr.* **1995**, *28* (6), 717–728.

(5) MolecularProbes. *Quant-iT ™ OliGreen ® ssDNA Reagent and Kit*; 2008.

APPENDIX B

[1] S. E. Lohse, J. A. Dahl, J. E. Hutchison, *Langmuir* **2010**, *26*, 7504–7511.

[2] B. L. Baldock, J. E. Hutchison, *Anal. Chem.* **prepared for submission.**

APPENDIX C

(1) Lohse, S. E.; Dahl, J. A.; Hutchison, J. E. Direct Synthesis of Large Water-Soluble Functionalized Gold Nanoparticles Using Bunte Salts as Ligand Precursors. *Langmuir* **2010**, *26*, 7504–7511.

(2) Randeria, P. S.; Jones, M. R.; Kohlstedt, K. L.; Banga, R. J.; Olvera de la Cruz, M.; Schatz, G. C.; Mirkin, C. A. What Controls the Hybridization Thermodynamics of Spherical Nucleic Acids? *J. Am. Chem. Soc.* **2015**, 150304145409002.

(3) Monserud, J. H.; Schwartz, D. K. Mechanisms of Surface-Mediated DNA Hybridization Mechanisms of Surface-Mediated DNA Hybridization. **2014**, 4488–4499.

(4) Bhatt, N.; Huang, P. J. J.; Dave, N.; Liu, J. Dissociation and Degradation of Thiol-Modified DNA on Gold Nanoparticles in Aqueous and Organic Solvents. *Langmuir* **2011**, *27*, 6132–6137.

(5) Bdelwahed, W.; Degobert, G.; Stainmesse, S.; Fessi, H. Freeze-Drying of Nanoparticles: Formulation, Process and Storage Considerations☆. *Adv. Drug Deliv. Rev.* **2006**, *58*, 1688–1713.

(6) Liu, J.; Mazumdar, D.; Lu, Y. A Simple and Sensitive "Dipstick" Test in Serum Based on Lateral Flow Separation of Aptamer-Linked Nanostructures. *Angew. Chemie - Int. Ed.* **2006**, *45*, 7955–7959.